**Università degli Studi di Padova**

Department of Pharmaceutical Sciences

---

Doctoral Course in Molecular Sciences-

Curriculum in Pharmaceutical Sciences

XXXIV Cycle

# Optimization of biomimetic nanovesicles for the treatment of solid tumors and inflammation in the child and adult.

**Redacted with the financial contribution of:** Fondazione “Città della Speranza”

**Coordinator:** Chiar.mo Prof Leonard Prins

**Supervisor:** Prof. Paolo Caliceti

**Co-supervisor:** Dr. Marco Agostini, PhD

**PhD Student:** Riccardo Rampado

# Summary

# Abbreviations:

5-FC: 5-Fluorocistein

5-FU: 5-Fluorouracil

ADEPT: Antibody Directed Enzyme Prodrug Therapy

Apo: Apolipoprotein

BBB: Blood-Brain Barrier

BCA: Bicinchoninic Acid

BN: Boron-Nitride

BSA: Bovine Serum Albumin

Cas9: CRISPR-associated protein

Ce6: Chlorine e6

CML: Chronic Myeloid Leukemia

CNS: Central Nervous System

CpG: CpG Oligodeoxynucleotide

CRC: Colorectal Cancer

CRISPR: clustered regularly interspaced short palindromic repeats

CSC: Cancer Stem Cells

Cy5.5: Cyanin-5.5

DC: Dendritic Cells

DDS: Drug Delivery System

DLS: Dynamic Light Scattering

DoE: Design of Experiment

DOPC: Dioleoylphosphatidylcholine

DOXO: Doxorubicin

DPPC: Dipalmitoylphosphatidylcholine

DSS: Dextran Sodium Sulphate

DTT: Dithiothreitol

EB: Extraction Buffer

EC: Endothelial Cells

ECM: Extra-Cellular Matrix

EMT: Epithelial to Mesenchymal Transition

EPR: Enhanced Permeability and Retention

ESCRT: Endosomal Sorting Complexes Required for Transport

EtOH: Ethanol

EVs: Extracellular Vesicles

FRET: Fluorescence Resonance Energy Transfer

FRR: Flow Rate Ratio

GM1: Ganglioside M1

GPI-AP: Glycosyl Phosphatidyl Inositol -Anchored Protein

HSA: Human Serum Albumin

HIV: Human Immunodeficiency Virus

HUVEC: Human Umbilical Vein Endothelial Cells

IBD: Inflammatory Bowel Disease

IL: Interleukin

IR: Infra-Red

ISEV: International Society of Extracellular Vesicles

IV: Intra-Venous

KIT: commercial Kit used for membrane proteins extraction

Lipo: Liposomes

Leuko: Leukosomes

LPS: Lipopolysaccharide

MDR: Multi-Drug Resistance

miRNA: micro-RNA

MPI: Magnetic Particle Imaging

MRSA: Methicillin-resistant Staphylococcus Aureus

MVB: Multi-Vesicular Bodies

NEXT: New Extraction protocol

NG: Nano-Ghost

NIR: Near Infra-Red

NP: Nanoparticle

OS: Osteosarcoma

RGD: Arginylglycylaspartic acid

ROS: Reactive Oxygen Species

PAMAM: Poly-Amido-Amine

PARP: Poly-(ADP)-ribose polymerase-

PBS: Phosphate Buffered Saline

PC: Protein Corona

PDI: Polydispersity Index

PDT: Photo-Dynamic Therapy

PEG: Poly-Ethylene Glycol

PET: Positron Emission Tomography

PLGA: Poly-Lactic-co-Glycolic Acid

PMA: Phorbol 12-myristate 13-acetate

PT: Platelets

PTX: Paclitaxel

RBCs: Red Blood Cells

RVG-29: Rabies Virus Glycoprotein 29

siRNA: small interfering RNA

SLN: Solid Lipids Nanoparticle

SPION: Super-Paramagnetic Iron Oxide Nanoparticles

TCL: Total Cell Lysate

TGF: Tissue Growth Factor

TfR: Transferrin Receptor

TFR: Total Flow Rate

TNF-α: Tissue Necrosis Factor Alpha

TPP: Tri-Phenyl Phosphine

US: Ultra-Sound

# Abstract:

This research project is focused on the optimization of biomimetic nanovesicles derived from leukocytes with the ability to selectively target inflamed tissues and solid tumors, termed Leukosomes (Leukos). These nanovectors are designed to deliver anti-inflammatory and antitumor drugs in the inflamed tissues that characterize chronic and acute inflammatory pathologies and some neoplasms, to increase the drugs accumulation into the target organs and at the same time reduce the exposure of healthy tissues. This would lead to an increase in their efficacy, a reduction of side effects and thus a reduction of the required dose.

In the past, many studies developed nanovectors for drug delivery using many different materials, both synthetic and natural. Most of these formulations rely on the principles of passive and active targeting to deliver their therapeutic payload. However, most systems have been designed using a “bottom-up” approach, in which the basic components of the nanovector become assembled to achieve a progressively more complex and specific behavior. Despite offering fine control over the formulative conditions, the complexity of some systems makes this strategy very cumbersome and difficult to scale-up to a hypothetical industrial production.

Thus, the use of biomimetic nanovesicles complements this strategy with a “top-down strategy”, in which membrane proteins derived from leukocytes are engrafted within phospholipid bilayer of nanovesicles, forming Leuko. The use of membrane proteins of white blood cells bestows our nanoparticles (NPs) with the leukocytes’ biological identity and some of their functions, including their ability to circulate in the blood for long time, mediated by proteins such as CD45 and CD47; on the other hand, proteins including CD11b, LFA-1 and integrins mediate the ability to adhere to the endothelia of inflamed blood vessels. Furthermore, the nano-range size of our particles allows exploiting the enhanced permeability and retention (EPR) effect to further increase their accumulation into vascularized solid tumors.

Therefore, the first step of this project was the optimization of a fast, cheap and reproducible protocol for the extraction and purification of membrane proteins form leukocytes (Figure 1). We employed human and murine monocytes stabilized cell cultures as proofs of concept, since their fast growth and ease of culture yields a lot of starting cells with a stable phenotype.

The new membrane protein extraction protocol (NEXT) is based on three main steps divided by sequential centrifugations: the first one consists in cells washing to remove the cell culture medium proteins; the second is the cell permeabilization to induce the efflux of cytosolic and cytoskeletal proteins, using an aqueous buffer containing a mild detergent (i.e., Digitonin 0.015%

m/v, extraction buffer 1, EB1); in the final step, cell plasma membrane solubilization is performed using another buffer containing a stronger but non-denaturing detergent (i.e., Triton X-100, extraction buffer 2, EB2) with the dual function of extracting the proteins from the membranes and stabilizing them by including the protein hydrophobic domains within the detergent micelles. The NEXT extracts were compared with a gold standard commercial extraction kit (KIT) for final protein yield and purity of the extracts.

After performing the washing procedure, the first step was optimized by testing different ratios between EB1 volume and number of starting cells, measuring their permeabilization via turbidimetric assay. Thus, the minimal amount of buffer to achieve complete monocytes permeabilization has been established to be 100 μL of EB1 per million of starting cells. The same analysis was performed on the final step, in this case using even different Triton X-100 concentrations (i.e., 0.1% and 0.5% v/v). This latter optimization demonstrated how the increase in the amount of detergent in EB2 can improve membranes solubilization, resulting in a higher protein yield (up to 2.5mg of proteins per ml of extracts, comparable with KIT), without specific volume requirements. These results validated the scalability of NEXT as a protocol that can be applied to different cell numbers by simple adjusting the EB1 and EB2 volumes. The extracts purity was also assessed using SDS-PAGE and Western Blot analyses with a specific panel of membrane and non-membrane proteins. This semi-quantitative investigation showed how the membrane proteins (i.e., CD11b and Calnexin) were indeed enriched in the NEXT extracts compared to the total cell lysate (TCL) up to five times, and conversely, the cytosolic proteins (i.e., β-actin and GAPDH) as well as the nuclear ones (i.e., NP-62) were greatly reduced or absent, with comparable purity to the KIT. Furthermore, the membrane proteins purity increased with detergent concentration in EB2. Finally, these results were confirmed using the orthogonal mass spectrometry technique, which demonstrated an overall reduction in the amount of different proteins present in the extracts from KIT (402) and NEXT (227) compared to TCL (516), with at the same time a higher percentage of membrane proteins in NEXT extracts (17,9%) compared to KIT (12.3%) and TCL (9.1%).

After the optimization of membrane protein extractions, the second step was their engraftment within the nanovesicles phospholipid bilayer, yielding Leukos (Figure 1). However, many Leuko features should be optimized to make them suitable for preclinical testing. Leukos should have a hydrodynamic diameter between 50 and 200 nm, homogeneous size distribution (PDI≈0.2 or lower) and efficient membrane protein engraftment.

To formulate Leukos, we employed the Nanoassemblr™ equipment. This approach is based on the fast and homogeneous mixing of an aqueous and an organic phase. The Nanoassemblr™

allows for the fast and scalable self-assembly of many lipid-based NPs by the change in polarity in the solvent during the mixing. In particular, the Leuko aqueous phase is composed of solubilized membrane proteins dispersed in a 250 mM ammonium sulphate buffer that enables the remote loading of the antitumor drug doxorubicin (DOXO); on the other hand, the organic phase is a cholesterol and phospholipids solution in ethanol. Thus, Leuko self-assembly and membrane protein engraftment occur simultaneously.

However, the experimental parameters for this process, including the system total flow rate (TFR), the flow rate ratio between the phases (FRR), and the proteins to lipids weight ratio should be optimized to yield Leukos with the desired features. Thus, Leuko features including size, PDI and protein loading were optimized using a Design of Experiment (DoE) approach to select the optimal parametric values while using the minimal number of required experimental runs.

The DoE approach allows creating different combinations of the considered parametric values that can cover many different experimental conditions. In our optimization, we selected a range of parametric values going from 1mL/min to 10mL/min for TFR, from 1:1 to 1:5 (organic : aqueous) for FRR and from 1:300 to 1:20 for the membrane to lipid ratio. Each single combination corresponds to an experimental run with unique conditions. The experimental results have been analyzed and interpolated to create a mathematical model that predicts the results of the process for any given parameter combinations within the evaluation range. On the bases of our prediction model, the optimal parameters were found to be a 1mL/min TFR, a 1:4.88 FRR, and 1:20 lipid to protein ratio. These conditions yielded Leukos with diameter of 150nm, a PDI≈0.23, and a very negative surface charge (i.e., Zeta Potential, -25mV), that suggested the efficient engraftment of membrane proteins. Membrane proteins functionalization was orthogonally confirmed using flow cytometry with a wide screen of antibodies directed against several immune cells markers, confirming both their presence compared to bare liposomes (Lipos) and correct orientation.

Leukos have been then loaded with the model antitumor drug DOXO using a remote loading strategy that yielded a 70% encapsulation efficiency. DOXO release has also been studied, and Leukos showed gradual and pH-dependent release profile. Specifically, DOXO is released faster in slightly acidic conditions (pH=6), corresponding to lisosomal pH. Therefore, DOXO is expected to be not released during Leukos circulation in the blood at physiologic pH (pH=7.4), while it is released within the cell after endocytosis.

In the last part of the project (Figure 1), we demonstrated Leuko ability to adhere to inflamed endothelial cells using fluorescence microscopy, as well as their internalization rate in osteosarcoma

SAOS-2 cells and colorectal cancer HCT-116 cells. In the latter ones, the internalization increased with time, and the Leuko intracellular punctate pattern suggests an endocytic mechanism of uptake. Finally, we tested the cytotoxicity of Lipo and Leuko loaded with DOXO on the above-mentioned cancer cell lines, using both “flat” cell culture conditions and tumor spheroids using a hydrogel as bioactive scaffold to enable tumor spheroids growth (Geltrex$^{TM}$). DOXO loaded Leukos showed improved cytotoxic effect compared to free DOXO against tumor cells both in 2D and in 3D.

The results of this project constitute a proof of concept to establish a framework for the optimization of biomimetic drug delivery systems that can be formulated using many different starting cell lines and with many different potential applications in a with set of pathologies. Furthermore, the establishment of more biomimetic nanoplatforms paves the way to the formulation of personalized therapeutics using patient-derived “self” cells with not only high efficacy but improved biocompatibility.

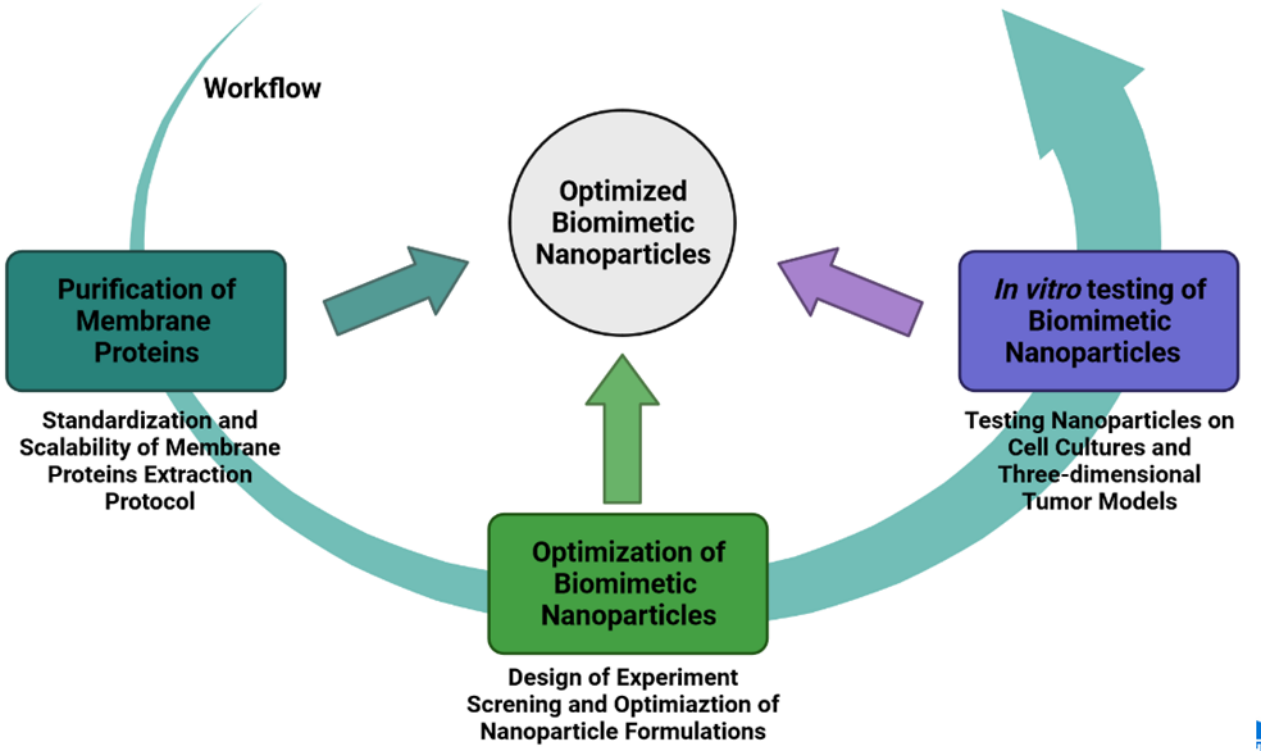


**Figure 1** Schematic representation of the project

# Riassunto:

Questo progetto di ricerca è volto all'ottimizzazione di nanovescicole biomimetiche derivate da leucociti denominate Leucosomi (Leuko) con la capacità di veicolare farmaci selettivamente a tessuti infiammati e tumori solidi. Questi nanovettori sono disegnati per veicolare farmaci a ntinfiammatori e antitumorali nei tessuti infiammati che caratterizzano patologie infiammatorie croniche e in alcune neoplasie, al fine di aumentare il loro accumulo negli organi target e ridurne l'esposizione a tessuti sani con un miglioramento della loro efficacia, minimizzazione dei loro gravi effetti collaterali e delle dosi necessarie.

In passato, molti nanovettori sono stati sviluppati usando diversi materiali naturali e sintetici. La maggior parte di queste formulazioni si basano sui principi di targeting attivo e passivo per il direzionamento al tessuto target. Tuttavia, questi sistemi sono progettati seguendo una strategia "bottom-up", in cui le diverse componenti del nanovettore vengono assemblate per ottenere formulazioni con un comportamento sempre più complesso e specifico. Anche se questo approccio offre un eccellente controllo sulle condizioni di produzione, la complessità di alcuni sistemi lo rende molto laborioso e difficile da sviluppare su larga scala per la produzione industriale.

L'uso di vescicole biomimetiche permette di combinare questa strategia con un approccio "top-down", in cui proteine di membrana purificate dai leucociti sono inserite nello strato fosfolipidico di vescicole formando i Leuko. In particolare, l'uso di proteine di membrana derivate da globuli bianchi fornisce alle particelle l'identità biologica e le funzioni dei leucociti stessi, incluse la loro capacità di circolare nel sangue a lungo, mediata da proteine quali CD45 e CD47. Inoltre, proteine come CD11b, LFA-1 ed integrine mediano l'adesione all' endotelio nei tessuti infiammati. La dimensione nanometrica di queste vescicole permette loro di sfruttare l'effetto EPR per aumentare ulteriormente il loro targeting nei tumori solidi.

Nella prima fase di questo progetto è stato ottimizzato un protocollo per l'estrazione e purificazione di proteine di membrana che fosse semplice, economico e riproducibile (Figura 1). Nella fattispecie, sono state usate linee cellulari di monociti umani e murini, visto che la rapida replicazione e facilità di coltura fornisce molte cellule di partenza con un fenotipo relativamente stabile.

Il protocollo di estrazione delle proteine di membrana (NEXT) si è basato su tre passaggi principali: il primo consiste nel lavaggio delle cellule per rimuovere le proteine presenti nel terreno di coltura; il secondo nella permeabilizzazione delle cellule per permettere l'efflusso di proteine citosoliche e del citoscheletro, usando un buffer contenente un detergente blando (Digitonina 0,015%

m/v, buffer di estrazione 1, EB1); nell'ultimo passaggio viene effettuata la solubilizzazione della membrana plasmatica con un detergente non denaturante ma più forte (Triton X-100, buffer di estrazione 2, EB2) il quale permette anche di stabilizzare le proteine di membrana includendo i loro domini idrofobici nelle micelle. La resa e purezza finale delle proteine ottenute con NEXT sono state paragonate con quelle ottenute con un kit commerciale (KIT).

Dopo aver effettuato i lavaggi, il primo step è stato ottimizzato valutando diversi rapporti tra EB1 e numero di cellule, misurando la loro permeabilizzazione con saggi turbidimetrici. La quantità di EB1 minima per ottenere la completa permeabilizzazione dei monociti è risultata 100 µL di EB1 per milione di cellule. La stessa analisi è stata effettuata sul secondo passaggio, in questo caso utilizzando diverse concentrazioni di Triton X-100 (0.1% e 0.5% v/v). Questa ottimizzazione ha dimostrato come l'aumento di detergente presente in EB2 potesse migliorare significativamente la solubilizzazione delle membrane e risultasse in una resa proteica più alta (fino a 2,5 mg di proteine per mL di estratto, comparabile al KIT), senza specifici requisiti di volume. Questi risultati hanno validato il protocollo NEXT che può essere applicato a differenti quantità di cellule variando i volumi di EB1 ed EB2. La purezza degli estratti ottenuti con NEXT sono anche stati analizzati usando SDS-PAGE e Western Blot con uno specifico set di proteine di membrana e di altri compartimenti cellulari. Questa analisi semi-quantitativa ha dimostrato come le proteine di membrana (CD11b e Calnexina) erano effettivamente arricchite negli estratti ottenuti da NEXT rispetto al lisato cellulare completo (TCL), fino a cinque volte di più, e le proteine citosoliche (β-actina e GAPDH), oltre a quelle nucleari (NP-62) sono risultate molto ridotte o assenti. Inoltre, la purezza delle proteine di membrana aumentava con la quantità di detergente presente in EB2. Infine, i risultati sono stati confermati usando la spettrometria di massa, la quale ha mostrato una complessiva riduzione nel numero complessivo di diverse proteine negli estratti ottenuti dal KIT (402) e nel NEXT (227) rispetto al TCL (516), con allo stesso tempo una percentuale più alta di proteine di membrana negli estratti di NEXT (17,9%), rispetto al KIT (12.3%) ed al TCL (9.1%).

Dopo aver effettuato l'estrazione delle proteine di membrana, il secondo step del consiste nell'inserirle nello strato fosfolipidico delle nanovescicole, ottenendo i Leuko (Figura 1). Tuttavia, molte caratteristiche dei Leuko devono essere ottimizzate per rendere questa formulazione adatta agli studi preclinici. In particolare, i Leuko dovrebbero avere un diametro idrodinamico tra i 50 ed i 200 nm, una distribuzione di dimensioni omogenea (con un PDI di 0,2 o minore) e una buona funzionalizzazione con le proteine di membrana.

Per formulare i Leuko, è stato utilizzato il sistema di microfluidica Nanoassemblr™. Questo approccio si basa sulla miscelazione veloce ed omogenea di una fase liquida acquosa ed una organica.

Il Nanoassemblr™ permette l'auto-assemblamento rapido e scalabile di molte nanoparticelle (NPs) con base lipidica per cambiamento nella polarità del solvente durante il processo di miscelazione. In particolare, la fase acquosa dei Leuko è composta da proteine di membrana disperse in un tampone di ammonio solfato 250 mM per permettere il caricamento remoto di doxorubicina (DOXO). La fase organica consiste in una soluzione di fosfolipidi e colesterolo in etanolo. Di conseguenza, l'assemblamento dei Leuko e l'inserimento delle proteine di membrana avvengono in un solo step.

I parametri sperimentali per questo processo, inclusi la velocità totale di flusso nel sistema (TFR), il rapporto di flusso tra le fasi (FRR) e quello tra proteine di membrana ed i lipidi devono essere ottimizzati per ottenere Leuko con le caratteristiche desiderate. Dunque, le caratteristiche dei Leuko tra cui diametro idrodinamico, distribuzione di dimensioni, e loading di proteine sono state ottimizzate mediante Design of Experiment (DoE) al fine di selezionare i valori dei parametri considerati ottimali, usando il minor numero possibile di corse sperimentali con diversi valori parametrici. L'approccio DoE permette infatti di creare combinazioni di valori dei parametri sperimentali considerati che coprano molte condizioni diverse simultaneamente. Nella nostra ottimizzazione abbiamo selezionato range di valori parametrici da 1mL/min a 10mL/min per il TFR, da 1:1 a 1:5 per il FRR, e da 1:300 a 1:20 per il rapporto tra proteine e lipidi. Ciascuna combinazione corrisponde ad una corsa sperimentale con specifiche condizioni. I dati sperimentali sono stati analizzati e interpolati per creare un modello matematico che permettesse di prevedere i risultati del processo sulla base dei valori parametrici utilizzati. Sulla base delle predizioni offerte dal nostro modello, i parametri ottimali si sono rivelati essere un TFR di 1mL/min, un FRR di 4.88:1 (fase acquosa di fase alcolica, v/v) ed un rapporto di massa tra lipidi e proteine di 20:1. Questa combinazione di parametri ha permesso di ottenere Leuko con un diametro di 150 nm, un PDI≈0.2, ed un potenziale zeta molto negativo (-25mV), che suggerisce un efficiente inserimento delle proteine di membrana. L'inserimento delle proteine di membrana sui Leuko è stato anche confermato con la tecnica ortogonale di citofluorimetria, in cui abbiamo utilizzato un ampio screen di anticorpi contro diversi marker espressi delle cellule immunitarie. Questa tecnica ha confermato la presenza di numerosi marker immunitari ed il loro corretto orientamento sui Leuko rispetto ai semplici Lipo.

I Leuko sono stati dunque caricati con il farmaco antitumorale modello doxorubicina (DOXO) usando un metodo di loading remoto con un'efficienza di incapsulamento del 70%. È stato anche studiato il rilascio del farmaco, dimostrando un profilo di rilascio graduale e dipendente da pH. Nello specifico, DOXO viene rilasciata dai Leuko più velocemente a pH leggermente acido (pH=6), corrispondente al pH dei lisosomi. Questo profilo è adeguato per il rilascio intracellulare di DOXO dopo endocitosi e previene il rilascio nel circolo sanguigno (pH=7,4).

Nell'ultima parte del progetto (Figura 1), si è valutata la capacità dei Leuko di aderire a cellule endoteliali infiammate usando la microscopia a fluorescenza, oltre al tasso di internalizzazione dei Leuko da parte delle cellule di osteosarcoma SAOS-2 e delle cellule di cancro colon-retto HCT-116. In quest'ultime, l'internalizzazione ha dimostrato di crescere col tempo. Inoltre, il pattern intracellulare puntato citosolico delineato dalle NPs suggerisce un meccanismo di internalizzazione endocitico. Infine, abbiamo testato la citotossicità di Lipo e Leuko caricati con DOXO sulle linnee di cellule tumorali sopra specificate sia in condizioni di coltura "piatta", sia su sferoidi tumorali ottenuti coltivando le cellule in un idrogel che funzioni da supporto bioattivo per la crescita di sferoidi tumorali (Geltrex$^{TM}$). I Leuko caricati con DOXO hanno dimostrato in entrambi i modelli una citotossicità verso cellule tumorali superiore a quella della DOXO libera. La citotossicità delle particelle è stata testata anche su organoidi di cancro colon-rettale derivati da pazienze.

I risultati di questo progetto costituiscono un *proof-of-concept* al fine di stabilire un framework per l'ottimizzazione di sistemi biomimetici per il *drug delivery* che possano essere formulati utilizzando diverse linee cellulari di partenza e con numerose possibili applicazioni in contesti patologici sia tumorali che di infiammazione acuta e cronica. Lo sviluppo di nuovi sistemi biomimetici inoltre aprirebbe la via alla formulazione di terapie personalizzate ottenute da cellule "self" derivate da paziente che coniughino alta efficacia con una migliore biocompatibilità.

# Introduction

## The main features of Cancer

Cancer is among the main causes of global deaths and is responsible for about 25% of overall mortality in the United States and United Kingdom (1). At the same time, almost three quarters of all cancer-related casualties happen in low income and developing countries, with fast changes in their lifestyle resulting in similarly rapid cancer rates (1).

### Carcinogenesis

Under normal conditions, cell proliferation and turnover in healthy tissues is finely regulated in a mostly constant equilibrium, with specific molecules that induce cell proliferative and anti-proliferative biochemical signals (2). This dynamic equilibrium determines cell replication and growth rates when required, for example during the organism growth, enable the repair of damaged tissues and maintains the tissue homeostasis.

All neoplasms originate from cells that uncontrollably replicate (3). Cancers invading surrounding tissues are defined as malignant; conversely, benign tumors are normally not invasive, remaining in their organs of origin without physiological function (4). Other than fast replication, tumor cells often acquire the ability to create new blood vessels by over-secretion of specific molecular signals in a process called neo-angiogenesis (5). Malignant tumor cells in their more advanced state can extravasate form the primary tumor site into the systemic blood circulation using the novel tumor vessels, avoid their removal by the immune system, and exploit it as a fast route to reach and invade distant organs, creating tumor metastases (6). Furthermore, many tumors become resistant to anticancer drugs over time, even during the treatment, making their eradication especially challenging (7).

To date, more than one hundred different tumor types have been identified. Since tumors can affect virtually every organ and tissue in the human body, neoplasms are classified by the tissue and cell population they originate from (4).

Despite the many origins and heterogeneity among tumor types, the molecular root of cancer can be pinpointed to some main genetic damages or alterations in genes (8). Pre-cancerous cells normally acquire genetic mutations that cannot be fixed by physiological DNA repair mechanisms like nucleotide- and base-excision repair, homologous recombination, end joining, and mismatch repair. The two main classes of mutation that can occur and result in the development of tumors are either the excessive activation of genes that promote cell division, tissue invasion and immune

evasion (termed as oncogenic), or the inactivation of genes responsible for the repair of genetic damage and in apoptosis (called onco-suppressors) (9). Thus, the activation of oncogenic genes is the main responsible for fast and uncontrolled cell death. Conversely, onco-suppressors inactivation results in further genetic damage due non-functioning repair mechanisms, and cells insensitivity to DNA damage-induced cell death.

These genetic mutations can be spontaneous (10), deriving from DNA replication errors, it can be hereditary (11), or be caused by environmental agents such as ultraviolet (UV) light, ionizing radiations, genotoxic compounds, and even infective agents such as viruses and bacteria (12).

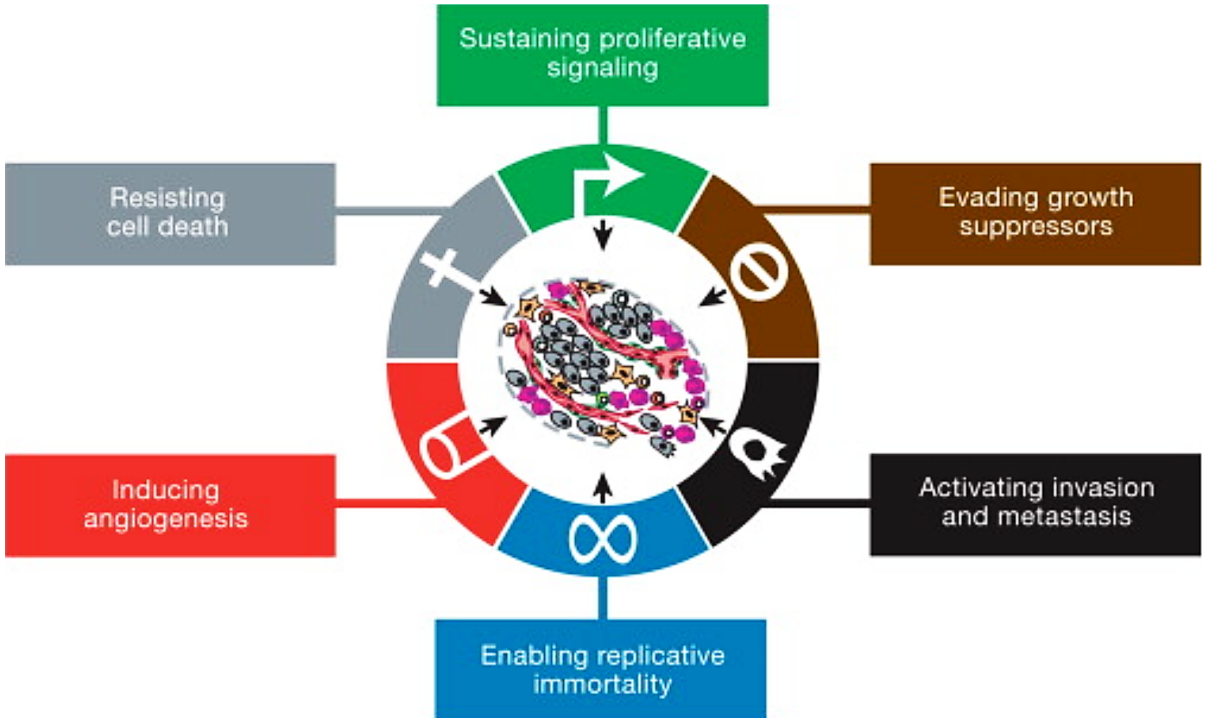


**Figure 2** Schematic representation of the main hallmarks of cancer during its development. Figure was taken from (3).

Carcinogenesis is normally classified in four principal steps (13). The first one is initiation and is characterized by permanent DNA damages previously described; it is considered quite fast in time and poses the bases for the fast growth and further genetic instability of tumor cells. The second step is the promotion, during which cells tend to increase the amount of DNA to support their fast division and accumulate further mutations that are defined as promoters, enabling the tumor to support its own growth by metabolic changes that would not be per se oncogenic. The third step is the malignant transformation, during which the cells become undifferentiated and do not resemble their original population and acquire the ability to invade the surrounding tissue. The final step is progression during malignant neoplasms gain genetic alterations, which leads to karyotype change. Furthermore, the degeneration of chromosomal structure provides new abnormal cellular features,

such as the tissue invasion, metastatic colonization, and anaplasia.

Along these four phases, cancer develops several features that are defined as the “hallmarks of cancer” (Figure 2):

- Cell increase growth signaling (14): this can occur through different processes, such as the dysfunction of physiological feedback intracellular mechanisms, which results in the overexpression of secreted growth signals with autocrine action, the abnormal proliferative intracellular signaling, the overexpression of membrane receptors responsible for the binding to growth factors, or the re-programming of surrounding cells to produce paracrine growth factors.
- Insensitivity to growth suppression and malignancy promotion (14): essential proteins for gene stability such as p53 and RB become inactivated, making cells continue to proliferate even in cases of otherwise lethal genetic mutations. Furthermore, cancer cells undergo signaling changes that makes them insensitive to tumor suppressing signaling factors or even changing the cells response to them towards a proliferative response. Tumor cells can also overcome the inhibitions deriving from cell-to-cell contact. An example of this is TGF-β, which is considered an anti-proliferative agent, which however become pro-proliferative in several tumors, promoting the epithelial to mesenchymal transition (EMT), resulting high-grade malignancy to cancer cells.
- Resistance to cell death (15): the main mechanisms of cell death that tumor cells tend to avoid are the ones that occur physiologically. The first one is apoptosis, which is a programmed cell death process caused by oncogenic activation, DNA damage, natural embryonic development, or cells senescence. The increased activation of anti-apoptotic mechanisms or the inactivation of pro-apoptotic function can result in cells resistance to this form of death. The second cell death process is autophagy, normally considered a mechanism for cells to recycle their molecules by the formation of large cytosolic vesicles termed autophagosomes. Normally, the strong induction of autophagy results in cells death and tumor suppression, but the contribution of these mechanisms to tumor eradication is not straightforward. The third form of cell death, necrosis, is normally caused by chemical or physical stress that induces cell eruption and cannot be escaped by metabolic or genetic mutations. Necrosis normally results in the release of intracellular, immunogenic material that can elicit an antitumor immune response, and its induction is thus considered advantageous against cancer.
- Achieving unlimited replication: in physiological conditions, healthy cells can replicate only a finite number of times before undergoing senescence and subsequent apoptosis. From a

molecular standpoint, this process is regulated by the gradual shortening of telomeres, which are genetic non-coding structures at the end of chromosomes. After telomeres become gradually consumed with each cells division, cells naturally undergo apoptosis. Thus, in many tumors the embryonic telomerase enzyme is activated abnormally, causing the elongation of telomeres and making cells *de facto* able to divide virtually an infinite amount of time.

- Neo-angiogenesis (5): the creation of new blood vessels is a process normally present during the embryonic development and in damaged adult tissues during their repair. Many solid tumors however gain the ability of secreting pro-angiogenic factors, leading to the tumor infiltration of blood vessels, which provide the neoplasm with nutrients and even more growth factors.
- Tissue invasion and metastasis (6): after invading their primary region, tumor cells can penetrate within the blood vessels and reach blood circulation, using which they can colonize even distant organs by extravasation and invasion of the tissue parenchyma. This process can occur also via the lymphatic drainage, in which tumor cells can accumulate into the lymph nodes. In this way, cancers can compromise the function of many organs.
- Immune evasion and reprogramming (16): The immune system is normally able to rapidly identify and remove somatic cells with an altered phenotype, such as most spontaneously occurring neoplastic cells. Thus, only a small percentage of actual tumors can bypass the immune system and further proliferate. This immune evasion can occur via the secretion by tumor cells of immune suppressive signaling molecules, the expression of surface receptors that inhibit immune-induced death and phagocytosis, or even reprogram immune cells to produce molecules that promote tumor growth.

Of note, the sequence of mutations leading to a tumor origin and development follows an evolutionary mechanism (17). First, the increase in cells proliferation and their lack of genetic repair mechanisms pose the foundations for other fast mutations, and in the case of rapid growth, gives the tumor cells advantage compared to healthy tissues with slow and well-regulated growth. The resistance of tumor cells to apoptosis and unlimited replication further provides them with independence from the surrounding tissue inhibition mechanisms, letting the tumor overcome the surrounding cells. Angiogenesis provides the tumor with higher amount of nutrients compared to the surrounding tissue, and metastasis enables the tumor to spread across the organism, actively acquiring new space and nutrients in secondary organs. Similarly, tumor cells resistance to drugs also derived from the selective pressure exerted by cytotoxic agents onto the cell population, eradicating sensitive cells and intrinsically providing drug/resistant cells with more space and nutrients left by the removed cells. The tumor deregulated activation of many mechanisms associated with wound healing led the

tumor to be often referred at as “the wound that does not heal” (18).

It is important to note that the tumor cells population is often not homogeneous and is composed by heterogeneous subpopulations with different metabolic1 and genetic profile (19). Thus, tumor cells are not only in competition with the surrounding environment but also among themselves, and many treatments targeted to specific tumor features could work only on a fraction of the overall tumor mass.

**Pathophysiology of tumors**

Despite the wealth of knowledge available on the metabolism and genetic profile of tumors, the frequent onset of drug resistance and even lack of response underlines the limits of this tumor-centric approach in drug development.

Recently, the importance of the tumor surrounding tissue and environment considered and its relevance in promoting tumor growth unveiled. This led to known Paget’s comparison of tumors to “seeds” that require a “soil” (the tumor microenvironment) with specific features to enable its successful development, invasion, and distal metastasis (20). Thus, the tumor metabolism and is microenvironment became the focus for the design of novel antitumor treatments that leverage these peculiar features a further level of selectively to achieve tumor ablation without affecting healthy organs. Among the main characteristic of the tumor milieu there are:

- Local hypoxia: the fast proliferation rate of tumor cells is a feature of many solid tumors. In turn, this leads to an increase consumption of oxygen compared to healthy tissues. In these conditions, the resulting low oxygen pressure is termed as hypoxia (21). This condition has important repercussions onto the tumor development, since it can induce partial tumor necrosis and a metabolic shift of tumor cells towards non-oxidative metabolism (referred at as the Warburg Effect), and induce tumor cells to start angiogenesis to increase oxygen delivery to the neoplastic mass, even activating oncogenic genes such as *Ras*.

  Low oxygen pressure can also lead to the production of reactive oxygen species (ROS), which can cause further DNA damage and favor tumor progression (22). The high tumor concentration of ROS can be exploited to design materials that are susceptible to oxidative stress, such as polymers that can dissociate in presence of these reactive molecules, offering a potential handle for tumor microenvironment selective drug release for systemically administered nanomaterials.
- Local acidosis (23): the local acidic pH that characterizes many solid tumor parenchyma is often a result of the mentioned metabolic shift of tumor cells towards anaerobic metabolism,

which results in the production of a high amount of metabolites such as lactic acid by lactate dehydrogenase. Another acidosis-inducing factor is also the high amount of carbon dioxide produced by tumor cells, which can be promptly converted to carbonic acid via the carbonic anhydrase enzyme. Acidosis can also be exploited as an environmental feature to design materials that can release antitumor drugs in acidic pH.

- Tumor vasculature: the hypoxic conditions of solid tumors and acidosis require an increase in the supply of nutrients and more efficient waste removal (5). This need results in angiogenesis, with the infiltration of new vessels into the tumor mass that can support the growth of tumor cells situated at the center of the tumor mass and thus less exposed to systemic circulation. Notably, since the tumor neo-vessels are prompted by an imbalance of pro- and anti- angiogenic factors, their structure is quite irregular, with their shape being very convoluted, the basal membranes are often lacking, and the endothelium itself present fenestrations in size range of 100-800 nm. In turn, this “leaky” architecture, together with a lack of parallel increase in lymphatic drainage, contributes to the increase in local pressure of the tumor due the extravasation of many high molecular weight molecules that would be otherwise retained in the bloodstream, making the tumor “desmoplastic”.

Vasculature has important repercussions on the use of chemotherapy, since the non-homogeneous distribution of tumor vessels through which chemotherapeutics normally reach tumor cells makes the drug distribution uneven across the tumor mass, and some cells are not as exposed to treatment, resulting in lackluster efficacy. Furthermore, the high local pressure of the tumor prevents the drugs from penetrating the tissue via active filtration, instead relying only on slower passive diffusion. These same features of tumor vasculature have been employed for the delivery of nanomaterials to solid tumor using the enhanced permeability and retention (EPR) effect (24). Specifically, after intravenous administration, NPs can reach the tumor vessels via systemic circulation, extravasate through the vessels fenestrations and accumulate into the tumor thanks to the relatively inefficient lymphatic drainage, increasing the accumulation of antitumor drugs into the tumor itself. However, the relevance of the EPR effect in improving nanoparticles delivery efficiency has been somewhat been reconsidered since only a fraction of tumor presents extended neo-vasculature and the fenestrations size is very inconsistent among different tumors and even different patients. Furthermore, some recent studies demonstrated how NPs could accumulate into the tumor also using non-EPR pathways such as transcytosis.

## Anticancer therapies

The aim of anticancer therapy is eradicating the tumor cells with minimal side effects on healthy cells. Several strategies are available to this end, and their choice depends on several factors including the location of the tumor, its stage, genetic and metabolic features, as well as the patient health condition. The main classes of antitumor therapy are:

- Surgical resection: this approach normally involved the excision of the tumor mass via direct surgical intervention (25). However, recently new techniques have been developed such as cryosurgery (freezing the tumor mass using local application of low temperatures), and hyperthermia (ablating the tumor mass using by topical high temperatures).
- Radiotherapy: local doses of ionizing radiation can be used to induce tumor cell death without exposing healthy tissues to toxic radiation dose (26). This is achieved either by external irradiation or by the administration of radioactive isotopes.
- Chemotherapy: consists in the administration of cytotoxic drugs, which normally target DNA structure and synthesis, cell replication or active metabolic pathways, all features that are more present in tumor cells compared to healthy ones, resulting in preferential toxic effects against the former (27). This approach also includes hormone therapy (28), which employs specific hormones inhibitors to stop the growth of hormone-dependent cancers. Angiogenesis inhibitors to inhibit the formation of new blood vessels to reduce the influx of nutrients to tumor cells (29). Targeted therapies that manipulate very specific signaling pathways that are activated exclusively in certain tumor subtypes, making these agents highly selective and avoiding toxic effects on healthy tissues (30). On the basis of the time of chemotherapy administration chemotherapy can be classified in:
    - Neoadjuvant therapy: used to reduce the tumor size before surgery, allowing surgical resection or radiotherapy.
    - Adjuvant therapy: after a surgical tumor excision, chemotherapy is administered to remove potential tumor leftovers or undetected metastases.
- Immunotherapy: consists in a group of different strategies that aim at inducing the activation of the immune system against tumor cells, employing the organism’s natural defense mechanisms to achieve tumor eradication (31). Some of these approaches include immune checkpoint blockade agents, induction of immunogenic cell death, or administration of vaccines containing tumor neoantigens.
- Gene therapy: this recent approach aims at genetically manipulating the tumor cells by introducing new onco-suppressive genes or restoring their function, or by the selective deactivation of oncogenic ones (32). This strategy takes advantage of the recent developments

in RNA delivery as well as highly innovative gene editing strategies such as CRISPR-Cas9 and antisense oligonucleotides.

- Stem cell transplant: stem cells are administered to replace the ones ablated by chemotherapy or radiotherapy.

Chemotherapy is widely used therapy normally used in combination with other approaches. However, a serious drawback of this treatment is that since these drugs act preferentially in fast-replicating cells, they can act on both tumor cells and other healthy proliferating tissues such as epithelial and bone marrow cells. This leads in turn to serious toxicity such as myelosuppression, gastrointestinal disturbances, as well as skin and cutaneous annexes dysfunction, normally accompanied by systemic effects such as fatigue, nausea, and vomiting, associated with the organism's response to perceived toxic molecules (33).

Another critical issue in chemotherapy is the development of multidrug resistance (MDR), a phenomenon consisting in tumor cells not responding to cytotoxic agents (7). This adaptation to therapy can occur via different mechanisms including the expression of membrane efflux pumps that remove chemotherapeutics from the cells, the activation of drug catabolizing enzymes, or downregulating drug targets that makes cells less sensitive to their action. To circumvent this problem, in most cases antitumor drugs are normally administered in combination. This allows for targeting of many different tumor cells pathways at the same time, reducing the chance for tumor cells to survive by modifying only single drug targets. The use of different drugs together also enables drug synergy, exerting a superior antitumor effect compared to the sum of each molecule (34). Furthermore, chemotherapy is used in combination with the above-mentioned physical treatments obtaining a similar synergistic effect.

In summary, tumor therapy requires a multidisciplinary approach with the aim to improve treatment outcome and minimizing side effects, ultimately improving the patients' quality of life.

**Cancer and inflammation**

Inflammation is an essential physiological function involved in the resolution of tissue damage and infection (35). However, this feature can become a double-edged sword since its dysregulation can cause many different autoimmune and chronic inflammatory diseases. It is important to note however, that inflammation has two functions: removing damaged tissues and external bodies, but also promote tissue regeneration and wound healing.

Inflammation and more generally the immune system have a pivotal role in every step of cancer insurgence and progression. The interplay between the immune system and neoplasms is

bilateral and dynamic. When Dovrak defined cancer as a “wound that does not heal”, he underlined several aspects of its progression, including angiogenesis (36), cellular proliferation, but also the presence of local inflammation and immune cells infiltration (37; 3). Of note, all these aspects are included in the tissue regeneration function of inflammation.

Tumor associated inflammation can have different origins, including pre-existing chronic inflammatory or autoimmune conditions, like in the case of Crohn’s disease and Ulcerative colitis, two chronic inflammatory gastrointestinal conditions considered major risk factors for the development of colorectal cancer (CRC) (38).

The complex contribution of the immune system to tumor growth sparked the use of a complex terminology that defines tumors as either immunologically “hot”, “cold”, or “deserts” depending on the number of infiltrated leukocytes present in the tumor milieu (39). However, this loose classification assumes that the activity of local immune cells would be inherently anti-tumor and does not consider the ability of tumor cells to leverage immunity to their advantage. In fact, immune cells in physiological conditions can substantially hinder tumor growth through the elimination of aberrant neoplastic cells, but in more progressed tumors, the selective pressure of immune cells can eliminate more antigenic cells and indirectly promote the growth of immune-escaping cancer cells. Furthermore, tumors cells are not only able to escape the immune system, but they can also reprogram locally infiltrated immune cells to create a more favorable environment for its growth and tissue invasion via the production of growth factors for themselves (40).

Indeed, tumors can induce the differentiation of local macrophages from as their M1 phenotype (associated with cancer 1removal) to their modulatory M2 phenotype (associated with wound healing and cells proliferation) (41). In a few cases, tumors can induce the differentiation of local T-regulatory leukocytes that induce apoptosis of pro-inflammatory immune cells. Tumor cells can reprogram local fibroblasts to produce growth factors to sustain their proliferation (42).

Tumors can maintain the presence of favorable inflammatory conditions by producing pro-angiogenic signaling molecules and cytokines that induce the proliferation of blood vessels and the expression onto their surface of adhesion molecules that work as a homing device for circulating immune cells, which can become reprogrammed by the tumor cells *in situ* (5).

These features have been exploited as potential therapeutic targets to immune-modulate the tumor microenvironment. Among these, the main strategies include:

- Inhibition of tumor neo-angiogenesis: there are already in the clinic therapeutic tools that specifically aim at reducing the formation of new blood vessels around the tumor. Antibodies such as bevacizumab and small molecules inhibitors such as vandetanib and sorafenib that target the VEGF/VEGF-R and PDGF/PDGF-R signaling, both essential in tumoral neo-angiogenesis. This approach aims to starve the tumor, inducing cells necrosis and indirectly stimulate tumor immune clearance, although it is used normally in combination with traditional chemotherapy (36).
- Tumor vessels have been used also as an active targeting handle for nanomedicines since they tend to overexpress molecules such as integrins that enable immune cells accumulation (43). These nanosystems therefore would accumulate in the same tumor milieu, and at the same time could occupy the adhesion site, preventing tumor-promoting immune cells to accumulate in the tissue.
- Elicit an immune response: this can be achieved using many different approaches such as the development of tumor vaccine that can present tumor antigens to immune cells and therefore educate immune cells to attack the tumor mass (44); cause tumor cells immunogenic death, either via chemotherapy or physical treatment *in situ* (e.g., temperature, radiation, or the use of nanomaterials and external stimuli to induce thermal or mechanical ablation) (45). This in turn would lead to the release of death associated molecular patterns that can elicit antitumor response.

A more recent approach relies on the use of immune checkpoint inhibitors (46). Tumor cells can prevent phagocytosis through the expression of surface markers such as PD-L1, which can bind to the receptor PD-1 on T cells, inhibiting their antitumor effect. Conversely, tumor antigen can be exposed by antigen presenting cells (APCs) to T-cells via the co-stimulatory proteins CD80 and CD86, which bind to the T-cell receptor CTLA-4, causing the development of “anergic” leukocytes that are unable to attack tumor cells. These mechanisms are defined as immune checkpoints. Thus, antibodies against PD-L1, PD-1 and CTLA-4 have been developed to inhibit these immune-suppressive processes, facilitating the immune destruction of tumor cells. Despite the elegance of this strategy, immune checkpoint inhibitors were successful only in a small fraction of patients with already immune-infiltrated cancers.

## Basic concepts of nanomedicine

In the last decades, many new drugs reached the clinical practice (47). However, their pharmacokinetics profiles still leave a lot to be desired, with only a very small fraction of the administered therapeutics reaching its molecular target (48). The off-target accumulation in other

tissues can results in undesired side effects and adverse reaction.

Thus, the chemotherapeutics should be administered and absorbed efficiently, navigate the organism without affecting it, and reach the target tissue selectively, following the intuition of Paul Elrich who defined the ideal drugs as “magic bullet”. Nanotechnology applied to drug delivery has received a lot of interest as an innovative strategy to control drugs biodistribution and release (49). NPs loaded with different drugs offer the advantage of increasing drugs apparent solubility, reduce their degradation and excretion, and improve their targeting using different strategies. Furthermore, nanomaterials have intrinsic and peculiar features that can synergize with the drugs in disease treatment and diagnosis (50).

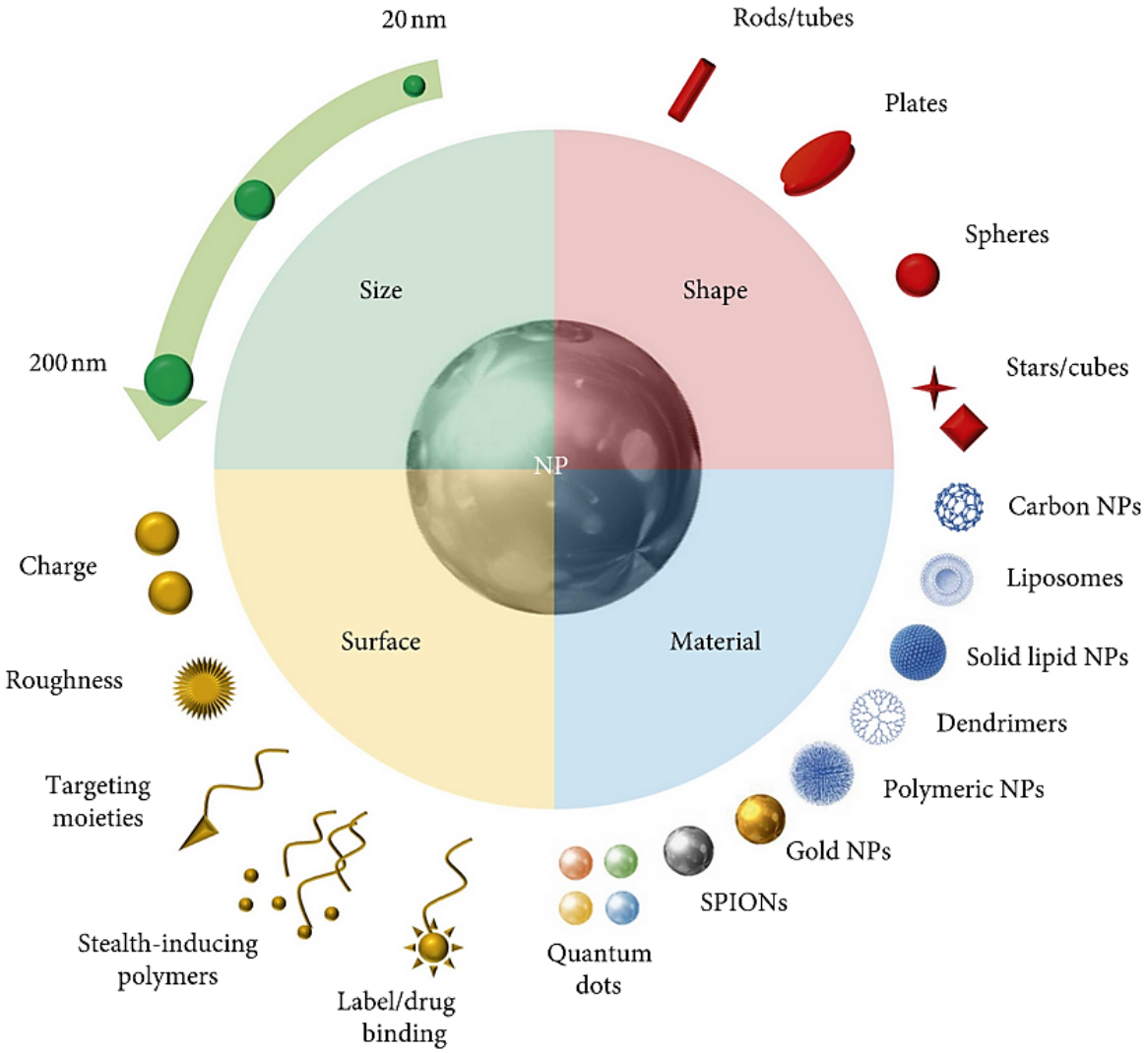


**Figure 3** Schematic representation of the main features of nanomaterials used for drug delivery and nanomedicine against tumors. Image was taken from (51).

Despite all these advantages and the many nanovectors described in the literature, only a few nanomedicine-based formulations have reached the bedside. The reasons for such a high failure rate

can be attributed to different factors: importantly, many NPs formulations are complex platforms with many components to assemble, and this makes their industrial scaling-up process exceptionally complicated (52); secondly, many nanovectors fail late clinical trials due a lack of benefit compared to traditional treatment or safety concerns, underlining how there is a long way to go to further improve NPs targeting efficacy and understand their potential toxicities; finally, there are still no clear regulatory requirements specific for nanomedicine, making their final approval difficult and cumbersome since it has to rely on guidelines designed for traditional drugs (53).

Most nanomedicines are injected intravenously. Despite the parenteral administration route overcoming important biological barriers, NPs are still faced with many hurdles that separate them from their final target. In particular, the immune system, specific organ barriers (e.g., the blood brain barrier), and clearing organs are all major concerns that should be considered when designing nanovectors for drug delivery (54).

One of the staples of nanomedicines used for drug delivery is the use of EPR effect. First described by Maeda et al, this passive targeting process relies on the extravasation of nano-sized colloids, including drug loaded NPs, through the fenestration that characterize many solid tumors newly formed blood vessel (24). At the same time, the relatively low lymphatic drainage also results in improved NPs retention into the tumor milieu. The main NPs features necessary for achieving EPR effect are (Figure 3):

- Size. NP size has important and complex repercussions on their behavior. Specifically, healthy blood vessels present only very small gaps, in the range of few nanometers (2-6 nm), and thus does not enable NPs filtration. However, other organs such as the liver, spleen and kidneys, present larger fenestrations due to their natural filtrating function (in the wide range of 40 to 500 nm, depending on the specific organ). This results in most NPs formulations considerably accumulating in these tissues after systemic administration, often significantly reducing their targeting efficacy, end even very small particles being quickly cleared by kidney glomeruli. Conversely, materials in the range of micrometers in size result in their fast accumulation in capillaries including lung vessels and can result in micro-embolisms. Thus, nanomaterials for systemic administration are designed to be in the size range of 50 to 200 nm (55).
- Surface charge. The electrical charge onto the surface of nanoparticles determines not only their biodistribution but also their toxicity. Positively charged materials after intravenous administration tend to quickly adsorb on their surface a high amount of plasma proteins,

resulting often in NPs aggregation and ultimately in their fast clearance (56). Furthermore, cationic NPs can strongly interact with the cellular membranes and endocytosed very quickly but could also result in membrane damage and cellular toxicity. Conversely, neutral or slightly negative charged particles demonstrate lower protein adsorption, longer *in vivo* colloidal stability, and ultimately longer circulation time (57).

- Shape. Nanomaterials geometric shape has also relevant effect in their biodistribution. For example, despite most nanomaterials assembling in spheroidal shape, many materials have been generated with specific purposes. For example, discoidal particles appear to interact very efficiently with blood vessels. Conversely, elongated, needle shaped particles with the same mass as their spherical counterparts demonstrated increased circulation time, perhaps due to their reduced hydrodynamic diameter enabled by their aspect ratio (58).
- Stealth behavior. To improve the NPs circulation time, nanovectors are often coated with hydrophilic flexible materials that neutralize their surface charge, greatly reducing the adsorption of plasma proteins, and reducing their clearance from circulation. For the longest time, nanomaterials have been coated with polyethylene glycol (PEG), a biocompatible polymer with all the mentioned features, that is to date considered the gold standards to generate stealthy nanomaterials. Nevertheless, PEG has still some limitations including its non-biodegradability, which could result in organ accumulation, and the chronic production of anti-PEG antibodies, which can result in paradoxical fast particles clearance (56).

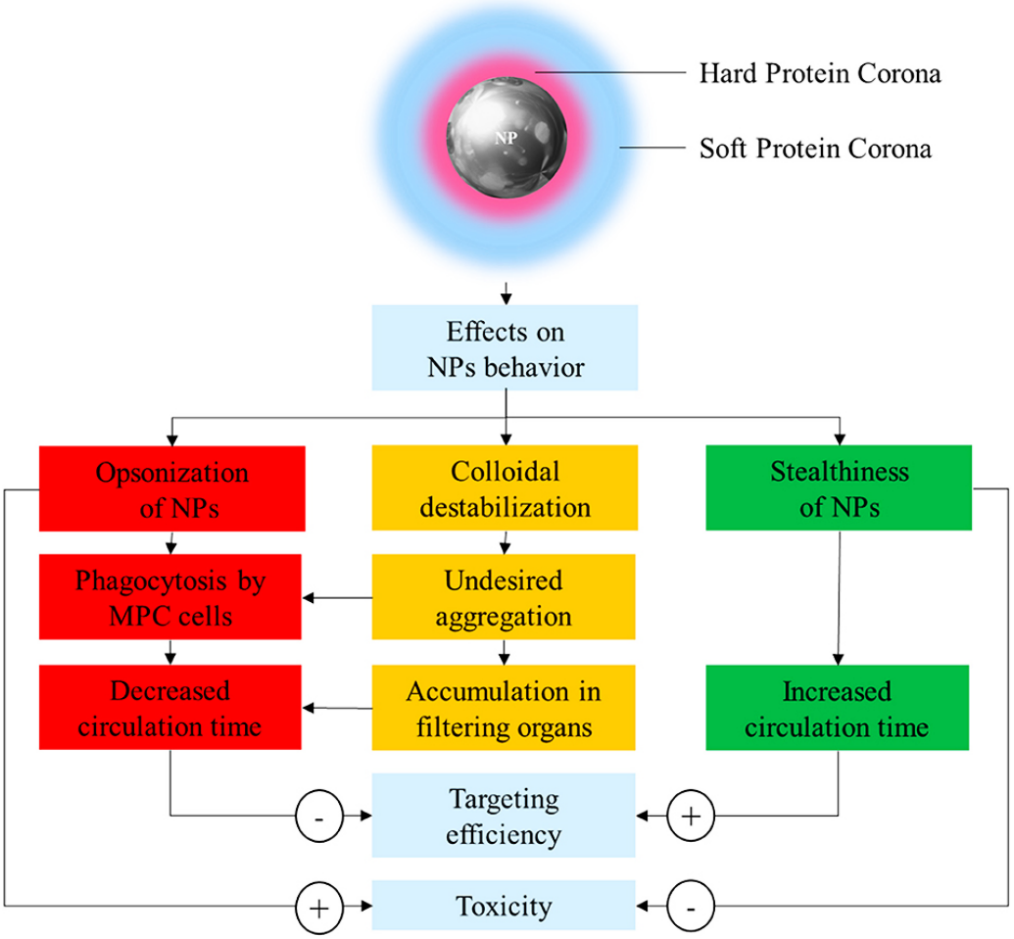


**Figure 4** Schematic representation of the main effects of PC formation on NPs behavior after intravenous administration. The image was adapted from (56)

Despite the EPR effect relevance in the design of antitumor nanomedicines, it was demonstrated how its relevance is highly variable depending on the extent of tumor vasculature and its permeability.

- Immune evasion: after NPs are administered, they always become rapidly coated by many different plasma proteins, forming the so-called protein corona (PC) (56). This phenomenon is highly dynamic and depends on NPs features including their size, surface charge and chemistry, and shape. The composition and extent of the PC can determine the fate of NPs, since the absorption of immune-related proteins such as immunoglobulins and complement proteins can make the nanomaterial easy to recognize by the immune system, resulting in its fast removal from systemic circulation (Figure 4). The use of stealth inducing polymers focuses on the reduction of PC formation on the NPs surface. However, more recent and innovative nanomaterials have leveraged the wealth of knowledge on the PC components and function to create particles able to manipulate the PC formation and adsorb proteins, which are able to prolong their half-life in the blood circulation (Table 1).

**Table 1** Main contributions of different nanomaterials features to the formation of the PC. (56)

| Feature | Influence on NP interactions with proteins |
|---|---|
| Size | • Larger particles have lower and offer more surface interaction for each protein.<br>• Smaller particles have higher surface curvature. This leads to less influence on the protein's conformation. |
| Shape | • Shape change the mass/surface ratio of NPs. Spherical NPs (maximum mass/minimal surface) thus minimize the interactions with the environment.<br>• Shape changes the curvature of NPs, with the above-mentioned repercussion of protein conformations. |
| Hydrophilicity/ hydrophobicity | • Hydrophobic NPs interact with hydrophobic proteins through Wan der Waals or π-π interactions.<br>• Hydrophobic surfaces could favor protein denaturation/conformational chances, by forcing to expose their hydrophobic domains.<br>• Hydrophilic NPs interact with more charged proteins through electrostatic interactions. |
| Surface charge | • More densely charged NPs tend to have thicker and denser PCs.<br>• Highly positively charged NPs interact very quickly and very strongly with proteins having an IP <5.5.<br>• Highly negatively charged NPs interact mostly with proteins with an IP >5.5.<br>• Slightly negatively charged proteins appear to have lower interactions with proteins. |

A complementary approach to passive targeting and the EPR effect is active targeting. This strategy relies on the surface functionalization of NPs using an array of different ligands for receptors that overexpressed by the target tumor cells (59). Importantly, the use of active targeting moieties does not provide any active force that drives NPs to their target, but can only work in addition to passive targeting, increasing the particles affinity to their target cells after they reach them. Furthermore, higher active targeting ligand surface density results in improved nanovectors adhesion and uptake. This is of paramount importance because NPs are too large to simply diffuse across the cellular membrane and therefore require active uptake mechanisms such as endocytosis and phagocytosis. Active targeting therefore can also improve the NPs uptake kinetics.

Drug release from nanovectors can occur via two different mechanisms: in the first case, NPs release the drugs in the tumor microenvironment after reaching its proximity; in the second case, NPs are internalized by tumor cells via endocytosis and the drug is released from the endosomal compartment into the cytosol where it elicits its function. The drug can either be physically released from nanovectors during their degradation or can be chemically cleaved by the NPs scaffold if it was chemically conjugated.

The drug release can be controlled using different endogenous and exogenous features (60):

- Temperature: thermo-sensitive materials can undergo phase transition, dissolution or degradation over a specific temperature value and therefore it could be possible to elicit this condition in the tumor via external light irradiation of using specific nanomaterials that can artificially increase the local temperature. Furthermore, the high metabolic activity of tumors can also result in slightly higher temperatures compared to healthy tissue, providing an endogenous stimulus for drug release.
- pH: tumor acidosis can be used to trigger the degradation of the NPs matrixes and achieve drug release inly in the tumor milieu. Another possible approach involves the chemical

conjugation of the drugs to the NPs via pH dependent chemical bonds that can be cleaved under acidic conditions.

- Light and ultrasounds (US): these external stimuli can be used to respectively induce the *in-situ* degradation of NPs via the triggering of peculiar light-sensitive drug reactions, or via thermal and mechanical stress. Importantly, US can penetrate tissues much more in depth than visible or IR light without causing intrinsic tissue damage.

## Biomimetic nanoparticles for drug delivery

Nanomaterials have been formulated mainly according to "bottom-up" approach, in which the single chemical components are assembled or even chemically synthesized to obtain the final nanovector (61). This approach led to important scientific milestones and even the approval of nano formulations for the treatment of many diseases, consolidating nanotechnology as an innovative and fruitful field of inquiry. The aim to improve synthetic NPs tissue specificity sparked the formulation of nanomaterials with disparate features such as materials with pH dependent (62; 63), temperature dependent, redox dependent (64), and enzyme responsive (65) features. Thus, these nanosystems intricacy increased following a "bottom-up" approach, in which more layers of specificity are added upon the system. However, over the years, this quest for nanomaterials with increasingly complex behaviors and higher targeting efficiencies led to the creation of a swath of very complex nanoplatforms, which however presented limited applications *in vitro* and even less success when tested *in vivo*. Furthermore, many of these "smart" materials require cumbersome chemical synthesis. This in turn creates the artificial hurdle of recreating their complexity on a large scale, potentially hindering their clinical translation. Finally, synthetic materials applied to biomedical applications always pose the important issue of biocompatibility.

On the other side of the spectrum of innovative therapeutic approaches, there are biological therapies, which include a variegate class of different strategies, ranging from monoclonal antibodies (66), viral vectors (67) and extracellular vesicles (68), to the use of entire cells as therapy (69). These therapies proved to be true game changers, providing not only new therapeutic agents, but also even entirely new technologies and way to think about the treatment of many pathologies. However, the complexity of the biological therapies and their production steps poses some issues such as their reproducibility on a large scale. Furthermore, safety concerns over the use of some among these treatments such as viral vectors and cellular therapies stem from their complexity and difficulty in complete characterization.

In the last years, the concern about "over-engineered" synthetic nanomaterials led to a renewed interest in using formulations with simpler designs, focusing of biocompatibility and

scalability of production. On the other hand, the quest to streamline the production of biological-based therapies led to the adoption of a “top-down” approach, selecting the essential components of biologicals necessary to achieve the desired effect.

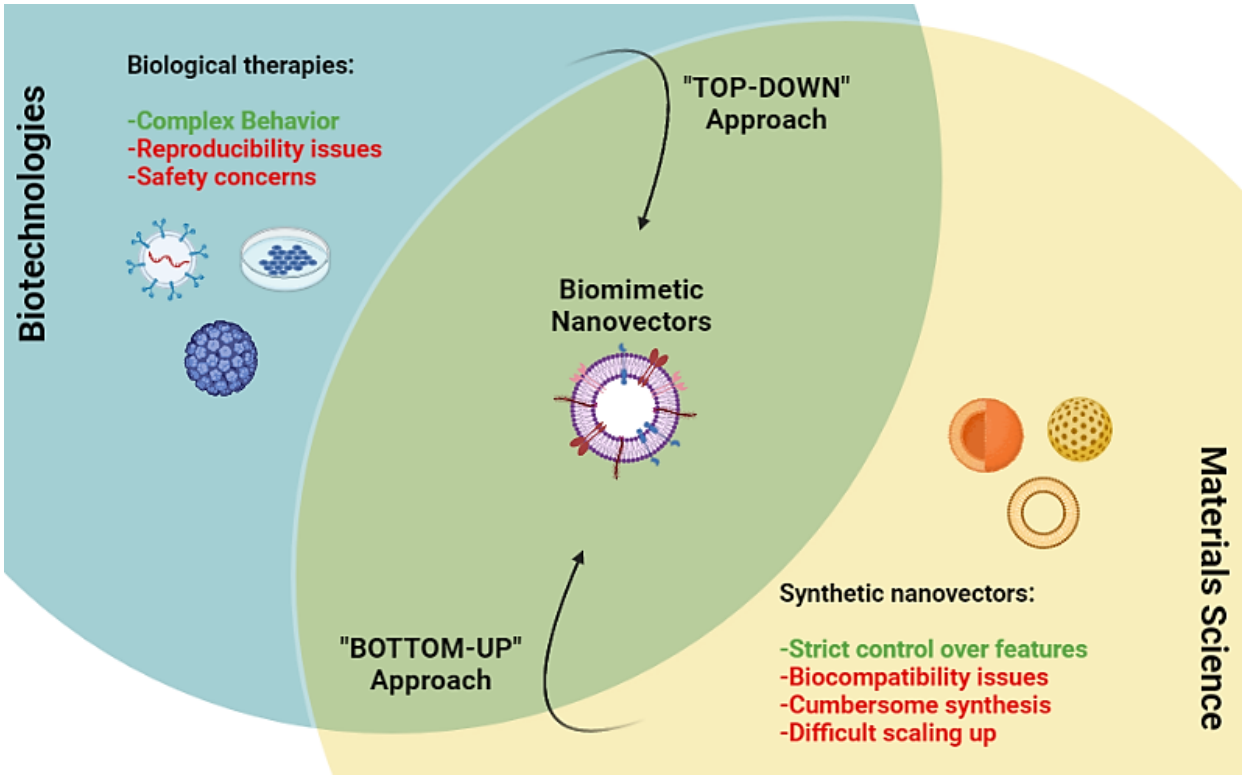


**Figure 5** Schematic representation of how biomimetic nanovectors fit at the crossroads of biological therapies and synthetic nanovectors. This image was created using Biorender.com.

In particular, among the many different approaches investigated to improve the circulation time and targeting efficiency, the use of cell membrane and their components has emerged as a fascinating opportunity (70). Specifically, the plasma membrane of cells and the markers expressed on it essentially separates the inside of cells from their environment. Since the membrane works as a boundary between intracellular space and its surroundings, has many essential functions, including mediating their biochemical interactions with soluble molecules that work as signals to modulate the cells behavior, with other cells, including their recognition as “self" by the immune system and the homing ability of circulating cells to specific tissues via adhesion molecules, and their interaction with the extracellular matrix. The plasma membrane ultimately defines the biological identity and some of the behavior of cells. Since all these proprieties are intrinsically provided by the cellular membrane through its receptors, recapitulating the membrane features on the surface of nanomaterials can also modulate their behavior, depending on the cells the membranes or membrane markers are derived from. This nature-mimicking approach has been defined as “biomimetic”. The rise of biomimetic nanomaterials attempts to address this call to reductionist innovation. Thus,

biomimetic nanovectors bridge the gap between biological therapies and synthetic nanovectors, providing at the same time simpler synthesis, improved biocompatibility, and simpler scalability (Figure 5).

The use of biomimetic nanomaterials offers the unprecedented opportunity to employ highly biocompatible formulations with a wide range of complex behaviors that can be adapted to many pathological contexts, including the ability to efficiently avoid immune clearance, deliver the cargo through specific surface receptors, bypass biological barriers, and absorb toxic molecules (71).

More specifically, three main functional protein classes can be defined, as summarized in Figure 6.

The first one is represented by membrane proteins, which are ligands for specific molecules on the surface of other cells or tissue matrix, providing biocompatible active targeting options this group of proteins includes integrins and adhesion molecules normally expressed by immune cells and platelets. It is important also to note that these targeting molecules could exert their biological function upon binding to their target, triggering intracellular responses. This makes often biomimetic nanomaterials not only biocompatible, but also bioactive on their own. This class also includes antigens that are recognized by immune cells and are normally used to formulate nanovaccines with specific purposes.

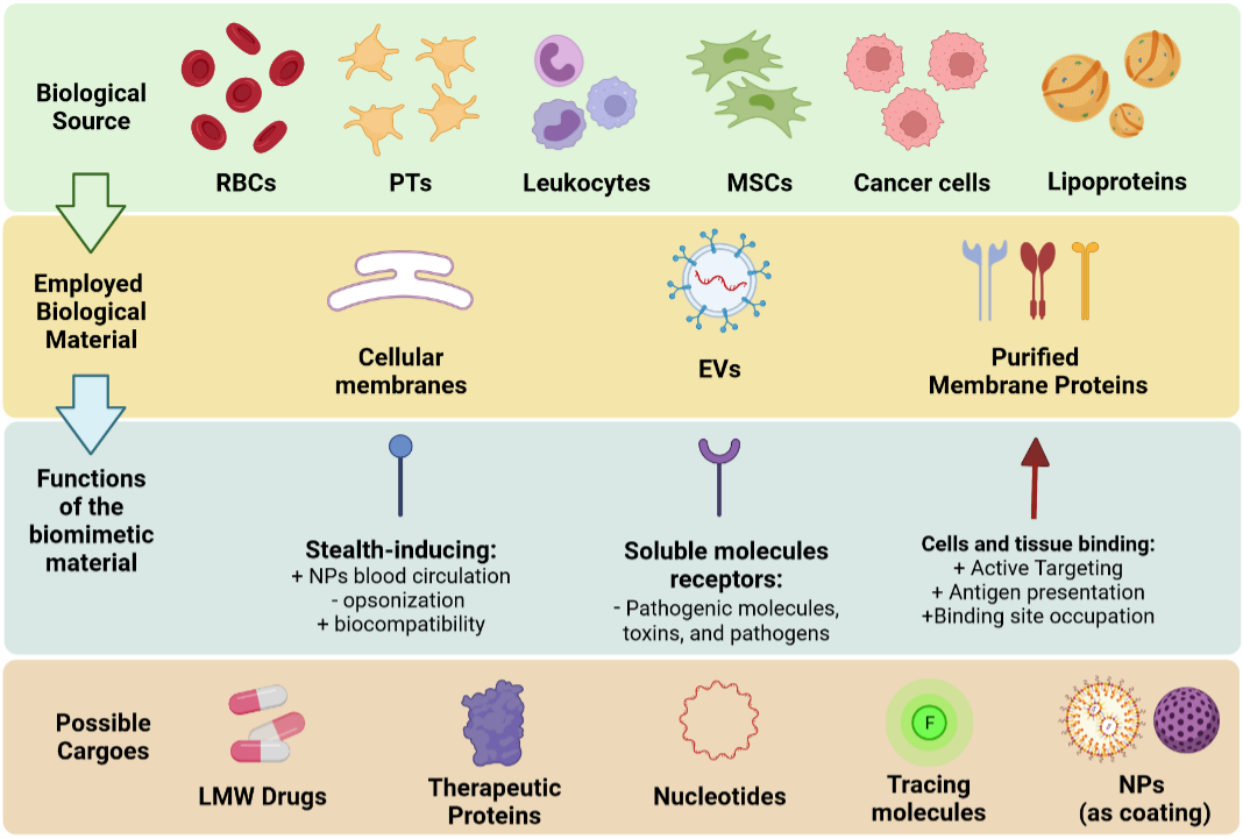

**Figure 6:** Schematic representation of the current biomimetic approach toolbox in term of source cells, biomimetic strategies, membrane proteins functions, and cargoes. This image was created with Biorender.

The second class is constituted by proteins that help the biomimetic systems to be recognized as "self-entities", normally by inhibiting complement activation, or by avoiding immune clearance by phagocytosis during circulation or residence into tissues. This class includes molecules such as CD47 that can bind to the SIRPα onto the macrophages, inhibiting phagocytosis (72).

The third group of protein instead includes proteins that are receptors for soluble molecules that can be found in circulation and in the tissues, and they can bind specifically to a wanted molecule, removing it from free circulation and preventing its interaction with the target cells, inhibiting their function and working as "decoys". This class includes all receptors for chemokines, interleukins, and growth factors (73).

It is important to note that these classes are purely functional and allow us to better rationalize the use of cellular membranes and membrane proteins, but a protein could belong to different or multiple of these classes depending on the contest of application of the system. Therefore, there is a spectrum of complexity regarding the reconstitution of the cellular membrane on the surface of biomimetics (Figure 7).

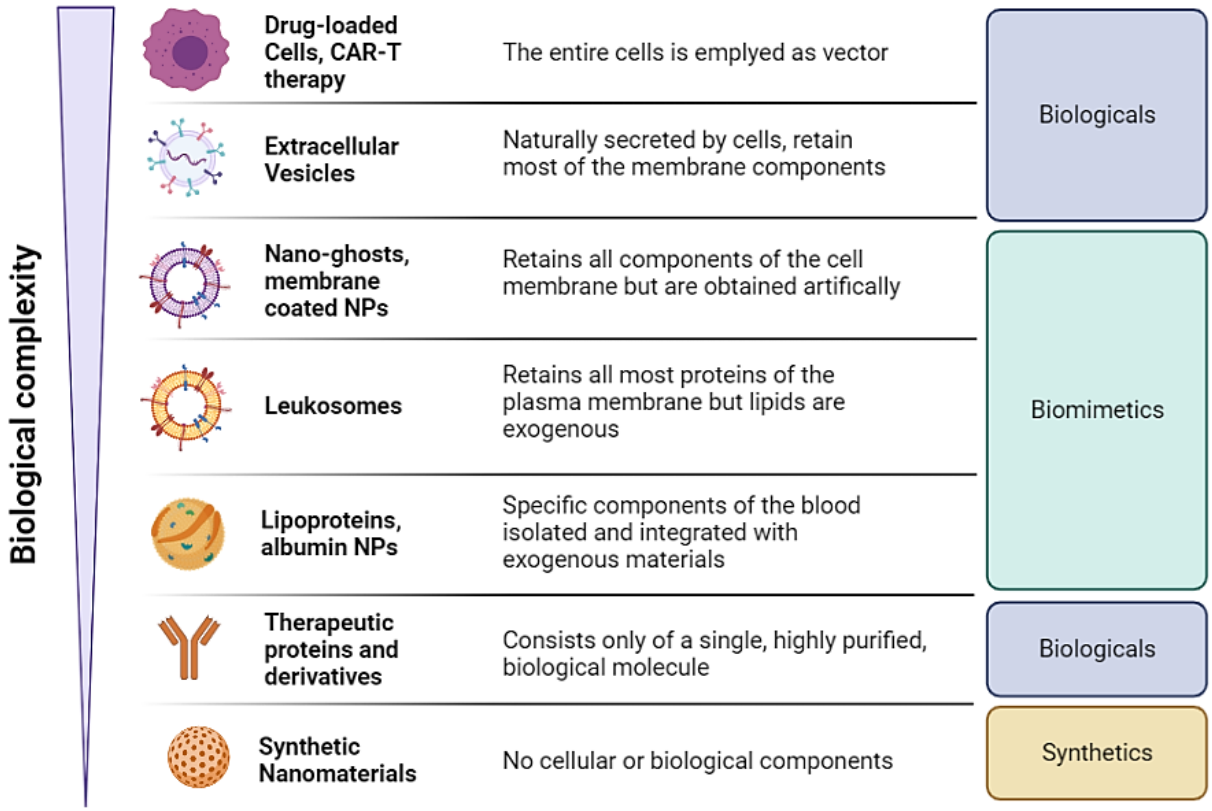


**Figure 7:** Schematic representation of biological therapies classified based on their resemblance to actual cells. This figure was produced using Biorender.

## Membrane coated and membrane-based nanomaterials

An interesting approach to formulate biomimetic nanovectors is the use of whole cellular membranes as a coating for the particles or as stand-alone nanovectors. This approach aims to completely translate on nanovectors the entirety of the plasma membrane (74). This is normally achieved by isolating the cellular membranes through the hypotonic treatment of the source cells to obtain “Cells ghosts”, and their subsequent sonication or extrusion to reduce their size and PDI to the nano range, or to coat NPs respectively.

However, this strategy presents some complications: since there is the chance of including intracellular components on the surface of nanoparticles, which could result in the immune recognition of these components as part of apoptotic bodies or other cells fragments, and thus rapidly cleared after injection (75). This also goes for lipids, since the use of the entire membranes could also lead to lipids scrambling, exposing apoptosis associated lipids on the particles surface, working as a signal of cell death (76).

Among the many cell types that have been used for particle coating, the most popular are certainly red blood cells (RBCs) (77), platelets (PTs) (78), and leukocytes (79) (Figure 6). This is not surprising if we consider that most NPs are designed to be administered IV. Therefore, cells that are normally present in the systemic circulation are in principle prime candidates for this endeavor, since they would not be considered as “out of place” by the organism immune system.

RBC membranes present on their surface specific proteins such as CD47 that can bind to receptors on the leukocytes’ membrane, inhibiting their clearance and providing the coated NPs with a much longer plasmatic half-life. Similar receptors are also present on the surface of platelets (PTs) and leukocytes. Another advantage given specifically by RBCs and PTs it their lack of nuclei and most intracellular organelles, which makes them natural “cells ghosts” which can be readily used to coat NPs. RBCs and PTs are also quite abundant and easy to isolate from the blood via simple techniques such as centrifugation, enabling the possibility of using a patient’s own cells for particle coating, further increasing the biocompatibility of nanomaterials and following the innovative path of personalized therapy.

Furthermore, PTs and leukocytes express specific adhesion molecules. These targeting moieties enable PT to efficiently accumulate onto the surface of damaged endothelium, like in the case of externally induced damages, local inflammatory states, arterial damage due to stenosis, and even towards some tumors (80). Conversely, leukocytes are naturally capable to home towards inflamed endothelia that express adhesion molecules such as PECAM-1, VECAM-1, ICAM-1 and

ICAM-2 (81). This inflammatory state is common to acute and chronic inflammatory pathologies, as well solid tumors.

Other interesting options for NPs coating are mesenchymal stem cells (MSCs) membranes, which have recently gained much attention for their ability to selectively accumulate into tumor tissues (82).

The other option could be the use of actual tumor cells. In most cases, the rationale is to formulate these cellular components with specific adjuvants to obtain novel anticancer nanovaccines to induce an antitumor immune response though the presence on the particle of tumor neoantigens (83). Another intuition aims to create “artificial EVs” to exploit the homologous targeting of tumoral EVs towards their own original tissue.

**Membrane-coated NPs**

In the present section, we provide some recent and scientifically relevant examples of membrane coated nanomaterials for anticancer treatment as well for other applications.

***RBCs coated NPs***

An example of RBC membrane application is offered by a work of Zhou et al. In this study, DOXO-loaded, pH sensitive dextran nanoparticles are coated with RBC membrane functionalized with the active targeting moiety Angiopep-2, which can bind to low density lipoproteins-related receptors expressed by the blood brain barrier (BBB) vessels and by glioblastoma cells. These particles were uptaken at a fast rate by glioblastoma U87MG cells with remarkable cytotoxic effect. Furthermore, they prolonged the DOXO half-life *in vivo* by an order of magnitude compared to uncoated particles and accumulated with high efficiency in the tumor in *in vivo* orthotropic murine glioblastoma models, crossing the BBB and prolonging animals’ survival compared to the free drug (more than 20 days more), almost eradicating the tumor mass.

A similar study by Fu et al (84) focused on the development of vincristine-loaded solid lipid nanoparticles (SLNs) coated with RBC membrane functionalized with the T7 and NGR peptides, to target the transferrin receptor (TfR) expressed by the BBB, and the tumor-expressed CD13 markers respectively, as a drug delivery vector against glioma. These particles were able to efficiently target the brain in both zebrafish and mice orthotropic models, and reduced tumor growth by over 50%, almost doubling the animals’ survival time.

Another example is provided by Han et al, who used resveratrol loaded SLNs coated with the RBC membrane and functionalized with rabies virus glycoprotein (RVG29) and triphenylphosphine cation (TPP) to enable BBB crossing and accumulation into neuronal mitochondria (85). These

particles not only efficiently reached the impervious CNS compartment but also reduced ROS stress in neurons, as well restoring the animals' brain activity in an Alzheimer's model.

RBC coating has been used for more traditional drug delivery applications, such as their use to cloak PLGA NPs loaded with the Hedgehog inhibitor cyclopamine to treat pancreatic ductal adenocarcinoma (86), which resulted in much prolonged drug half-life and slightly improved drug accumulation into the tumor, reducing tumor growth by 80% in a xenograft pancreatic adenocarcinoma murine model.

Another work by Liu et al (87) investigated ROS-sensitive arylboronic ester-based biomimetic nanocarriers loaded with the photosensitizer chlorine e6 (Ce6) and a hypoxia-activated prodrug tirapazamine to target tumor hypoxia and achieve combined photodynamic therapy (PDT) and chemotherapy. The RBCs coating not only enabled the colloidal stabilization of NPs, but also increased the uptake by tumor cells, especially when functionalized with the RGD peptide, which binds αV integrins and neuropilin-1 receptors overexpressed in breast cancer. These nanovectors very efficiently targeted tumor tissues (with comparable levels to the liver) in breast tumor bearing mice and upon near infrared light (NIR) irradiation reduced tumor growth and weight by over 90%, with no detectable systemic or organ toxicity.

RBCs coated PLGA-NPs were used also to deliver DOXO to lymphoma cells, using the cellular coating as an innovative stealth inducing material to improve the drug half-life and tumor accumulation (88). This formulation demonstrated improved efficacy in an ectopic murine model of lymphoma, inhibiting tumor growth of over 70% and improving animals' survival compared to free DOXO, which instead did not improve survival compared to the untreated subjects, perhaps due to serious side effects.

However, the mere chemical composition of the particles is not the only factor to consider. For example, a recent work by Li et al (89) demonstrated how smaller, spherical RBC membrane-coated PLGA particles (80nm) had a longer half-life and reduced liver accumulation compared to bigger particles (100 and 200nm particles). This could be due to reduced liver filtration via sinusoids capillaries. Thus, smaller particles appear to be more suitable to enable long circulation time.

Another study applied Hyaluronidase sensitive, PTX and PheoA-loaded particles coated with RBCs membranes for the treatment of breast cancer, which also presented don their surface a PD-L1 binding peptide as synergistic molecules for immunotherapy (90). These particles confirmed the size trends exposed before, with bigger particles being cleared faster *in vivo*. Furthermore, these particles accumulated into the tumor tissue of breast cancer-bearing mice, inducing immunogenic cell death,

and the accumulation of CD4+ and CD8+ T-cells, ultimately hindering tumor growth, with no visible systemic toxicity in the animals. This study is an example of how biomimetic strategies could complement even combinatorial, complex system such as this.

Another iteration of this approach is presented by Zhang et al (91), who formulated RBC membrane-coated PLGA NPs loaded with gambogic acid and functionalized with anti-EGFR iRGD peptide for CRC treatment. These particles showed remarkable colloidal stability and very slow drug release, suitable for long circulation, and at the same time efficient tumor cells targeting *in vitro* and *in vivo*, completely abolishing CRC tumor growth and improving survival by 60%.

RBC membranes can be used also to improve the stability and biocompatibility of inorganic nanoparticles for diagnostic purposes. In a study from Meng et al (92), SPIONs were coated with RBC membranes and then functionalized with antibodies to bind against circulating prostate cancer cells. In this case, RBC membranes also provide the colloidal stability to SPIONs, reducing the absorption of plasma proteins onto their surface that could hinder their binding to the cancer antigens. These particles isolated successfully tumor cells from prostate cancer patients' samples, with an efficiency over 95%, compared to the 60% of the bare particles, demonstrating the synergistic activity of RBCs coating and antibody labelling.

However, the cell membrane coating of particles presents some technical challenges. Specifically, the process of membrane coating normally occurs randomly, and does not follow necessarily, the important in-out orientation of the cellular membrane. This could result in the wrong orientation of proteins on the surface of the particles, leading to the outer exposure of otherwise intracellular protein domain, which are not functional towards the NPs environment but could also result immunogenic. This concern was addressed in a recent work by Xie et al (93), in which cationic liposomes were functionalized with a peptide ligand that bound the intracellular domain of Band 3, an important protein present onto RBCs. By coating these liposomes with RBC membranes, the authors ensured the correct orientation of band 3 protein. This system resulted in RBC-coated liposomes with good stability and PEG-like levels of immune escape. Furthermore, the particles could efficiently target the infected tissues of *Candida Albicans* bearing mice, and even efficiently absorbed the fungal toxins, greatly increasing animal survival.

Liang Fang Zhang was among the first to use RBCs coating as a nanosponge against bacterial infections (94). A remarkable example of this concept is offered in a recent work (95), in which PLGA NPs were coated with RBC membranes, and greatly reduced the hemolytic abilities of *Staphylococcus Aureus* toxins bot *in vitro* and *in vivo*, even resulting in an increase of survival in

animal models, reducing both the toxins damage to lungs and systemic inflammation markers. Importantly this approach resulted very useful even in treating drug resistant bacteria, underlining its utility as synergistic treatment for other pathologies.

This system was improved on by using a liquid oil core instead of PLGA NPs as core for RBC membranes. The use of a liquid core makes the nanosponges able to first bind strongly to hydrophobic toxins via their receptors on the RBCs membranes, which then get partitioned into the core itself. This results in a sink condition in which the core works as an actual functional compartment in the nanoparticle formulation. The value of this intuition was demonstrated by Chen et al (96), who used this platform to reduce the toxicity of different acetyl cholinesterase toxins (i.e., paraoxon, diisopropyl fluorophosphates, and dichlorvos). These particles demonstrated good binding activity and removal of the toxins *in vitro*, which translated in efficient systemic detoxification *in vivo*, rescuing by 40% acetyl cholinesterase activity and greatly improving animal survival. This study further builds on the past success of RBCs coating for detoxification, integrating the decoy activity with an active absorptive lipophilic core.

Luk et al (97) have also used RBCs coated NPs as a decoy for autoimmune hemolysis, a pathology in which the immune system produces antibodies against its own RBCs, causing complement and immune mediate hemolysis. In this case, RBC membrane-coated PLGA NPs efficiently bound to anti-RBC sensitized B cells *in vitro*, and efficiently targeted this cell population in a murine *in vivo* model of autoimmune hemolysis. However, this study did not investigate the therapeutic efficacy of this treatment in reducing overall hemolysis.

The same principle has been applied in a wide variety of infections models, including ocular infection (98), different bacteria secreting pore forming toxins (99), sepsis (100), and in autoimmune diseases and using a variety of different cellular coatings (101).

RBC membrane coating has also been used by Lee et al (102) to deliver the radioisotope Zr-89 for tumor imaging. This formulation demonstrated longer half-life and good tumor targeting in CRC cells bearing mice, enabling efficient positron emission (PET) imaging.

RBCs coating has also been used for regenerative medicine purposes. Specifically, Liang et al (103) encapsulated growth factors derived from MSC-conditioned medium into PLGA particles and coated with RBC membranes to induce liver regeneration after acute hepatic failure. This platform demonstrated good stability, slow factors release, and the ability to promote hepatocytes activity *in vitro*. This translated in a marked increase in liver function markers (i.e., ALT and AST) and reduction of inflammatory markers (IL-6, IL-1beta and TNF-α) in murine carbon chloride induced

hepatic failure, with much higher animal survival.

A similar study by the same group used RBCs-coated PLGA NPs to prevent the hemolytic activity of group B *Staphylococcus* toxins (104). This system not only demonstrated the ability to rescue hemolysis from infection, but also improved macrophage survival, improved bacteria killing and decreased the secretion of IL-1B. All these mechanisms of action are highly synergistic and provide evidence of the many functions that biomimetic nanosystems can recapitulate, overcoming the somewhat limited scope of traditional and antibody-based therapy, which instead focus on single molecules and pathways.

***PTs coated NPs***

Wang et al (105) offer an interesting example of the use of PT membranes as NPs coating. In this study, bufalin-loaded PLGA NPs formulated via nanoprecipitation were coated with PT membranes derived from blood to provide them with long circulation and tumor homing abilities through the P-selectin surface protein interaction with hepatocarcinoma cells expressing CD44. The authors demonstrated how the coated NPs alone were highly biocompatible and colloidally stable in PBS and cell culture medium. Their uptake was mediated by P-selectin since non-coated particles were not uptaken and anti-selectin treatment reduced their uptake by blocking the targeted receptors. When used *in vivo*, these particles did not show any toxic effect while accumulating efficiently in the tumor tissue in an ectopic murine hepatocarcinoma model and delivering the antitumor molecules bufalin, reducing tumor volume and weight by 80%.

Another study by Liu et al (106) focused on the use of PT membranes fused with pH dependent phospholipids to create “platesomes” to deliver DOXO to colorectal and breast cancer. These vesicles were prepared by hydration and the PT membrane were fused with them via extrusion. The particles maintained both their size (around 150nm), the protein profile of the membranes (CD41 and CD62) and showed pH dependent DOXO release in acidic conditions (pH=5.5). Furthermore, these NPs were efficiently endocytosed by different tumor cells lines and demonstrated increased cytotoxicity compared to free DOXO and non-PT coated liposomes. This improvement in targeting and therapeutic efficacy was also observed *in vivo* in ectopic murine models of CRC and breast cancer, reducing tumor by 80% and 50% respectively with no systemic nor organ toxicity.

A recent study by Zuo et al (107) encapsulated metformin and $W_{18}O_{49}$, to reduce tumor hypoxia and enable PDT therapy, respectively. These particles were stable and successfully targeted the tumor in Raji lymphoma cells bearing mice, both reducing its oxygen consumption and causing tumor death upon irradiation, without affecting mayor organs or influencing animals’ health.

In study from Li et al (108), magnetite NPs and L-arginine were loaded into PTs membranes to achieve efficient targeting of thrombi after stroke, with the aim to induce NO production by L-arginine, causing blood vessels dilation and reducing platelets aggregation on the thrombi themselves. Magnetite NPs provide the possibility to induce NPs accumulation into the affected site by applying an external magnetic field. These particles efficiently accumulated into central nervous system (CNS) blood vessels *in vivo* in murine stroke models, reducing by over 60% platelets local aggregation and partially restoring blood flow into the affected tissue.

The use of PTs membrane for endothelium target have been employed as well by Wang et al (109), who created a poly-amino-amide (PAMAM) dendrimer-based nanoclusters loaded with the endothelia protective agent JQ1 and coated with PTs membranes for the targeting and treatment of arterial stenosis, as an alternative to the drug loaded highly invasive stents. This innovative approach, upon IV injection, efficiently targeted only the affected sites in a similar way as the actual PTs, remodulate gene expression in stenotic arteries of murine models, increasing the vessels lumen and decreasing the hyperplasia of the endothelia.

PTs have also been used, similarly to RBCs, as decoy mechanism to protect from toxic molecules. One example of this intuition is offered by Kim et al (110), who used PT-coated PLGA NPs as a dampening agent to protect against the toxins secreted by *Staphylococcus Aureus*. These particles not only prevented toxins from damaging actual circulating PTs, but also prevented toxic damage against macrophages and neutrophils. Remarkably, these NPs demonstrated the ability to boost PTs activation, as well as macrophages and neutrophils oxidative stress, reinforcing their bactericidal activity both *in vitro* and *in vivo* in a model of systemic *Staphylococcus Aureus* infection, resulting in a lower expression of pro-inflammatory cytokines, but also lower bacterial count and greatly improved survival. This study is quite interesting because it evidences not only the efficacy of PTs as decoy, but also their potential ability to modulate the immune system as intrinsically active nanomaterials.

A similar type of particles (111), loaded with the TLR8 activator resiquimod successfully delivered their cargo to different CRC and breast cancer cell lines *in vitro,* and elicited immune cells activation by increasing the expression of inflammatory markers such as CD80, CD86, CD45, CD11b and CD11c. *In vivo,* these particles accumulated into the tumor tissue of tumor bearing mice and demonstrated prolonged retention when injected intratumorally, promoting a significant increase in MHC-II expression in distal lymph nodes, eradicating tumor growth in a murine CRC model and hindering by almost 90% tumor volume in a breast cancer mouse model while preventing the formation of metastatic noduli. Importantly, all this remarkable antitumor activity was performed in

avoidance of the serious side effects normally associated with resiquimod.

Another decoy-based use of PT coating is their use to remove anti-platelets antibodies in immune thrombocytopenia. In this pathology, the body produces antibodies against its own PTs, resulting in their fast clearance and coagulation dysfunction. A recent work by Wei et al (112) demonstrated how this coating onto PLGA particles very efficiently bonded anti-platelets antibodies *in vitro*. This resulted in remarkable detoxifying effects in a murine model of immune thrombocytopenia, in which the anti-PTs immunoglobulins titer was much decreased, rescuing the amount of platelets and the bleeding time to normal values.

***Leukocytes coated NPs***

Another important option for the generation of biomimetic nanovectors is offered by leukocytes. This broad family of cells have both inflammation tropism and are intrinsically well tolerated when in circulation. Thus, engrafting their membrane proteins onto nanovesicles thus enables to complement the already successful liposomes with these functions.

Cell membrane-coated NPs can also work as a molecular nano-sponge by binding to specific pathology-related molecules or viruses. An example of this it given by the study of Wei et al (113), in which PLGA nanoparticles were coated with CD4 T-cells against HIV infection. These particles demonstrated to retain all the major membrane markers of T-cells including CD4, CCR5 and CXCR4, all receptors involved in HIV virus internalization. T-cells coated particles were able to bind HIV receptors *in vitro* very efficiently, reducing by over 80% the T-cells death caused by HIV virus itself. This remarkable proof-of-concept demonstrates the versatility of biomimetic membrane coated NPs for the treatment of a wide variety of pathologies.

The use of nanosponges as decoys against infective agents was also demonstrated on viruses, like in a recent work by Zhang et al (114), who formulated PLGA NPs coated with either lung epithelial cells or macrophages plasma membranes as binding agents against the SARS-CoV-2 virus. Both these cell types present on their surface the receptors that the virus needs to penetrate within its target cells and infect them. These particles demonstrated remarkable biocompatibility and very high affinity in binding viral particles *in vitro*, consolidating this decoy strategy as highly versatile in many pathological contexts.

NPs can also be used for the delivery of enzymes to treat metabolic diseases, re-establishing the biochemical homeostasis of specific substances. One such example is gout, which is caused by an excess of circulating uric acid, resulting in its accumulation in the extremities as small crystals. The amount of circulating uric acid can be reduced by the administration of the uricase enzyme to convert

uric acid in the more soluble allantoin. This protein however is quickly removed from systemic circulation. To increase the half-life of the enzyme, Zhuang et al (115) encapsulated it into metal organic framework NPs coated with either RBC membranes or macrophage membranes. Both coated formulations demonstrated good stability and biocompatibility, maintaining the enzyme conversion and improving its half-life. However, macrophage membranes also preserved several cytokines receptors (i.e., IL-1R, TNF-α receptor, and IL-6R), being capable of binding these inflammatory molecules which are increased in gout. Thus, macrophage particles demonstrated *in vivo* improved therapeutic efficacy thanks to the dual activity of the enzyme and the molecular sponge action of the particles themselves, providing evidence of the potential synergy the biomimetic strategy can provide to other therapy.

***Tumor cells coated NPs***

Tumor cell coated nanoparticles can have multiple functions such as antigen presentation and interfering with the tumor reprogramming of parenchymal cells. A study by Jin et al (116) demonstrated how U87 tumor cells membrane coated PLGA NPs had the dual action of reducing tumor cells interactions with fibroblasts, reducing their migration and at the same time provide tumor neoantigens. These activities were also present in *in vivo* models of metastatic breast cancer, in which these particles circulated for longer time than bare PLGA NPs, reduced the number and size of metastases by over 90%, and were also able to accumulate in lymph nodes, presenting their antigen to immune cells and thus stimulating CD4 and CD8 T-cells.

Tumor cell-coated NPs as tumor vaccines can also be modulated using genetic engineering (117). A recent work by Jiang et al (118)focused on the use of B16 melanoma cells as a starting material to create membrane coated PLGA NPs for antigen presentation with the aim to induce an antitumor immune response. However, the source tumor cells were transfected to induce the expression of the co-stimulatory receptor CD80 as an adjuvant to improve antigen presentation. These particles demonstrated good CD80 loading, remarkable stability, and efficiently induced the expression of several inflammatory markers by splenocytes *in vitro*. After IV injection, these particles both prevented tumor growth when used before tumor cells engraftment and to retard tumor growth in already tumor baring mice, confirming their accumulation in lymph nodes where they elicited T-cells stimulation and ultimately resulted in improved animals' survival.

Another approach for the formulation of antitumor nanovaccines have been established by Kroll et al (119) who loaded PLGA NPs with the adjuvant CpG oligodeoxynucleotide 1826 (CpG) to promote APC maturation and coated them with melanoma cells membrane to present multiple antigens, aiming at eliciting an antitumor immune multiantigen-based response. Importantly, the

multiantigen immunity can increase the change of the immune system to efficiently attack the entirety of a potentially heterogeneous tumor cells population, reducing the risk of tumor immune escape. This platform induced monocytes maturation more efficiently than either CpG or tumor cell membranes alone. Furthermore, the nanovaccine elicited an antitumor immune response both as prophylactic treatment and as treatment post-challenge in a melanoma murine model, working in synergy with immune checkpoint inhibitors.

Tumor cells membranes coating have also been used to functionalize Boron Nitride Nanospheres (BN) laded with DOXO. Specifically, in a study by Feng et al (120), HeLa cells membrane were able to greatly BN NPs, was able to improve drug loading and regulate drug release and demonstrated HeLa-selective uptake and subsequent cytotoxicity. When injected IV into HeLa tumor bearing mice, the particles demonstrated double targeting efficiency to the tumor with a 30% to 50%b reduction in liver and spleen accumulation, resulting in 80% tumor mass reduction.

A similar approach was also tested by Sun et al, who coated DOXO and ICG-loaded thermo-sensitive liposomes loaded with HepG2 hepatocellular carcinoma (HCC) cells to achieve joint chemotherapy and photothermal therapy. These NPs demonstrated very efficient temperature increase and drug release only upon NIR light irradiation, resulting in selective toxicity on UCC cells when activated by NIR light. Furthermore, this nanovector accumulated into the tumor tissue of HCC murine models and upon irradiation resulted in almost complete tumor ablation with no evident systemic side effects.

***Multiple membranes coated NPs***

The use of cellular membrane coating technology offers the possibility to combine membranes from different cells onto a single nanovector. This results in nanoparticles with the advantages of both the cell type membranes they are coated with. This hybrid-based strategy offers another level of complexity to biomimetic nanoparticles.

A proof of concept of this intuition is offered by Gong et al (121). In this work, DOXO loaded PLGA particles were coated with a mix of RAW264.7 murine macrophages and breast cancer 4T1 cells. The fusion of these membranes onto the surface of single particles was confirmed by Fluorescence Resonance Energy Transfer (FRET) analysis, demonstrating the close proximity of the two membranes via lipophilic FRET dyes within the membranes prior to fusion. Remarkably, the hybrid system demonstrated improved tumor cells targeting *in vitro* compared to either the macrophage or tumor cells coated NPs as well as improved tumor cell killing capacities. Furthermore, this new system demonstrated improved tumor accumulation (30% more than its respective control),

50% less liver accumulation, and almost 90% reduction of metastatic foci in murine models of metastatic breast cancer, more than doubling animals' survival.

Another example of this interesting approach is offered by Dehaini et al, (122) who coated PLGA nanoparticles with a mix of RBC and PT membranes. This system retained the proprieties of RBC membranes (including acetylcholinesterase activity) and PT tropism towards cancer cells and stenotic arteries while maintaining long circulation. This strategy offers the possibility to create NPs with complex behavior for therapeutic applications by the modular assembly of different cellular membranes.

Another exciting frontier in nanotechnology and nanomedicine is represented by the use of nanorobots (123). These constructs can perform relatively complex behavior, such as external or fuel-induced movement, making them suitable for precision medicine. However, nanorobots are normally composed of inorganic or non-physiologic material, a feature that can severely reduce their biocompatibility. E recent work from Esteban-Fernández de Ávila et al (124) aimed to overcome this limitation by coating gold nanowires with PT and RBC membranes to neutralize Multidrug Resistant *Staphylococcus Aureus* (MRSA) and its pore forming toxins. These metal NPs have the peculiar feature of propelling themselves in solution when exposed to US, making them suitable as mobile nanosponges to capture pathogens very quickly. Indeed, the coated nanorobots demonstrated improved movement *in vitro* in whole blood compared to bare nanowires, and at the same time removed very efficiently from the blood both pore forming toxins and MRSA. Although being a solely in vitro study, this proof of concept opens the way to many more application of biomimetic coating to a variety of nanorobots.

***NPs coated with other membranes***

Another interesting approach enabled by the biomimetic strategy is the use of pathogen-coated nanoparticles that can prevent the pathogen adhesion to the target tissue, hindering its successful colonization (125). This possibility was demonstrated by Zhang et al (126), who formulated *Helicobacter Pylori* membrane-coated PLGA NPs. These particles demonstrated the ability to adhere to the stomach epithelium and when the tissue was pretreated in an *ex vivo* model, they inhibited the actual bacteria adhesion in a dose and time dependent pattern.

The same group tested a complementary approach by coating PLGA NPs with the membrane of gastric epithelial cells (127). These NPs maintained the membrane markers of their source cells and efficiently adhered to *H. Pylori* colonies, and when loaded with the antibiotic clarithromycin in the polymeric core, demonstrated a steady release and a synergistic effect with improved antibacterial

efficacy *in vitro* and *in vivo*.

Another type of cells that are constantly exposed to the systemic circulation but are not circulating *per se* are blood vessels endothelial cells (ECs). Specifically, ECs have the intrinsic ability to adhere among themselves and been exposed to circulating immune cells without eliciting immune reactions. Thus, using their membranes for particle coating could result in highly biocompatible nanosystems which also have the ability to adhere to damaged endothelia. This concept was successfully applied by Gao et al (128), who coated manganese-albumin particles for the treatment of atherosclerotic plaques. Manganese ($Mn^{+}$) can induce the activation of integrin receptors on the plaques ECs, reducing in the reduced expression of pro-inflammatory genes. These particles demonstrated controlled $Mn^{+}$ release and reduced blood vessels lesion in an Apolipoproteins-knockout murine atherosclerosis model.

## Cell membrane and membrane derived nanovesicles

### *Nanoghosts*

Among the different biomimetic nanoplatforms, there is also the possibility to use the membranes to generate nanovesicles composed entirely of cellular membranes closed onto themselves. This strategy was followed by Oieni et al (129), who generated cell-derived nanoghosts (NGs) from many different cell lines. This technology employs a series of hypotonic treatment of cells, sequential centrifugation, and sonication to remove most of the cellular organelles and isolate the membranes. This technique is very fast and easy to perform, and can be applicated onto many different cells, yielding high amount of nano-sized nanovesicles. Similarly, to EVs, it is possible to perform drug loading or labelling of nanoghosts either by treating the source cells with the desired drugs, from which the cargo is maintained into NGs, or by post-loading, loading or labeling NGs during or after their production. NGs were thus successfully loaded with fluorescent labels, radioisotopes, and both small-molecules drugs as well as DNA (129; 130).

One example was provided by a recent study in which NGs were labelled using $C^{14}$-linoleic acid by incubating the source MSCs with this marker. NGs demonstrated good label encapsulation, resulted very biocompatible, and it was possible to efficiently trace them both *in vitro* and *in vivo* after IV injection in healthy nude and immune-competent mice.

NGs were also successfully applied to MSC transfection with an anti-miRNA-221 antisense oligonucleotide by post-loading via electroporation. In this work, NGs were efficiently endocytosed by MSCs via homologous uptake, accumulated in the endosomes and could release the oligonucleotide efficiently from the endo-lysosomal compartment, avoiding degradation and

comparable miRNA-221 knock-down efficiency to more cytotoxic cationic liposomes (131). Furthermore, these NGs were able to deliver their cargo to MSCs in a murine e osteochondral defect model.

A similar study from Kaneti et al (132) demonstrated that MSC-derived NGs can also be successfully loaded with plasmids. Specifically, the authors encapsulated a plasmid encoding for hemopexin-like domain, a protein with onco-suppressive function on both tumor cells and tumor vasculature. This nanovector induced tumor cells death and inhibited endothelial cells proliferation and migration, successfully increasing the expression of the transfected protein in the target cells. This translated to a 70% reduction in tumor growth *in vivo* in subcutaneous models of prostate cancer and significantly reduced the amount of tumor foci in a murine model of lung cancer. This system provided reliable results in very different pathological settings, demonstrating its versatility and high therapeutic potential.

An interesting frontier of tumor vaccines production is the use of carbohydrates-based antigens to elicit an antitumor response (133; 134). A recent work by Reuven et al fabricated RBC-derived NGs functionalized with N-glycolylneuraminic acid (Neu5Gc) as a highly biocompatible device to elicit the immune response against Neu5Gc positive tumors. This treatment was able to elicit a strong and durable anti-Neu5Gc humoral immune response, resulting in around 50% of tumor growth reduction in a murine model of CRC. Glycobiology represents a new and exciting frontier that could yield high impact results in tumor treatment, building on the increasing wealth of knowledge on the glycosylation of proteins.

NGs have also been formulated by enriching PT membranes doped with cholesterol to facilitate their re-assembly and then remotely loaded with antitumor and antibacterial small molecule drugs (135). This was proven in a recent work by Ying et al (136). Specifically, PT-derived nanovesicles were loaded with DOXO as an antitumor drug delivery system, and with Vancomycin as an antibacterial nanovector against MRSA. This platform demonstrated efficient drug loading in both cases and efficient tumor targeting in an ectopic murine model of breast cancer with improved tumor burden reduction compared to free DOXO. Conversely, PT NGs loaded with Vancomycin reduced significantly the amount of circulating MRSA in a murine model of systemic infection. This work demonstrates the high versatility of NGs and biomimetic systems in general in widely different pathological contexts.

***Membrane protein based nanovesicles***

Another step in the biomimetic strategy is focused on the isolation of membrane proteins and their engraftment on artificial phospholipids bilayers. This strategy allows the removal of intracellular proteins and yields high amounts of materials from virtually any cells. However, in this case the lipidic component of the membrane is lost, and it is not very well understood if the extraction of membrane proteins can isolate all of them with the same efficiency without losing some of them during the process, depending on the employed protocol.

In recent years, this intuition was successfully explored by Tasciotti, Molinaro, and Taraballi, creating the so called “Leukosomes” (Leuko) (137; 138). Leukos are phospholipid and cholesterol-based nanovesicles functionalized with monocytes-derived membrane proteins (Figure 8). This platform has been loaded with many different drugs, including DOXO, Ponatinib and paclitaxel among other molecules, and has been applied to several pathologies as osteosarcoma (139), breast cancer, sepsis (140), and inflammatory bowel disease (IBD) (141), demonstrating their remarkable versatility as drug delivery systems and targeting both acute inflammations caused by infections and tissue damage, but also the intrinsic inflammation that characterized the stroma of many tumors (142). In all these cases, Leukos demonstrated to be highly biocompatible and improved efficacy compared to the respective drug. Leuko have been produced using both the traditional thin layer hydration process and employing the faster, scalable, microfluidics based Nanoassemblr$^{TM}$ platform. In both cases, the successful engraftment of leukocytes membrane proteins on the particles surfaces was verified by western blot and flow cytometry (143). This latter technique also confirmed the correct orientation of membrane proteins onto the particle surface, which is a feature essential to assure that their domains responsible for the interaction with other cells and the surrounding environment are correctly exposed to the outside of the nanovesicles.

However, Leukos also demonstrated their therapeutic potential as stand-alone medical devices. Indeed, drug-free leukosomes were used to treat sepsis (140), a systemic inflammatory condition caused by circulating bacteria or their fragments. Leukosomes interacted with circulating monocytes in murine sepsis models, by modulating the expression of key genes in macrophages such as IL-1β, IL-6, IL-10, TNF-α and TGF-β towards an anti-inflammatory profile. Interestingly, this effect was produced only on inflamed macrophages but not onto inflamed ECs. This immune modulation resulted in an overall decreased sepsis score in mice and increased survival. However, the specific mechanism of action of Leukosomes in this context was not investigated.

A similar drug free application that hints at Leuko potential is their application in IBD. In this case, IV -administered Leukos efficiently accumulated into the intestinal tissue of via endothelial adhesion and exerted intrinsic anti-inflammatory activity in murine Dextran Sodium Sulphate (DSS) models of

IBD (141). Specifically, Leukos reduced the amount of immune cells and cytokines in the tissue, resulting in improved pathological score and significant reduction of intestinal lesions. This study also investigated the behavior of specialized Leukos obtained from macrophages stimulated with retinoic acid to induce the overexpression of integrins, resulting specialized Leuko (SLKs) in improved tissue targeting and therapeutic effect compared to traditional liposomes. The mechanisms of action of Leuko and SLKs could derive from their ability to occupy the adhesion molecules expressed by inflamed endothelial cells, preventing further accumulation of immune cells in the intestine and allowing for its recovery. It is also possible that Leukos can act as a molecular sponge, absorbing proinflammatory cytokines via their surface receptors. Their mechanism of action could also be a combination of the ones mentioned above or depend on some other interactions between L eukos and immune cells. Nevertheless, this study also provides the possibility to modulate the surface proteins profile of cells used as starting material for Leuko production, adding a new layer of complexity to biomimetic nanoparticles production. By reprogramming cells, the action of biomimetic nanoparticles can be improved and modulated to optimize them.

The use of the membrane proteins to enable the biomimetic strategy could also help to overcome the limitations of E production. Specifically, Vasquez-Rios et al (144) formulated EVs-like nanovesicles using the synthetic lipids with the same composition of EVs and engrafted on their surface the adhesion protein ITGα6β to enable their targeting to the lungs for lung cancer treatment. Furthermore, it was possible to efficiently load these nanovesicles with miRNA145 which was efficiently transfected to lung cancer cells *in vitro*. Remarkably, with regards to their biodistribution, the new vesicles accumulated less in the kidneys and liver compared to the actual EVs. This study opens the way to many new possibilities to create EVs live vesicles with more controllable feature, higher yield, and optimized composition, and with fast, scalable production.

Another study (145) studied the drug delivery potential of PT-derived NPs by functionalizing liposomes with membrane proteins derived from PTs and loaded with the IR dye RR-1048 that enables both tumor imaging and photo thermal therapy upon IR-II irradiation. The use of far IR light allows better tissue penetration and thus better tumor targeting. These particles showed remarkable efficacy in efficiently visualizing tumor cells and inhibiting tumor growth in murine models of pancreatic cancer, breast cancer and glioma murine models.

Another fascinating approach to engraft membrane proteins onto NPs has been offered by Lu et al (146), who produced phospholipid coated chitosan nanoparticles for VEGF siRNA delivery against cancer. In this study, the coated particles were functionalized with the EV-derived Cx43 protein using a cell-free synthesis strategy in which the particles are incubated in presence of the

Cx43 plasmid, the RNA polymerases and ribosomes to allow *in situ* synthesis of membrane proteins that become engrafted within the liposome bilayer. This approach gives the remarkable opportunity to create EV-like particles with well-defined proteins composition, with very defined features and higher yield than EVs. These particles demonstrated good transfection efficacy *in vitro* and cytotoxic effect upon VEGF siRNA delivery in tumor cells.

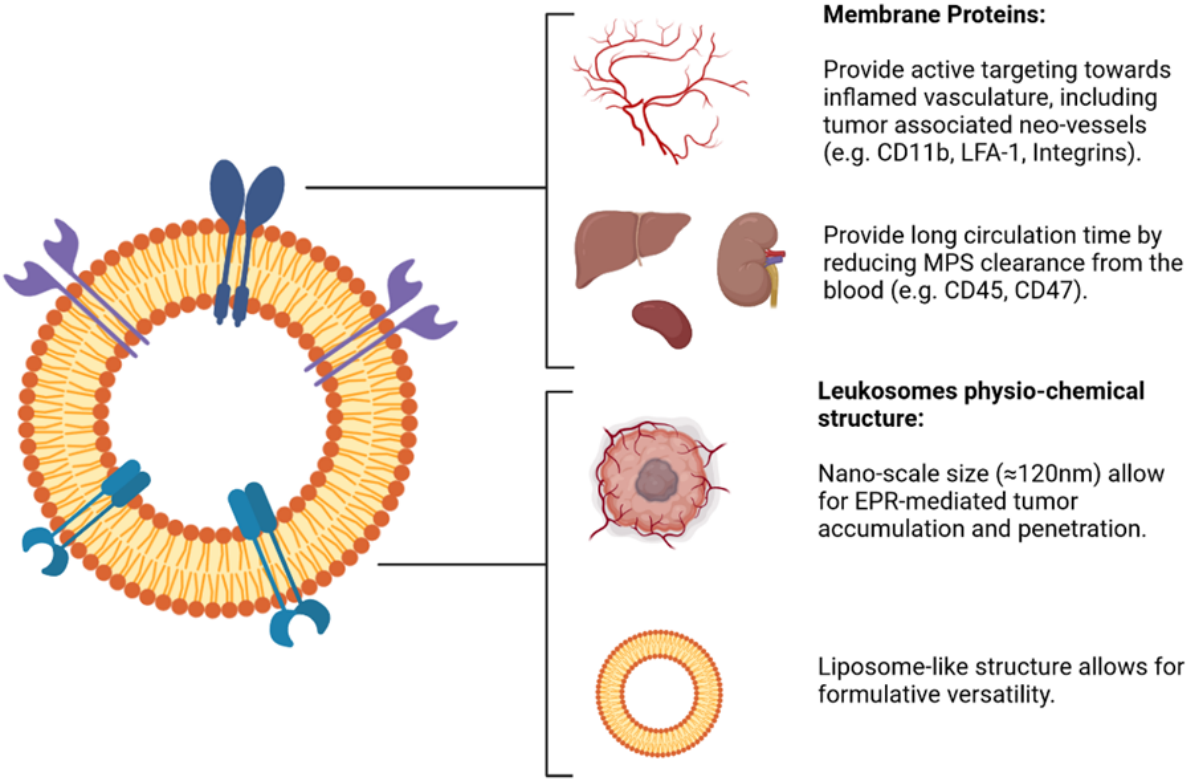


**Figure 8** Schematic representation of the structure and functions of Leuko. Image adapted from (147)

Another interesting example of cell components used as biomimetic coating is offered by Das et al, (148), who formulated PLGA NPs coated with the membrane component Ganglioside M1 (GM1). GM1 is the target surface receptor expressed by intestinal epithelia for the Cholera Toxin. By coating NPs with these molecules, it would be possible to create a decoy system to prevent Cholera-mediated intestinal damage. This concept was thus tested *in vitro* and *ex vivo*, since GM1 NPs efficiently bound cholera toxins both in solution and when disperse in the intestinal mucus and reduced intestinal epithelial cells damage *in vitro*. Furthermore, when administered orally, GM1 NPs almost completely recued the intestinal status of Cholera-infected mice, reducing the amount of secreted intestinal fluids.

**Non-cell based biomimetic nanovectors**

Another fascinating biomimetic strategy is to use non-cellular components of the blood, which are naturally able to circulate for long time and could easily shuttle nanomaterials through

systemic circulation, in some cases also providing intrinsic targeting activity to receptors expressed by the endothelium.

Albumins are highly biocompatible proteins which can circulate in the blood for long time and can also bind a variety of receptors, working both as carriers and targeting moieties (149). A clinically approved example of this concept is offered by the albumin-bound paclitaxel NPs (Abraxane™) used against tumors (150). Following this intuition, Liu et al (151) synthesized methotrexate-loaded albumin particles for the treatment of rheumatoid arthritis. These nanovectors were efficiently loaded with the drug and the protein retained its conformation. Furthermore, albumin -methotrexate particles efficiently bound the secreted protein acidic, and cysteine rich (SPARC) proteins overexpressed in the rheumatoid arthritis affected tissues synovial fluid, and induced Lymphocytes apoptosis, IL-6, IL-1β and TNF-α reduction, resulting in a substantial quenching of inflammation and even functional recovery of the limbs.

Another possibility is to exploit apolipoproteins to coat lipid and more generally hydrophobic particles. These proteins are normally present in the blood and carry lipids from and to the liver, and thus are invisible to the immune system, and by selecting the proper one, it is possible to direct the nanovectors to specific cellular receptors (152). This strategy is especially interesting to treat pathologies in which cells overexpress apolipoproteins receptors. One such case is atherosclerosis, in which part of the blood vessels walls becomes sclerotic and accumulates highly active macrophages (defined as foam cells) rich in lipids. Thus, foam cells overexpress apolipoproteins receptors which could be used as handle for active targeting. This opportunity was explored by Jiang et al (153), who generated Apolipoprotein E (Apo E) coated lipid NPs for the dual delivery of the cholesterol depleting drug pitavastatin to atherosclerotic plaques in combination with SR-A siRNA. SR-A inhibition is aimed at increasing the expression of the Apo E receptor CD36, creating a positive feedback loop of improved targeting. These formulations demonstrated the ability to accumulate into the plaques and reducing their extension as well as the number of macrophages in them, all hallmarks of improved atherosclerosis.

A similar study by Sheng et al (154) used ApoA-1 modified with the integrin targeting iRGD peptide to deliver indocyanine green to breast cancer. This system demonstrated colloidal stability over several weeks, demonstrated its reliability after multiple laser stimulations, resulted in extremely efficient tumor accumulation in a breast cancer mouse xenograft (almost double of the liver accumulation), and after irradiation resulted in complete tumor eradication with no detectable systemic side effects.

Another study by Qiang et al (155) employed only the lipids-binding part of Apo-B to create a targeting moiety functionalized with folic acid against HeLa cervix cancer cells. These particles were composed of the same lipids of actual lipoproteins, making them especially suitable for the loading of hydrophobic drugs such as paclitaxel. This formulation demonstrated gradual paclitaxel release and selective cytotoxic action against folate receptor-positive cancer cells, reducing the tumor burden by 75% in murine tumor models without affecting their body weight.

***Future perspectives on the development of biomimetic NPs***

However, the use of biomimetic nanosystems is not limited only to the development of drug delivery vectors, but also as medical devices to replace or reinforce physiological functions. RBC membranes coated NPs have been used as either hemoglobin carriers or as oxygen carriers to create semisynthetic RBCs (156) Conversely, a recent work by Hendrich et al (157) focused on the development of Lipoprotein mimics using soft synthetic cores as scaffolds to induce the assembly of lipids and Apolipoprotein-A1, creating analogs with not only the same size and structure, but also able to remove cholesterol from macrophages and deliver it to the hepatocytes *in vitro*. This could lead to the reduction of circulating cholesterol and its removal from atherosclerotic plaques.

All the approaches for the formulation of biomimetic NPs discussed above can achieve membrane reconstitution onto nanoparticles. However, all of them present some caveats and limitations that are worth considering.

A more general caveat for the use of biomimetic nanomaterials is a fruit of their own complexity. Specifically, it is quite difficult to understand the relevance of specific molecules in defining the nanomaterial behavior, since the entire membrane could present hundreds of different molecules. So far, only few studies have attempted to specifically block single membrane proteins using antibodies to study how the particle behavior changed without their function. However, it is possible that more proteins could redundantly have the same functions, or that some unexpected proteins provide important contribution to the formulations' behavior. Thus, the investigation of this complexity will require in the future more efforts with innovative techniques that offer a more "holistic" view. Expanding the knowledge and defining the "essential" molecules that are required for the desired particle function could ultimately lead to the production of "chimeric" biomimetic nanomaterials, in which single proteins that are found in disparate cell types can be combined on a single platform, taking the best of each protein source and bypassing the necessity to bring along a lot of unwanted cellular material. In turn, this could result in simpler formulations with more reproducible features and easier scalability.

Furthermore, despite the surface proteins having gathered the most attention from the research so far, the biological function of the cells' membrane can also be provided by the phospholipid bilayer they are inserted in, and by the complex sugars linked to the proteins and lipids. So far there are almost no studies on these specific components of the membranes, and further investigation could provide more options for innovative and multifunctional biomimetic nanosystems.

# Materials and Methods

## Cell culture and Materials

Murine monocytes (J774 A.1, ATCC® TIB-67™) and human monocytes (THP-1, ATCC® TIB-202™) were purchased from ATCC. J774 cells were cultured in 100 mm cell culture plates (Falcon™ Standard Tissue Culture Dishes) using High Glucose Dulbecco's Modified Eagles Medium (DMEM, Millipore Sigma, D5671-500ML) supplemented with 10% Fetal Bovine Serum (FBS, Atlas Biologicals, F-0500-A), 1% L-Glutamine (Fisher Scientific Gibco L-Glutamine Solution Cytology 100 mL - 25-030-081) and 1 % Penicillin and Streptomycin solution (Gibco™ Penicillin-Streptomycin (10,000 U/mL), 15140122). J774 were detached cells using cell scrapers, kept them under 20 passages from the original sample and amplified them when reaching about 80 % confluence. THP-1 cells were cultured in T175 cell culture flasks (Thermo Scientific™ Nunc™ EasYFlask™ Cell Culture Flasks, 159910) using RPMI-1640 medium (ATCC® 30-2001™) supplemented with 10 % FBS, 1 % L-Glutamine and 1 % Penicillin and Streptomycin solution. THP-1 cells were kept in suspension with a maximum cell density of 800,000 cells per ml of medium. All the cell lines were kept in a humidified incubator at 5 % CO2 pressure and 37º C (NuAire 200 L CO2 Incubator w/ decon 120V 60Hz). To induce THP-1 cells differentiation, Phorbol 12-myristate 13-acetate (PMA) was purchased from Merck (P1585). Human Umbilical Vein Endothelial Cells (HUVEC) were purchased from ATCC and culture in low serum medium (Biotechne, CCM027) and using gelatin coated cell culture plates and flasks. Gelatin derived from porcine skin was purchased from Merck (G1890-100G). To inflame HUVEC cells, lipopolysaccharide from *E. Coli* (LPS) was purchased from Merck (L4516-1MG). To stain cell nuclei, Hoechst 33258 solution was purchased also from Merck (94403)

Primary antibodies were purchased against nucleoporin-62 (NP-62) from Santa Cruz Biotechnology (SC-48389); antibodies for glyceraldehyde phosphate dehydrogenase (GAPDH) from Santa Cruz Biotechnology (SC-365062); antibodies against CD11b from Abcam (Ab75476); for Calnexin from Abcam (ab22595), for β actin from Sigma (A5441-2ML). The HRP-conjugated secondary anti-mouse polyclonal antibodies were purchased from Invitrogen (A16078).

For membrane protein extraction, PIPES (P6757-25G), sucrose (S0389-100G), Sodium Chloride (S9888-500G), EDTA (E5134-50G), magnesium chloride (M8266-100G), digitonin (D141-100MG), Triton X-100 (11332481001-50ML) were purchased by Sigma Aldrich. Phosphate buffer saline (PBS 10X, pH 7.4, 70011044) was purchased by GIBCO. Protease inhibitor cocktail (Halt™ Protease Inhibitor Cocktail 100X) was purchased by Thermo Scientific.

For NPs synthesis, ammonium sulphate was purchased from Sigma-Aldrich (A4418-100G), 1,2-Dipalmitoyl-sn-glycero-3-phosphocholine (DPPC), was purchased from Lipoid, 1,2-dioleoyl-sn-glycero-3-phosphocholine (DOPC, 850375P-200mg) was purchased from Avanti Polar Lipids, Cholesterol (C8667-500MG) was purchased from Sigma-Aldrich, absolute ethanol (1009832511) was purchased from Merck. Float-A-Lyzers™ were purchased from Spectrum (Spectrum™ G235036); sterilizing 0.22μm syringe filters were purchased from Merck (Z359904).

To perform the Stewart assay, iron (III) chloride hexahydrate (F2877), ammonium thiocyanate (A0302) and chloroform (C2432-2.5L) were purchased from Sigma-Aldrich.

## Protocol for membrane protein extraction

The commercial kit (KIT) used for membrane protein extraction was purchased from Calbiochem (ProteoExtract Native Membrane Protein Extraction Kit, Calbiochem, 444810). We used the kit according to the producer's specifications.

However, to make a direct comparison, the buffer / cell number ratios were the same as NEXT. Conversely, the protocol for NEXT was inspired by previous studies (158). The buffers for NEXT are composed as follows:

- Washing buffer: 1X PBS.

- Extraction buffer 1 (EB1 NEXT): 10 mM PIPES; 300 mM Sucrose; 100 mM Sodium Chloride; 5 mM EDTA; 0.015 % w/v digitonin and 1:100 diluted protease inhibitor cocktail diluted in MilliQ water (pH=6.8).

- Extraction buffer 2 (EB2 NEXT): 10 mM PIPES, P6757 Sigma-Aldrich; 300 mM Sucrose; 100 mM Sodium Chloride; 5 mM EDTA; 0.1 % or 0.5 % v/v Triton X-100 and 1:100 diluted protease inhibitor cocktail diluted in MilliQ water (pH=7.4).

We performed the membrane protein extractions as schematized in Figure 9 for both KIT and NEXT after removing them from the culture. In Step A, cells were rinsed twice with buffer to remove the FBS proteins present in the cell culture medium and centrifuged at 300 x g using an Eppendorf 5424R Refrigerated Centrifuge at 4° C.

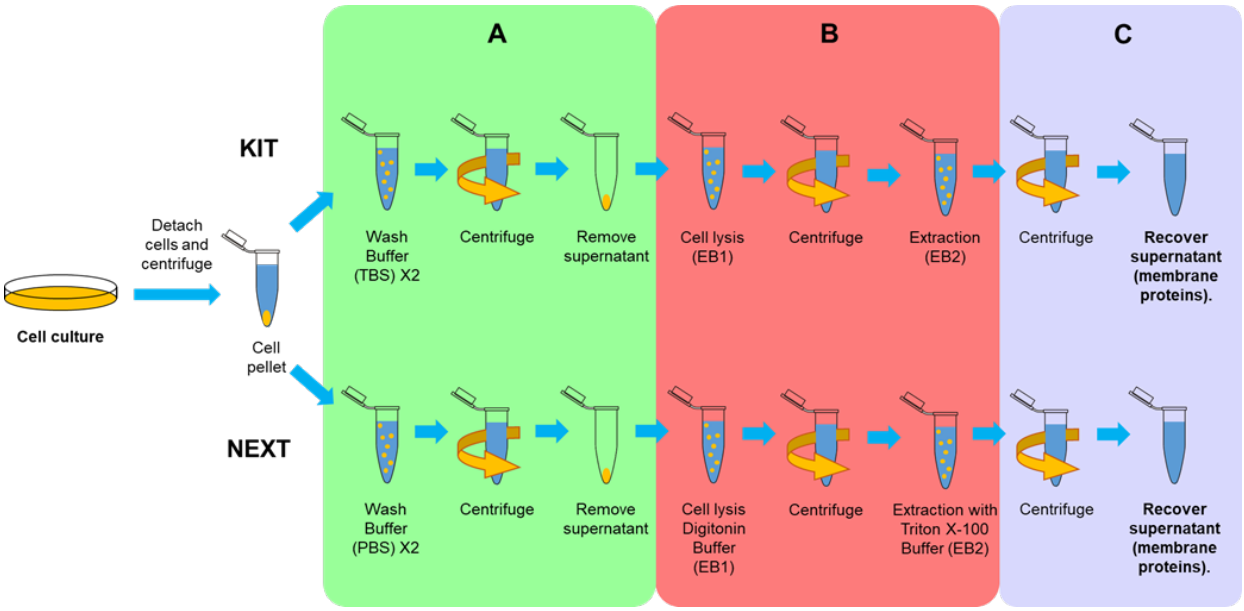


**Figure 9** Schematic description of the membrane extraction protocols using KIT and NEXT.

In Step B, cells were permeabilized by re-suspension in EB1 KIT or EB1 NEXT, allowing the efflux of cytosolic and cytoskeletal proteins and incubated for 10 minutes. Cells were then centrifuged at 16,000 x g for KIT and 1000 x g for NEXT, and the supernatant was removed.

In Step C, the pellets were re-suspended in EB2 KIT or EB2 NEXT to solubilize the cellular membranes and extract membrane proteins and incubated for 30 minutes. The suspensions were then centrifuged at 16,000 x g for the kit and at 5,000 x g for NEXT to remove the cells nuclei and organelles. The supernatants containing the purified membrane proteins were finally recovered for further analysis. All the washing, centrifugation, and incubation passages were performed at 4°C. Membrane protein extracts were stored at -20°C. These specific storage conditions were selected to replicate the ones advised for short-term storage of the commercial KIT, making the subsequent comparison clearer in terms of proteins stability.

## Assessment of cells permeabilization

To assess the complete permeabilization of the cells from EB1 in Step A, cells were observed using an inverted microscope (Nikon Eclipse TS 100) equipped with 10X phase contrast objective after treating them with Trypan Blue stain diluted 1:10 in 1X PBS and positioned into a hemocytometer. Images were collected using a Nikon Digital Sight DS-Ri1 camera system.

To perform turbidimetric analysis of the cell suspensions after permeabilization, 100 µL of the suspensions were added to a 96-wells plate and the absorbance was read at 950 nm light wavelength using a Tecan Spark® multimode microplate reader.

## Membrane proteins quantification and yield calculation

Protein concentration in the extracts was determined using BCA assay (Thermo Scientific™ Micro BCA™ Protein Assay Kit, 23235) according to the producer specifications. The proteins standard calibration curve was prepared using sequential dilutions of bovine serum albumin (BSA, Sigma – Aldrich, 100 g, 45ZV32) in the concentration range of 0-200 µg/mL. BSA dilutions were prepared in EB2 KIT or EB2 NEXT to account for possible interferences of the buffer components during the assay.

## SDS-PAGE/Western Blot

SDS-PAGE/Western Blot analysis was performed as follows. 20 µg of proteins per gel were loaded after diluting them with 4X Laemmle Buffer (4x Laemmle Sample Buffer #1610747 BIORAD), brought to volume with 1X PBS, and boiled at 95º C for 10 minutes. The samples were then loaded onto 4-20 % gradient poly-acrylamide gel (4–20% Mini-PROTEAN® TGX™ Precast Protein Gels, 10-well, 50 µl #4561094, BIORAD) in running buffer (10x Tris/Glycine/SDS #1610732, BIORAD). The gels were run using a Biorad apparatus (Mini-PROTEAN® Tetra Cell equipped with Biorad PowerPac Basic Electrophoresis Power Supply) at 100 V of voltage. Proteins blotting was performed using a fast-semi-dry apparatus (Trans-Blot® Turbo™ Transfer System, BIORAD) and were blotted onto PVDF membranes (Trans-Blot Turbo Mini 0.2 µm PVDF Transfer Packs #1704156, BIORAD). The successful blotting was assessed using Ponceau S solution (Ponceau S solution, P7170, Sigma Aldrich). The membranes were incubated with 5 % skimmed milk (Nonfat-Dried Milk bovine M 7409, Sigma-Aldrich) diluted in TBS supplemented with 0.1 % Tween 20 (P9416-100ML, Sigma Aldrich) (TBST).

Membranes were incubated overnight with monoclonal primary antibodies diluted in 5 % skimmed milk diluted in TBST. The next day, the primary antibodies were removed, and the membranes were washed three times with TBST. Then, the membranes were incubated with secondary HRP-conjugated polyclonal antibodies for 1 hour under gentle mixing. The secondary antibodies were removed, and the membranes washed again three times with TBST. The signal was then developed using ECL reactive (Clarity Western ECL Substrate, 500 ml #1705061, BIORAD) in the dark for 4 minutes. The membrane development was performed using a Versadoc instrument (Biorad Gel Doc EQ System w/ Universal Hood II).

The quantification of the blotted membranes was performed using the Image Lab software version 6.1 (BIORAD). The normalization of the signal was performed using the signal intensity form the total cell lysate after subtracting the background from a point of the membrane with no visible staining.

## DLS analysis of protein extracts

Dynamic light scattering (DLS) analysis was performed to assess possible proteins aggregation after extraction. We used disposable plastic cuvettes using a Zetasizer Nano ZS instrument. As negative controls, KIT and NEXT blank EB2 were analyzed. Conversely, as positive control for proteins aggregation, an aliquot of the different extracts was boiled at 95° C for 10 minutes on order to thermally destabilize proteins conformation. We did each reading in triplicated of 10 measurements each.

## Proteomics analysis – Mass Spectrometry

Samples preparation: samples (50 µL) were placed into Amicon Ultra 0.5 mL centrifugal filters (Millipore) to replace Triton-X100 with Protease Max Surfactant 0.2 % (Promega, 60 µL) which is MS compatible. The samples recovered were treated with 5 mM dithiothreitol (DTT) at 60° C for 30 mins and then with 15 mM iodoacetamide (IAA) at room temperature in the dark. Samples were further de-lipidated with methanol/chloroform extraction before digestion. Then trypsin digestions were performed overnight at 37° C (enzyme: substrate = 1:50 molar ratio). Reaction was stopped by adding 10% of formic acid and peptides were purified by SPE using Supel-Select HLB C18 column, volume 1 mL purchased by Sigma Aldrich (Sigma Aldrich, S.Louis, MO, USA ). Finally, peptides were dried using speedvac concentrator and sored at -20° C until analysis.

Data acquisition: An ACQUITY UPLC H-Class system coupled to a Waters Xevo G2-XS qTOF mass spectrometer (Waters UK, Elstree, UK) was used. Chromatographic separations were achieved using an ACQITY UPLC Peptide BEH C18, 1.7 µm, 1 × 50 mm (Waters UK, Elstree, UK) column. The mobile phases consisted of ultrapure H2O/0.025 % TFA (A) and CH3CN/0.025 % TFA (B) according to the following elution gradient: initial at 95 % solvent A for 0.5 min, then decreased to 65 % in 84.5 mins, then further decreased to 10 % in 7.0 mins and kept for 1.0 min before returning to initial conditions. The flow rate was set at 0.18 mL/min and the inject volume was set at 5 µL. The mass spectrometer parameters were set as follows: ESI(+), mass range, m/z 50–2000; capillary voltage, 2.75 kV; sampling cone, 45 V; source offset, 90 V; source temperature,120° C; desolvation gas (sheath gas) temperature, 350° C; cone gas, 50 L/h; desolvation gas, 800 L/h. To ensure for mass accuracy and reproducibility of the optimized MS conditions, leucine enkephalin (Leu-Enk, m/z 556.2771 in positive mode) was used as a lock mass

Data processing: mass spec data have been lock-mass corrected using Leu-Enk, peak picked, and converted into mzML format and processed by Proteome Discoverer 2.4 (ThermoFisher Scientific). Search parameters were set as follow: database, UniprotKB reference human proteome

UP000005640 (accession date 09/14/2021); enzyme, Trypsin (max 2 missed cleavages); taxonomy, Homo sapiens; precursor mass tolerance, 0.15 Da, fragment mass tolerance, 0.25 Da. Fixed modifications: carbamidomethyl (C). Dynamic modifications: oxidation (K, M, P); and deamidation (N, Q). An acceptable proteins false discovery rate (FDR) was set < 0.01 and a minimum of 2 non-redundant peptides was used to obtain proteins identification.

## Nanoassemblr™ formulation of Lipo and Leuko

Lipo and Leuko were formulated using the Nanoassemblr™ microfluidic equipped with its respective cartridges according to the producer's instructions.

The aqueous phase of the formulation was composed of a 250 mM ammonium sulphate buffer to enable later DOXO remote loading. After dissolution, the buffer was filtered using a 0.22 μm filters and its pH was adjusted pH 6.5 using a calibrated pH-meter. For Leuko, membrane proteins were diluted into the buffer in concentration adjusted on the basis if the FRR to achieve the desired lipids to protein ratio.

On the other hand, the organic phase was a solution of DPPC, DOPC, and Cholesterol in a 4:3:3 molar ratio dissolved in absolute ethanol to a final concentration of 10mg/mL.

The two solutions were then sealed in glass vials and kept at 45°C using a heating block. At the moment of formulation, the aqueous phase was loaded into a 3 mL syringe, while the organic phase was loaded in a 1ml syringe. The temperature of the solutions during the formulation were kept by installing another thermal block within the Nanoassemblr™. Thus, the syringes were loaded in the system and the Lipo or Leuko assembly were performed by setting the TFR, FRR (aqueous / organic) and lipids to protein ratio (w/w) as indicated by the DoE design. For the final formulations, the FRR was 4.88:1, the TFR was set to 1mL/min, and the lipids to protein ratio was 20:1. The pre-waste of the system and the post-waste were always set as 50μL and 150μL, respectively.

After synthesis, the NPs were dialyzed to remove the ethanol using a Float-A-Lyzer™ with a molecular weight cutoff of 300 kDa overnight at room temperature using PBS1X as external phase. Finally, particles were filtered using a sterilizing 0.22 μm filter under a sterile laminar flow hood.

Fluorescently labelled Lipo and Leuko were obtained by adding 0.05 mg Cy5.5 conjugated phosphatidylethianolamine (Cy5.5-PE) to the lipid phase before formulation (0.5% of the total lipid mass). To assess the particle fluorescence after formulation, Lipo or Leuko Cy5.5 were diluted 1:1,000 in MilliQ water and then 100μL of dispersion were added to a 96 well plate and fluoresce was read using a Tecan Spar plate reader using an excitation wavelength of 620 nm (20 nm bandwidth)

and an emission wavelength of 680 nm (30 nm bandwidth).

## Stewart assay for lipids quantification

The colorimetric Stewart assay was used to quantify the amount of lipids in the NP formulations. Briefly, the final NPs dispersion was diluted 1:50 in 2 mL of chloroform and thoroughly vortexed to endure complete lipids dissolution in the organic solvent.

Then, 2 mL of Stewart aqueous reagent were added to the lipid solution and the two phases were again thoroughly vortexed to allow for the reaction between the lipids and the reagent itself. The two phases were then separated by centrifugation for 10 min at 100 rpm. Then the reagent phase was removed, and the colored organic phase was spectrophotometrically analyzed at 485 nm wavelength. The concentration of lipids was calculated using a calibration curve to extrapolate the concentration from the net absorbance of the lipid solution.

To create a calibration curve, a freshly made chloroform solution of the lipids used for NP formulations in the same lipids' ratio was diluted to 0.05, 0.04, 0.03, 0.02, 0.01 and 0.005 mg/mL of total lipids and pure chloroform as a blank. The calibration curve and its relative equation are presented in the graph below.

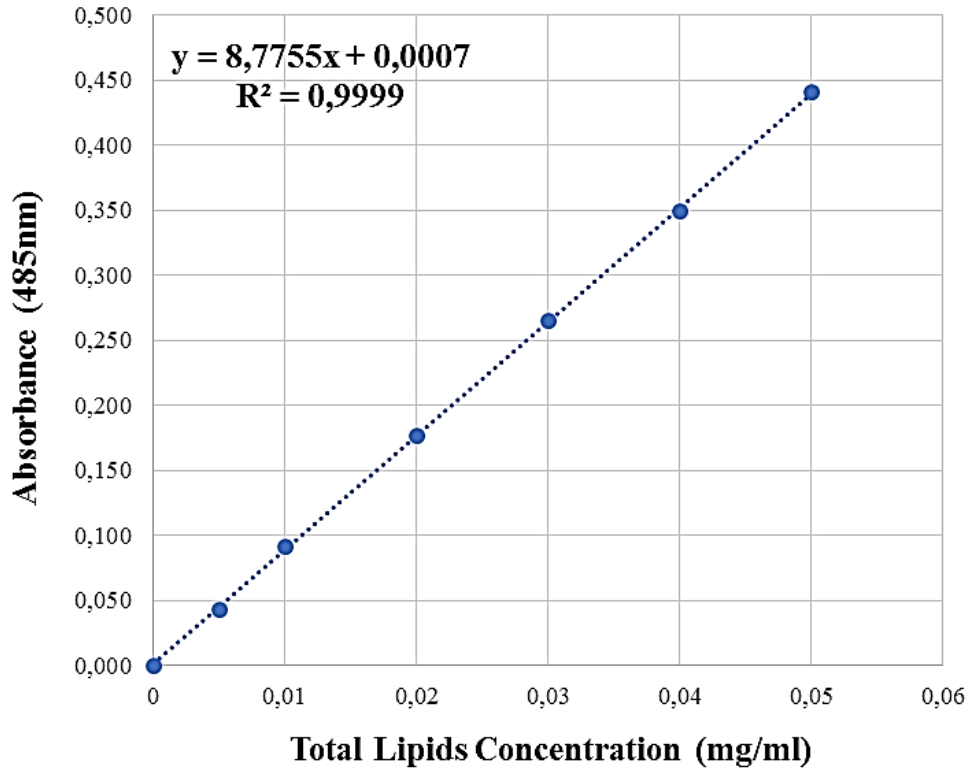


**Figure 10:** Calibration curve for the Stewart colorimetric assay used for lipids quantification

## DLS characterization of Lipo and Leuko

Lipo and Leuko hydrodynamic diameter, PDI, and zeta potential were measured using a Zetasizer DLS (Malvern). Particle solutions (1.2 mg/mL of lipids) were diluted 1:100 in fresh MilliQ water and measured using folded capillary cuvettes (DTS1070, Malvern) five sequential times for the size followed by three measurements of zeta potential, each interspaced by one-minute equilibration time.

## Particle tracking analysis of Lipo and Leuko

The number of NPs per milliliter of formulation was estimated using the Nanosight™ platform equipped with a 488nm laser. Lipo or Leuko were diluted 1:1000 in fresh MilliQ water prior to the analysis and then loaded into a 1mL syringe. For the analysis, the particles were injected at 1000-speed for 10 sec, followed by 120 sec of 100-injection speed prior to measurement. Each sample was measured while injected at a 100-injection speed in five sequential measurements of 60 sec each, keeping the camera level at 12. For data processing, the detection threshold was set at 7 for all measurements.

## Flow Cytometry Analysis and MACSPlex Exosome Assay

Human monocytic leukemia cell line THP-1 was analyzed by cell surface phenotyping using the BD FACSymphony (Becton Dickinson, San Diego, Ca, USA). In detail, THP-1 cells were counted and up to 0.5x106 cells were stained at 4°C with a selected panel of immune cell markers (mouse anti-human monoclonal antibodies CD45, CD19, CD3, CD4, CD8, CD56, CD11c, CD14, HLA-DR, HLA-ABC, CD86 and CD1c: all from BD Biosciences). A marker of cell viability (BD HorizonTM Fixable Viability Stain 780) was also added.

Leukos derived from THP-1 cells were characterized by cytofluorimetric analysis using the MACSPlex Exosome kit (Miltenyi Biotec, Bergisch Gladbach, Germany) following the manufacture's instruction. Briefly, three different Lipo and Leuko preparations (1*1010 particles) were added to the MACSPlex Buffer solution. Samples were then incubated for 2 hours with a cocktail of APC-conjugated detection antibodies against tetraspanins (CD9, CD63, and CD81) and phycoerythrin (PE)- and fluorescein isothiocyanate (FITC)-labeled capture beads, coated with antibodies against 37 different exosomal surface epitopes plus two isotype controls (REA and IgG1). Beads and detection antibodies were incubated without particles in MACSPlex Buffer and used as a negative control. After washing steps, samples were analyzed by flow cytometry using the BD FACSCanto II (Becton Dickinson, San Diego, Ca, USA), capable of detecting the necessary fluorescence signals. To eliminate a non-specific signal from the median fluorescence intensity (MFI) of each marker was subtracted the MFI of the negative control as well as of the isotype controls used

in the same experiment. Leukos specific signal from then obtained by subtracting the corresponding Lipos marker signal in each preparation. All the data were analyzed by FlowJo software version 10.8.1 (Becton Dickinson, San Josè, CA).

## DOXO loading into Lipo and Leuko

DOXO loading was performed using a remote loading approach. Specifically, DOXO hydrochloride was dissolved in fresh MilliQ water to a final concentration of 1mg/mL. Then, the DOXO solution was added to the NP suspension according to the desired Lipids to DOXO weight ratio, according to the following formula:

$$Vol\ DOXO\ solution\ (ml) = \frac{Lipid\ conc\ (\frac{mg}{ml}) \cdot Desired\ final\ Vol\ (ml)}{(Lipid{:}DOXO\ ratio\ \cdot Conc\ DOXO\ (\frac{mg}{ml})) + Lipids\ concentration(\frac{mg}{ml})}$$

The DOXO and NP mixture was then incubated in a thermal block at 45°C for 2 hours under 300 rpm stirring. Then, the NPs were dialyzed using a Float-A-Lyzer™ with a molecular weight cutoff of 300 kDa overnight at 4°C using PBS1X as external phase to remove the DOXO that was not loaded within the particles while avoiding drug leakage.

## Assessment of DOXO loading

DOXO quantification was performed using the intrinsic drug fluorescence. A Tecan Spark plate reader was used to measure the drug fluorescence by excitation at 485 nm and emission at 590 nm. A calibration line of DOXO in MilliQ water was created by using DOXO solutions in the range of 0 – 2 μg/mL (Figure 11).

To calculate DOXO encapsulation efficiency within the particles, we used a fluorescence-dequenching assay, in which Triton X-100 is used as a detergent to disassemble the nanovesicles and release the encapsulated DOXO sulphate crystals, which would then dissolve in water and restore the DOXO fluorescence that would otherwise be quenched in its crystalline form. NPs were diluted 1:2 in a 0.2% (v/v) solution of Triton X-100 in MilliQ water and stirred for 10 minutes. Then, 100 μL solution were added in triplicate in a 96 well plate and the reading was performed according to the previously reported plate reader settings. The encapsulation efficiency was calculated as follows:

$$Encapsulation\ Efficiency\ (\%) = \frac{DOXO\ amount\ loaded\ within\ the\ particles\ (mg)}{Initial\ amount\ of\ DOXO\ incubated\ (mg)} \cdot 100$$

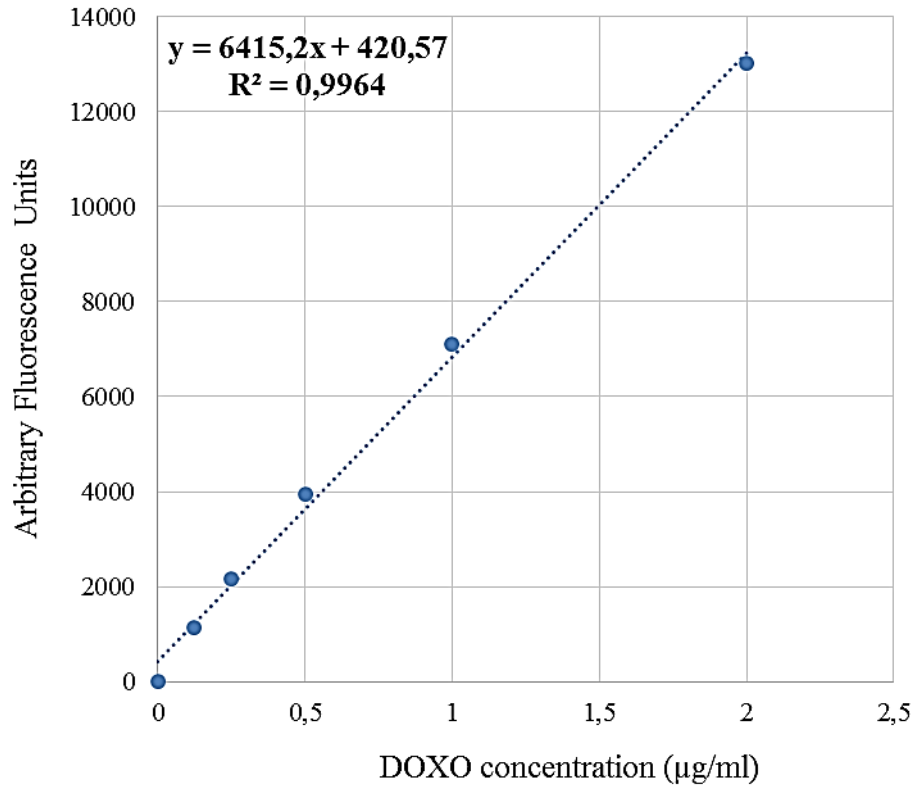


**Figure 11**. Calibration curve for DOXO quantification via fluorescence measurement.

## Assessment of DOXO release

DOXO release was performed by diluting Lipo or Leuko 1:50 in 2 mL of 1X PBS supplemented with 10% FBS (v/v) to simulate the cell culture medium. The release medium pH was either kept at pH 7.4 or adjusted at pH 6 to simulate the lysosomal compartment. The NP dispersion was then incubated in a thermal block at 37°C under 300 rpm stirring. At different time points 50 µL of the suspension were withdrawn and diluted either in water or in 0.2% Triton X-100 to measure the released DOXO and the total DOXO within the aliquot, respectively using the same fluorometric assay discussed in the previous section. The released DOXO percentage was calculating dividing the DOXO measured in water over the total DOXO within the aliquot, multiplied by 100.

## *In vitro* cytotoxicity assays

To perform cytotoxicity assays of DOXO and NPs, HCT-116 colorectal cancer cells or SAOS -2 osteosarcoma cells were seeded in a 96 well cell culture plate at a density of 10,000 cells per well and left to adhere overnight in complete culture medium. For 3D cell cultures, the same number of cells was diluted in 20 µL of Geltrex™ per well in a 24 well plate using the hanging drop approach to allow the hydrogel drops to solidify before adding the cell culture medium. The day after, the medium was withdrawn from the cells and replaced with either free DOXO, Lipo, Leuko, Lipo DOXO or Leuko DOXO in a dose range from 10 to 0.001 µM. The amount of DOXO-loaded particles added

was calculated based on the amount of DOXO they contained to make the treatment analogous to the free drug. Conversely, empty Lipo and Leuko were used in the same NP number as their respective DOXO loaded formulations. Then cells were incubated for 72h at 37°C, 5% $CO_2$. Afterwards, 20 µL of Resazurin solution (400µM) were added to each well and incubated for 2 hours. Finally, the fluorescence was measured using a Tecan Spark plate reader with excitation at 550 nm and emission at 590 nm.

The percentage of cell viability was calculated as the ratio between the fluorescence over the fluorescence of the untreated cells, multiplied by 100. After normalizing the viability data, the $IC_{50}$ values for each treatment were calculated using GraphPad Prism to fit a sigmoidal curve of percentage of viable cells versus the decimal Logarithm of the treatment concentration expressed as µ M.

## *In vitro* NPs uptake assay

To assess the internalization of NP uptake, tumor cells were seeded either in flat culture or embedded in Geltrex™ in the same conditions discussed in the previous section. Human umbilical veins endothelial cells (HUVEC) were seeded on gelatin coated 96 well plates at 10,000 cells per well density. To inflame endothelial cells, they were incubated with a 100 ng/mL solution of LPS in complete medium. Human THP-1 monocytes were instead seeded in 24 well plate as 50,000 cells per well in presence of PMA 100 mg/mL and left to differentiate into macrophages for 48 hours. Cells culture medium was then replaced with fluorescent Lipo Cy5.5. or Leuko Cy5.5 dispersed in complete cell culture medium at a final concentration of $1*10^{11}$ particles/mL. HCT-116 and SAOS-2 cells were then incubated for 6, 12 and 24 hours before imaging, while HUVEC and THP-1 cells were incubated for 3 hours before imaging. At the time of imaging, the cells culture medium was removed, and cells were washed with 1X PBS, stained for their nuclei by incubating them with a Hoechst solution 20µM for 5 minutes at 37°C. Cells were then imaged using a Zeiss AxioObserver fluorescence microscope equipped with a TL lamp for bright field imaging with 385nm laser for Hoechst visualization and with 630nm laser for Cy5.5 detection.

To perform the quantification of NP uptake, an ad hoc macro was created in FIJI to perform the NP fluorescence and the number of cells per image, following the workflow schematized in the figure below. Then, the NP fluorescence was normalized by the number of cells in its respective image, as presented in Scheme 1.

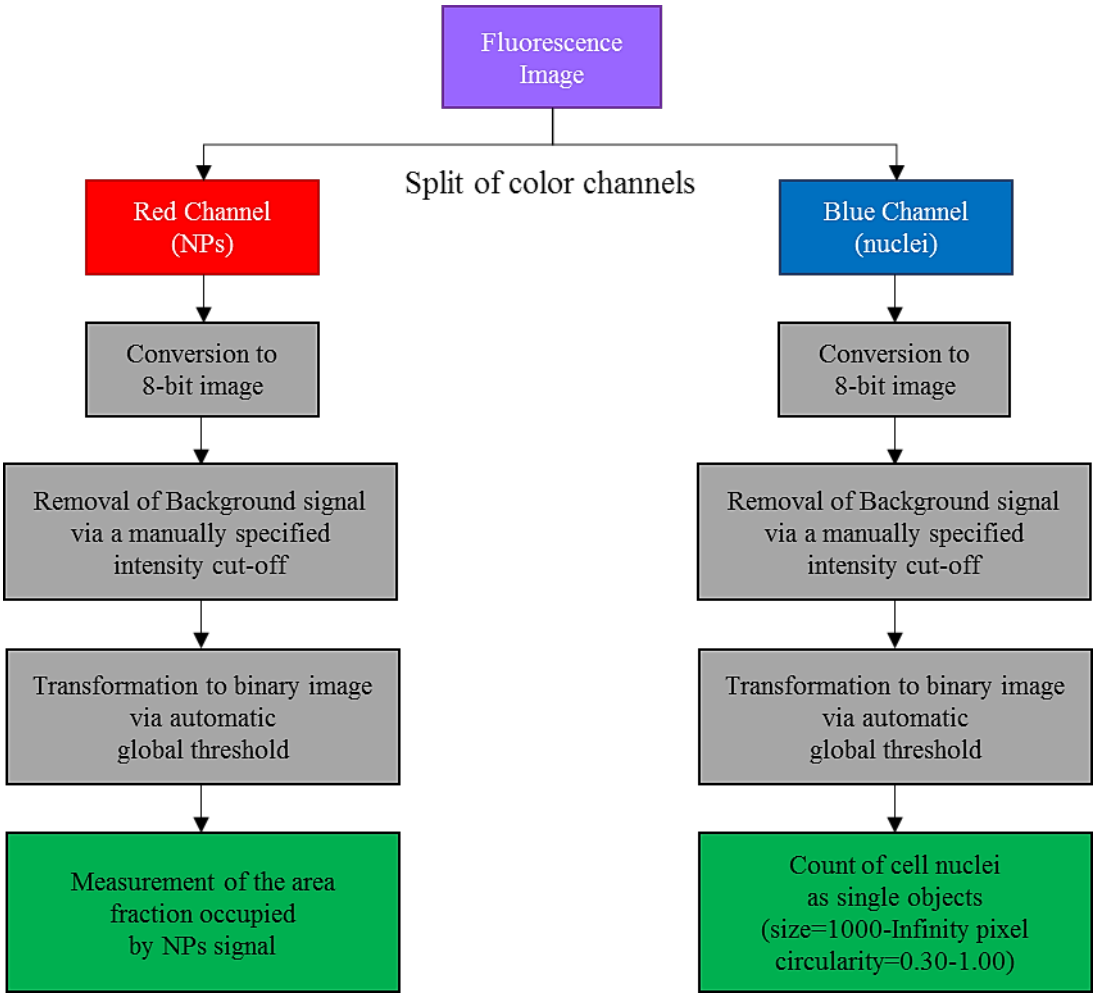


**Scheme 1.** Schematic representation of the workflow used for the processing of fluorescence images of tumor cells and spheroids to perform NPs uptake quantification

## Statistical analysis

All experiments were performed in triplicate, and statistically significant differences were assessed using 2-way ANOVA analysis for matching values.

# Results and discussion

## Turbidimetric optimization of EB1 volume/cell number ratio

The purification of membrane proteins from leukocytes was performed by two-step methods (KIT and NEXT) that were compared for their extraction efficiency. The study was carried out using different cell amounts to verify the reliability of the protocol under different conditions.

In step A, cells were prepared by washing with buffers specific for each method (KIT and NEXT), while in Step B the cell membranes were permeabilized with low concentration of digitonin, a glycoside derived from the plant species *Digitalis sp*. that, according its amphiphilic non-ionic properties, is a mild surfactant (159).

To assess the permeabilization efficacy of the digitonin-containing EB1 NEXT, increasing numbers of cells were suspended in 120 µl of EB1 KIT or EB1 NEXT. Cells were then diluted 1:1 v/v into a Trypan blue and its permeation though the cells membranes was observed.

Figure 12A shows the permeabilization profile of J774 cells. J774 cells suspended in PBS (negative control) were translucent, and therefore viable and non-permeabilized while after incubation with EB1 KIT all the cells up to 2.4 million/tube appeared dark blue and thus fully permeabilized. After treatment with EB1 NEXT, cells up to 1.2 million/tube were completely permeabilized while the cells in 2.4 millions/tube sample were partially translucent, indicating incomplete cells permeabilization. This result shows a different permeabilization efficiency of the two methods indicating that KIT is much more efficient than NEXT when high cell concentrations are processed.

To confirm this trend, turbidimetric analyses were performed. The absorbance of the cells suspensions was measured using a 950 nm light wavelength, since this light is not influenced by the inherent absorbance of cell components and is just scattered by the turbidity of the cells. Figure 12B shows that cells suspended in PBS had a linearly increasing optical density ($R^2$=0.9899). In agreement with previous data, cells suspended in EB1 KIT showed a much lower absorbance at all concentrations with respect to the control, deriving from efficient permeabilization. The slight increase in optical density could be caused by the biggest organelles within the suspension, which contribute to light scattering (160). Cells suspended in EB1 NEXT (0.203) had an overlapping optical density profile to EB1 KIT (0.170) up to 1.2 million cells. At 2.4 million cells, the absorbance of EB1 NEXT-suspended cells was similar to the control, confirming that no permeabilization was obtained under this condition.

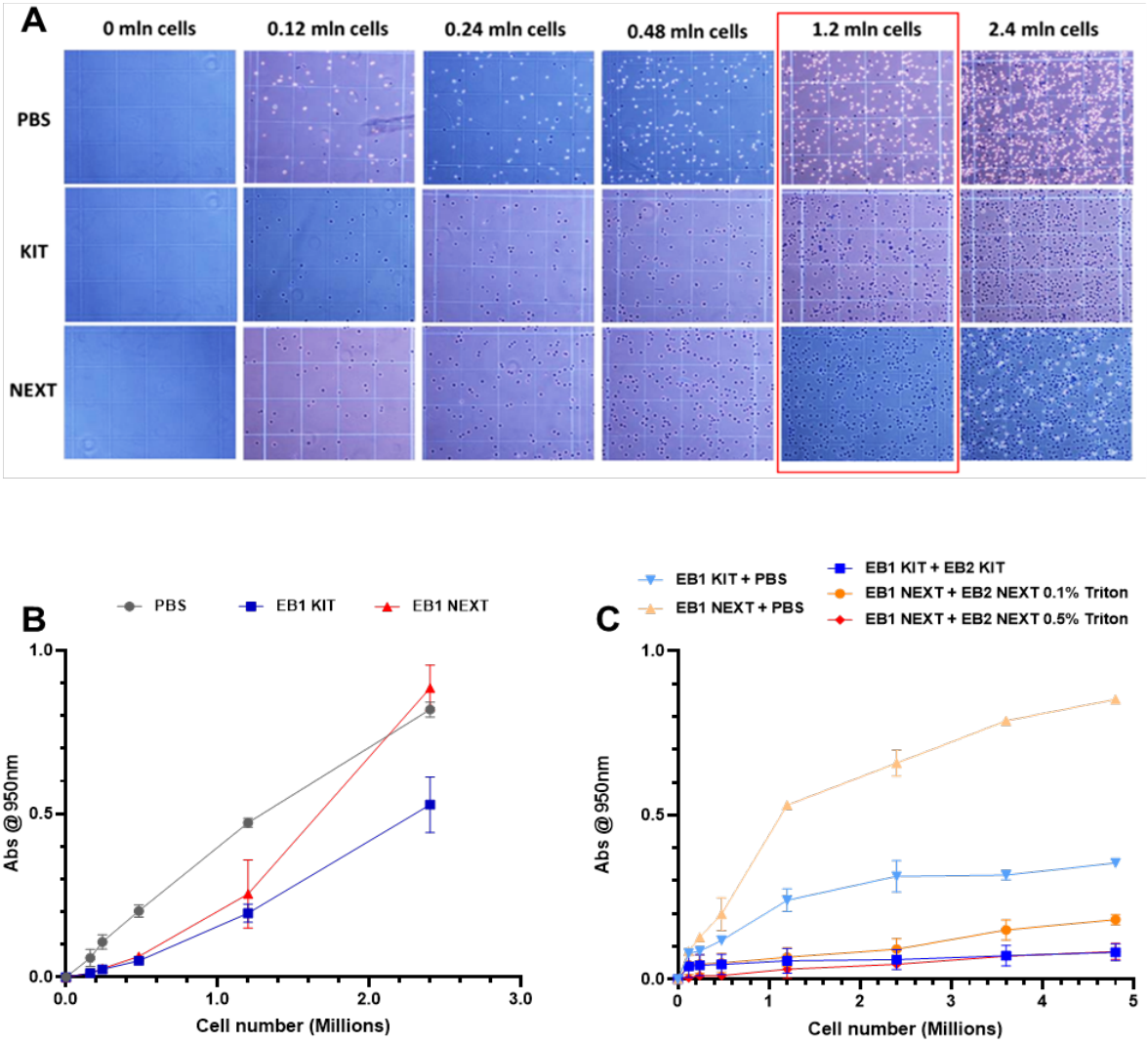


**Figure 12** A) Images of J774 cells after being permeabilized with KIT EB1 or NEXT EB1 and treatment with Trypan Blue; B) Turbidimetric profile of J774 murine monocytes suspended in PBS, KIT EB1 and NEXT EB1; C) Turbidimetric profile of J774 cells after permeabilization with KIT or NEXT EB1 and then in either PBS or KIT EB2 or NEXT EB2 containing 0.1% or 0.5% Triton X-100 (n=3 for all the graphs, error bars represent standard deviations).

Thus, the minimum volume of EB1 NEXT to completely permeabilize the cells is 120 µl per 1.2 million cells, corresponding to 100 µl of buffer per million cells. This ratio can be used to easily scale-up the extraction procedure using higher numbers of cells.

Once established the optimal condition for cell permeabilization, the same turbidimetric method was used to check the membrane solubilization by EB2 NEXT containing 0%, 0.1% or 0.5% v/v Triton X-100. Figure 12C shows that all samples treated with EB2 buffers display lower optical density is compared to cells suspended in PBS. However, samples preliminarily treated with EB1 NEXT presented significantly higher optical density than samples preliminarily treated with EB1 KIT . However, the treatment of cells previously processed with EB2 NEXT 0.5 % Triton, (EB1 NEXT+ EB2 NEXT 0.5 % Triton), yielded optical density overlapping the samples preliminarily treated with

EB1 KIT and then with EB2 KIT, (EB1 KIT+ EB2 KIT), indicating that in all the conditions all the cells were lysed, and that increasing the detergent amount in EB2 NEXT allowed for an improved membrane solubilization.

For proteins to retain their functions, it necessary that they maintain their three-dimensional conformation. Many techniques are available to assess the conformational status of proteins, including circular dichroism, X-Ray diffraction, small angle scattering, or Cryo-electron microscopy (161). However, all these techniques can be applied only with purified single protein solutions.

Conversely, our protein extracts are a complex mixture of proteins and detergents. Thus, we need a bulk method to assess the average stability of membrane proteins. Importantly, when membrane proteins lose their conformation and unfold, they tend to aggregate in larger protein complexes. A good endpoint for membrane protein physical stability in solution thus would be the presence of protein-detergent complexes of small size. Therefore, the protein extracts from EB1 KIT+ EB2 NEXT 0.1 % Triton and EB1 KIT+ EB2 NEXT 0.5 % Triton were analyzed using dynamic light scattering (DLS) to determine the size distribution of the protein complexes suspended in solution.

The results reported in Figure 13 show that KIT buffers without proteins had an average size of 12 nm while for NEXT buffers the size was a smaller 1.2 nm. These detected signals are considered detergent micelles present in the EBs. This difference could derive from the different detergents present in KIT and in NEXT buffers. As a positive control, a small aliquot of protein extracts from 4.8 million cells was heated at 95° C for 10 minutes to force protein denaturation and aggregation, and then cooled to room temperature. Even at a simple visual inspection, the heated extracts appeared opaque, evidencing the formation of bigger aggregates. This was confirmed by the DLS results showing that for all the tested extracts the population was composed of much bigger components than the normal extracts (around 1000 µm). For KIT and NEXT-derived extracts (Figure 13A, B, C), all the tested formulations had a size around 15 nm in diameter for KIT. Since the KIT claims that the extracted proteins are in their native conformation, this size distribution can be assumed the one of conformationally stable proteins-detergent micelles.

The Polydispersity Index (PDI) values of these extracts are around 0.5, and thus the size distribution is still quite polydisperse. This could be due to the many different proteins included into micelles. For NEXT 0.1 % Triton extracts, a similar size distribution was visible, indicating a similar conformation status of the proteins with an average size of 20 nm. However, the PDI of these extracts (PDI>0.6) was significantly higher than KIT extracts (PDI=0.3-0.5).

This suggests the presence of a small portion of protein aggregates, or the presence of native plasma membrane lipids that alter the structure of detergent micelles. Interestingly, despite the size of the aggregates being like KIT and NEXT 0.1% Triton, extracts from NEXT 0.5 % Triton had a lower PDI (PDI≈0.5). This could result from better protein solubilization and stabilization by the detergent, and / or better removal of native lipids.

Nevertheless, these data are very preliminary insights on the physical stability of protein in the final extracts and further investigations would be needed to better understand for how long the proteins are able to retain their conformations and functions under storage (162).

**A**

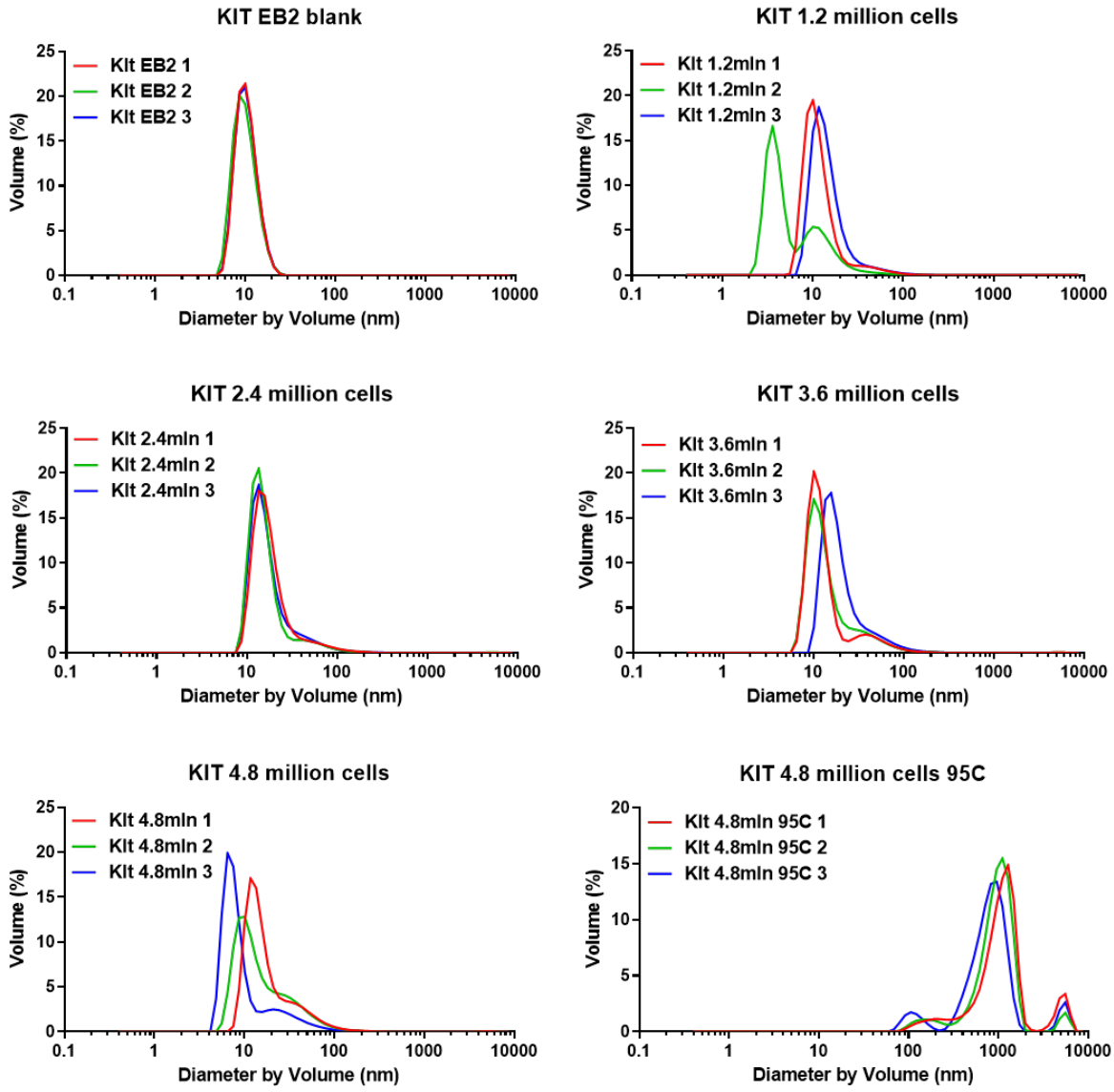

**B**

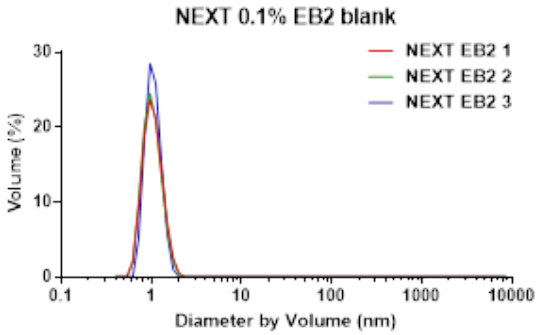
NEXT 0.1% EB2 blank
NEXT EB2 1
NEXT EB2 2
NEXT EB2 3
Volume (%)
Diameter by Volume (nm)

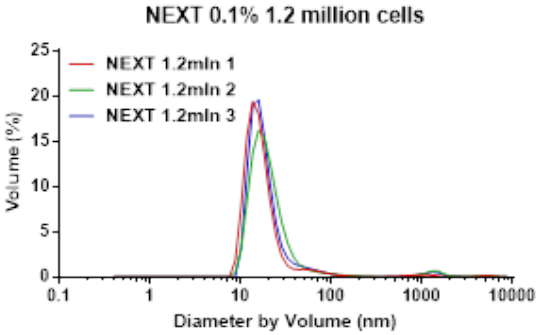
NEXT 0.1% 1.2 million cells
NEXT 1.2mln 1
NEXT 1.2mln 2
NEXT 1.2mln 3
Volume (%)
Diameter by Volume (nm)

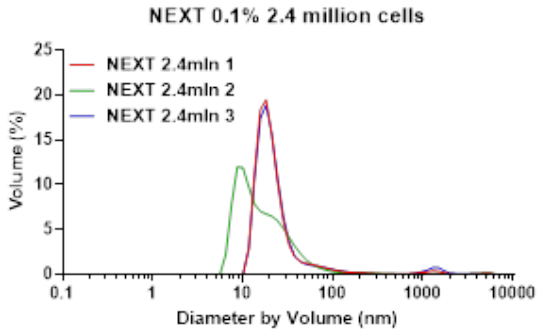
NEXT 0.1% 2.4 million cells
NEXT 2.4mln 1
NEXT 2.4mln 2
NEXT 2.4mln 3
Volume (%)
Diameter by Volume (nm)

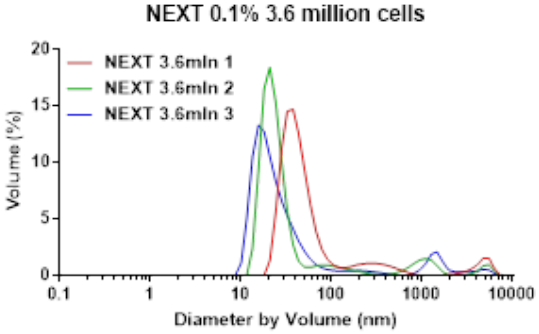
NEXT 0.1% 3.6 million cells
NEXT 3.6mln 1
NEXT 3.6mln 2
NEXT 3.6mln 3
Volume (%)
Diameter by Volume (nm)

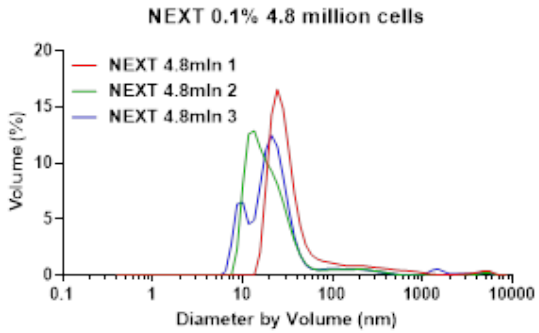
NEXT 0.1% 4.8 million cells
NEXT 4.8mln 1
NEXT 4.8mln 2
NEXT 4.8mln 3
Volume (%)
Diameter by Volume (nm)

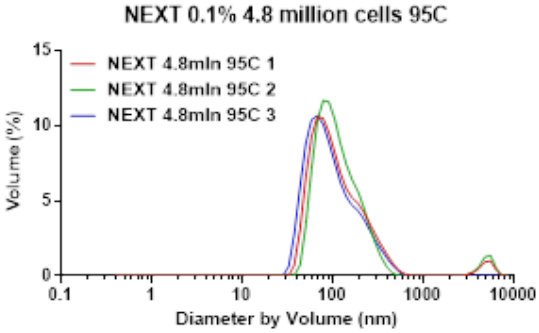
NEXT 0.1% 4.8 million cells 95C
NEXT 4.8mln 95C 1
NEXT 4.8mln 95C 2
NEXT 4.8mln 95C 3
Volume (%)
Diameter by Volume (nm)

**C**

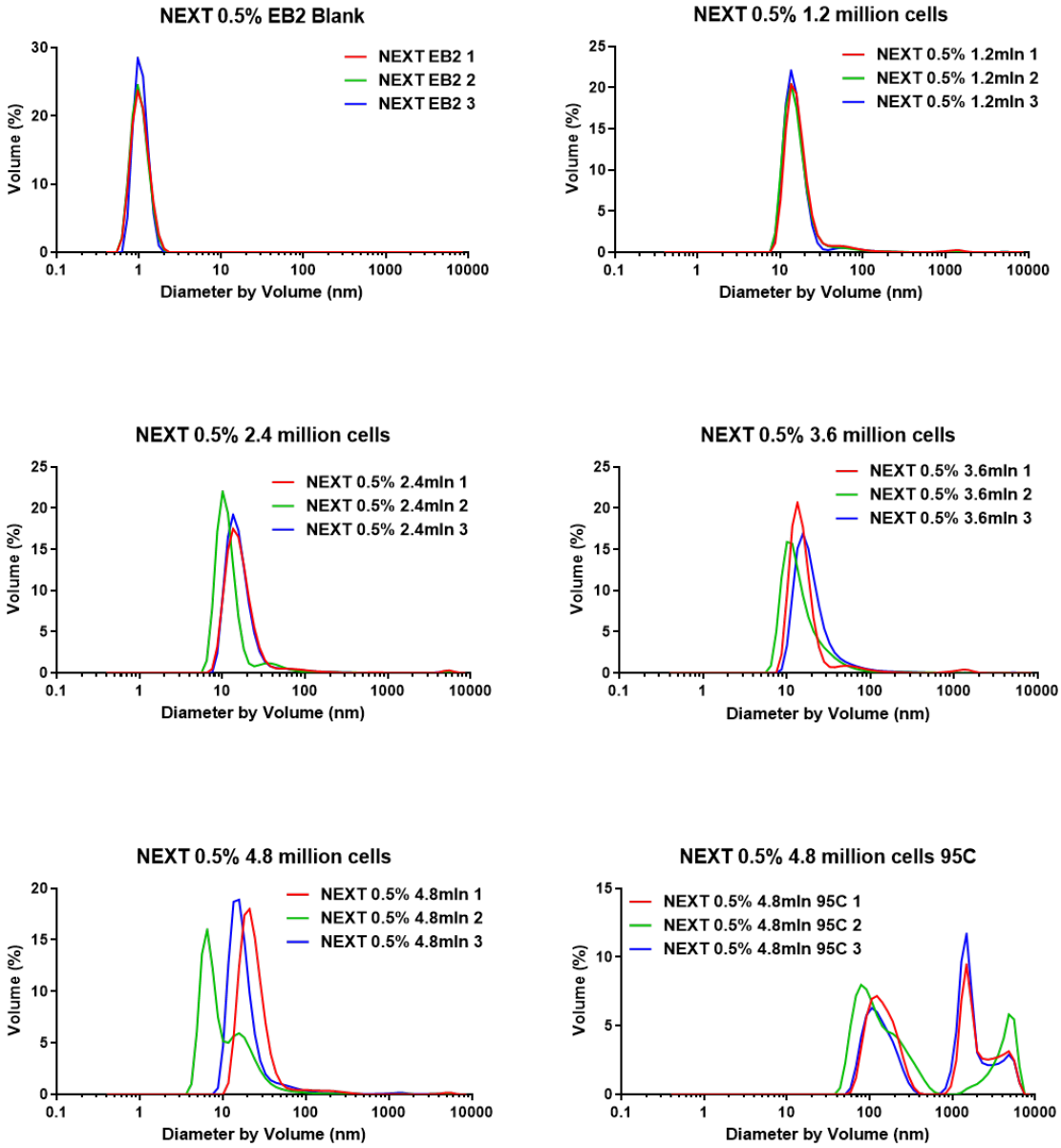


**Figure 13** DLS characterization of membrane protein extracts from KIT (A) NEXT 0.1% Triton (B) and NEXT 0.5% Triton (C).

## Membrane protein concentration and yield

The concentration and yield of proteins in the final extracts was assessed by BCA assay to evaluate the efficiency of membrane protein extraction by NEXT.

Figure 14A shows that all treatments yielded protein concentrations that increased linearly with the number of processed cells. The KIT extracts reached a maximum protein concentration (2.80 mg/mL) at 4.8 million cells. This was significantly higher than the concentration achieved by EB1

NEXT + EB2 NEXT Triton 0.1 %, which was 1.70 mg/mL with 4.8 million cells. Interestingly, EB1 NEXT + EB2 NEXT 0.5 % Triton yielded a protein concentration comparable to EB1 KIT + EB2 KIT (2.40 mg/mL at 4.8 million cells). This was in good correspondence with the turbidimetric data presented in Figure 12C, relating the better membrane solubilization to the higher final protein concentration.

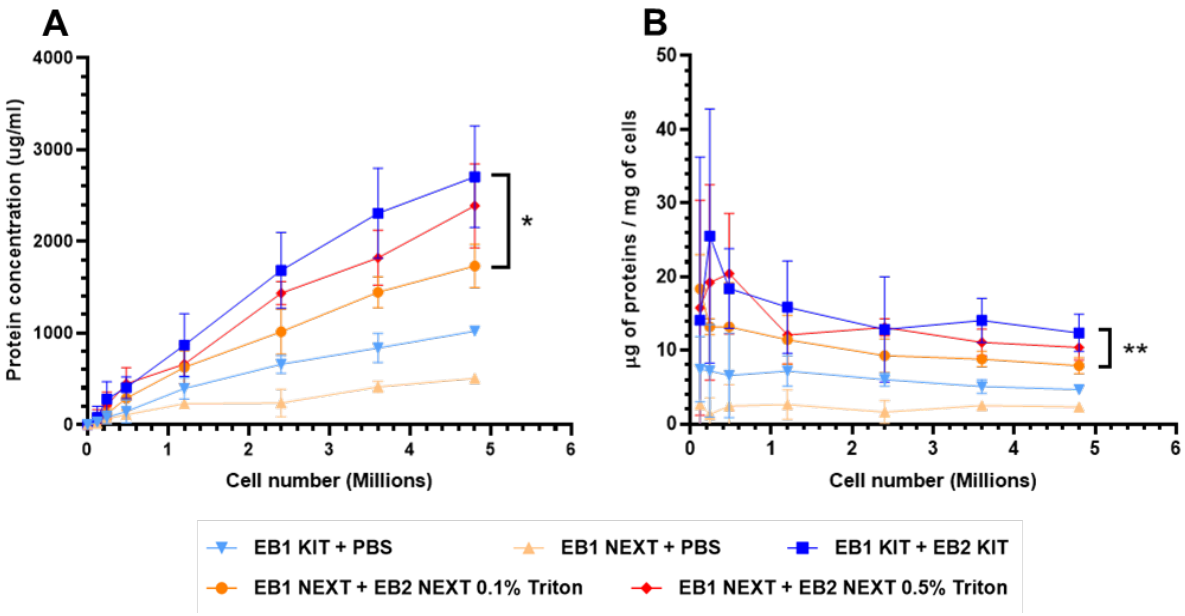


**Figure 14** A) Protein concentration profile estimated by BCA assay for the different membrane protein extracts; B) calculation of the relative membrane protein yield per mg of wet cell pellet for the different membrane protein extracts. (n=3 for all the graphs, error bars represent the standard deviation).

Notably, even the supernatant obtained from permeabilized cells contained a relevant amount of proteins. These proteins also increased linearly with cell number and corresponded to about 30 %, 25 % and 20% in the case of KIT EB1 + PBS and EB1 KIT + PBS, with respect to their extracted counterparts. The presence of proteins in the supernatant of non-solubilized cells could be a fraction of cytosolic proteins that was not completely removed in the previous passages. Accordingly, EB1 NEXT + EB2 NEXT 0.5 % Triton would yield protein extracts richer in membrane proteins than the EB1 KIT + EB2 KIT, and therefore purer.

The final protein yield was expressed as µg of proteins per mg of wet J774 cells pellet (Figure 14B). For all the tested conditions, the yield is mostly constant among different numbers of cells at the higher end of the tested range, with still significant differences between EB1 KIT + EB2 KIT (2.21 µg/mg of cells) and EB1 NEXT + EB2 NEXT 0.1 % Triton (0.78 µg/mg of cells). This confirms that the ratio between the extracted proteins and the original amount of biological material is roughly constant.

## Assessment of membrane proteins extracts purity

Despite EB1 NEXT + EB2 NEXT 0.5% Triton yielding a very similar final protein concentration to the KIT, it was essential to understand if NEXT can also achieve similar or improved membrane proteins purity into the extracts. To gain a first insight in this, we performed SDS-PAGE / Western blot analysis.

As a positive control for the presence of the wanted proteins, J774 complete cell lysate (TCL) was obtained by treating the cells pellets with RIPA buffer. A panel of proteins from different cellular locations was selected to gain clues on the general behavior of cellular components in the extractions. Specifically, CD11b is a cell membrane protein involved in leukocyte migration (163). Calnexin is a protein present in the endoplasmic reticulum and participates in proper protein folding (164). Nucleoporin (NP-62) is a protein located in the nuclear membrane (165). β-actin is an important component of the cytoskeleton (166). Finally, Glyceraldehyde 3-phosphate dehydrogenase (GAPDH) is a cytoplasmic protein involved in glycolysis (167).

In this analysis, only the cellular extracts obtained from higher number of cells were used (1.2, 2.4, 2.6 and 4.8 million cells), because the extracts from lower cells numbers had a concentration too low to be detectable using SDS-PAGE/Western blot. The analysis was performed directly comparing TCL, EB1 KIT and either EB2 NEXT 0.1 % Triton or EB2 NEXT 0.5 % Triton (Figure 15A) extracts, to assess the possible different effects of Triton X-100 concentration on extracts composition. Figure 15B shows the quantification profile for the analyzed proteins for NEXT 0.1 % Triton using ImageLab Software. The lane intensity for each condition was normalized by the TCL value.

For CD11b, KIT (Figure 15B) showed an increased purity with the number of cells up to five times the amount in TCL. This means that the percentage in CD11b increases by solubilizing more cellular membranes, leading to better purity. Conversely, CD11b in extracts from NEXT 0.1 % Triton (Figure 15B) shows a progressive decrease in its amount with increasing cell number (from 2.5 times TCL to the same amount). This could be due to the low amount of detergent. In fact, if too many membranes are present compared to the amount of detergent, they are not completely solubilized losing part of the proteins in the final centrifugation, reducing the efficiency of extraction. However, EB2 NEXT 0.5 % Triton extracts show a different profile. Figure 15G shows that CD11b increased with a very different profile from EB2 NEXT 0.1 % Triton. In fact, this protein present with a similar profile to the KIT (up to 5-fold compared to TCL), although to a lesser extent. This difference could be due to either a higher amount of detergent in KIT or to a higher affinity if CD11b for KIT detergents.

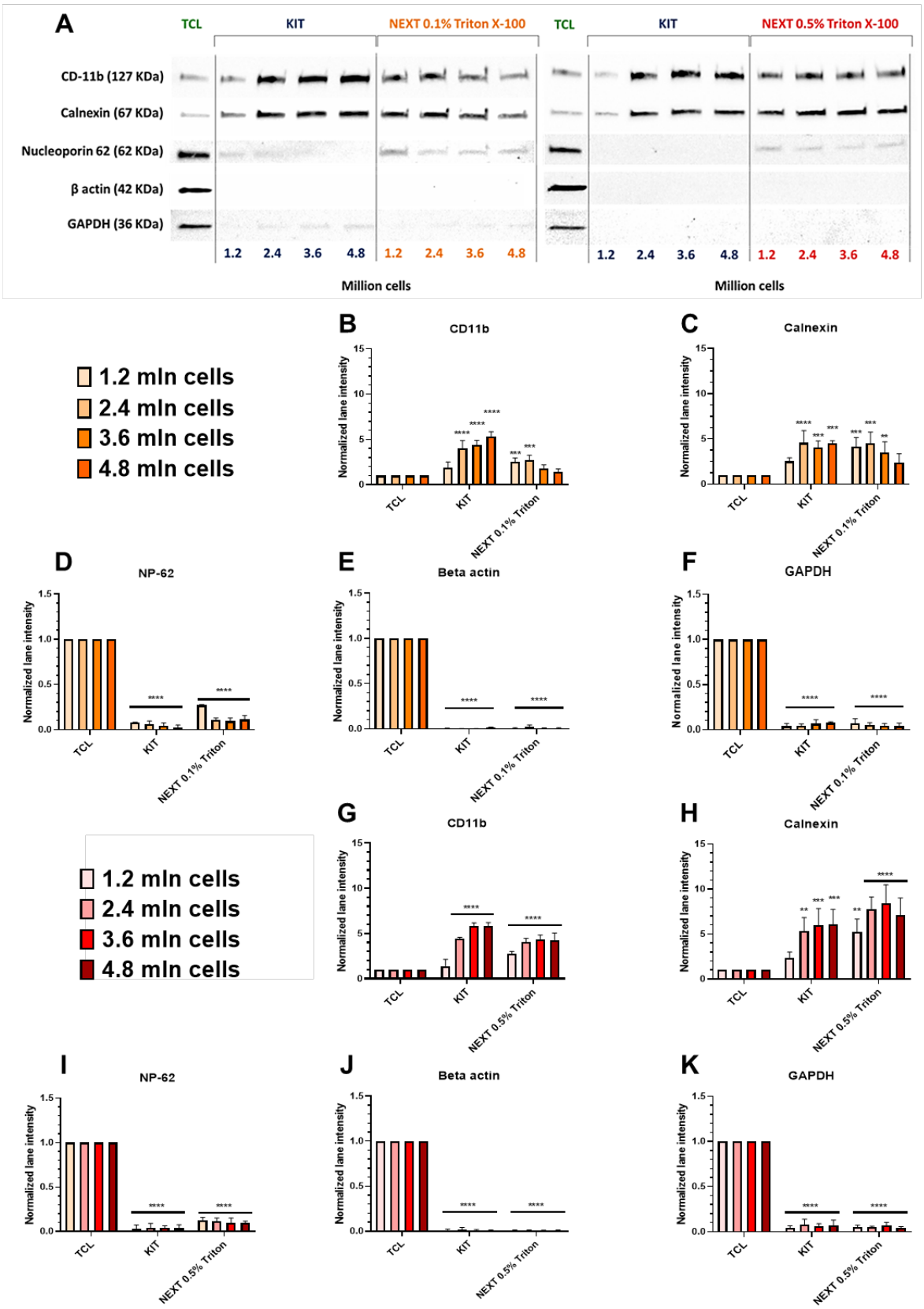


**Figure 15** A) SDS-PAGE / Western Blot profile of J774 cells lysed using RIPA buffer, and of J774 membrane protein extracts obtained from KIT, NEXT 0.1% Triton X-100 or NEXT 0.5% Triton X-100; B-K) Quantification of SDS-PAGE / Western Blot profile normalized lane intensity for membrane proteins extracts obtained from KIT and NEXT 0.1% Triton X-100; C) Quantification of SDS-PAGE / Western Blot profile normalized lane intensity for membrane proteins extracts obtained from KIT and NEXT 0.1% Triton X-100. (n=3 for all the graphs, error bars represent standard deviations; *= $p<0.05$; **=$p<0.01$; ***=$p<0.001$; ****=$p<0.0001$).

For Calnexin, the increase in purity in KIT derived extracts is less than for CD11b (Figure 15C, H, only up to 4.8-fold TCL). It appears that Calnexin is increased only to a maximum point. However, the reasons for this plateau are not clear. A similar decreasing profile is visible for NEXT 0.1 % Triton (Figure 15C, from 4-fould to 1.5-fold TCL with increasing cell number). It is interesting that Calnexin, despite not being in the plasma membrane, is still present in high amounts in all the final extracts, including KIT. This means the ER membrane in which Calnexin is integrated behaves similarly to the plasma membrane in presence of Triton, or that Calnexin itself has some structural motifs such as transmembrane domains that allow for its efficient extraction. Notably, Calnexin is much more present in EB2 NEXT 0.5 % (Figure 15H, increased 7 to 8-fold TCL) Triton than with EB2 NEXT 0.1 % Triton, and even more than KIT. This difference could be due to the higher amount of detergent in EB2 NEXT 0.5 % Triton than EB2 KIT or to the different efficiency of the KIT detergents. However, we do not know the composition of the latter.

Differently, NP-62 is almost completely absent from KIT extracts (Figure 15D, <10 % of TCL), evidencing a good removal of nuclear proteins, including the nuclear membrane ones. However, NEXT 0.1 % Triton and NEXT 0.5 % Triton extracts show some remnants of NP-62 are still present (Figure 15D, I, both around 10 % of TCL). This could mean that the nuclear membrane is more sensitive to Triton X-100 than the unknown detergents present in the KIT and therefore is partially solubilized.

β-actin was not detectable in any of the extracts (Figure 15E, J) indicating that cytoskeletal proteins are efficiently removed during the extraction. Similarly, GAPDH is almost completely removed by both protocols (Figure 15F, K), and only very faint signals are visible, suggesting an almost complete elimination of cytosolic proteins.

Taken together, these results suggest that the increase of Triton X-100 used in the extraction second step is critical to achieve good membrane proteins purity and can change the behavior of the proteins at increasing cell number.

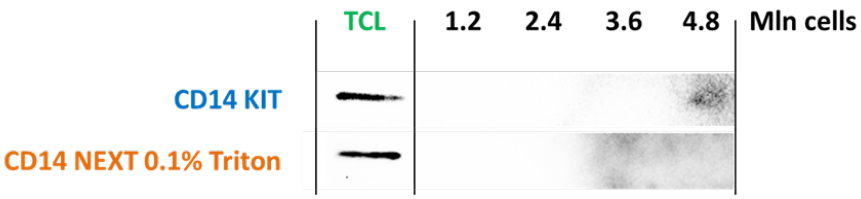


**Figure 16** SDS-PAGE/Western Blot profile of CD14 for KIT and NEXT 0.1% Triton.

Interestingly, CD14, a membrane protein involved in bacterial antigens recognition, was completely removed by both the KIT and NEXT derived extracts (Figure 16). This could depend on

the structural feature of CD14, which is a Glycosylphosphatidylinositol anchored protein (GPI-AP). This protein thus has no transmembrane domains but is linked to the plasma membrane through a phospholipid chain. Interestingly, GPI-APs tend to concentrate into plasma membrane patches defined as lipid rafts (168). Triton X-100, which is the detergent used in EB2 NEXT, was reported to not solubilize properly the lipid rafts, making them coalesce in detergent-resistant membranes (169).

These considerations could add another, unexpected level of complexity to the purification of membrane proteins. It was already demonstrated that different detergents tend to extract different sets of proteins depending on their association to lipid rafts (160). This complication, through adequate optimization, could become a novel tool to improve the proteins purity during the extraction, to exclude or concentrate lipid rafts-associated proteins.

## Translatability of the protocol to human cells

Considering the results obtained in membrane proteins purification, it is important to understand if this extraction protocol could be translated to other cells. To check this, THP-1 human monocytes were selected as a second cell line to test. These cells are different from J774 for several reasons: they are human cells, making their proteins of high interest for translational research; and they grow in medium suspension and not in adhesion. Validating NEXT in such a THP-1 cells would make it robust across potentially many different cell lines. To test THP-1 cells extraction, we selected 4.8 million cells as optimal condition, since it yielded the highest protein concentration.

Figure 17A shows the final protein concentration of THP-1 cells extracts compared to the ones from J774. The profile is very similar, with KIT (2.3 µg/mL for J774 and 2.1 µg/mL for THP-1) yielding a significantly higher concentration to NEXT 0.1 % (1.6 µg/mL and 1.55 µg/mL, respectively, $p<0.05$ using a p-test) and almost identical to NEXT 0.5 % (2.25 µg/mL and 1.9 µg/mL, respectively). The concentration of proteins in THP-1 extracts is slightly lower. This could be due to the slightly lower weight of the cells' pellets, which thus contain a generally smaller amount of proteins. This is confirmed by Figure 17B, since the yield of protein expressed by mass of protein/mg of wet cell pellet is almost identical to the one from J774 cells for the different protocols.

Following the previous workflow, Figure 17C shows the SDS-PAGE / Western Blot profile for these different extracts compared with THP-1 TCL, while Figure 17D shows their normalized quantification.

CD11b and Calnexin are both more present compared to TCL. Interestingly, the purity is much higher compared to J774 cells for both these membrane proteins. CD-11b is present 15-fold, 9-fold, and 13-fold more times than the TCL in KIT, NEXT 0.1 % Triton ad NEXT 0.5 % Triton,

respectively. Conversely, Calnexin is present 3.6-fold, 1.2-fold and 2.2-fold for KIT extracts, EB2 NEXT 0.1 % Triton extracts, and NEXT 0.5 % Triton extracts, respectively. Interestingly, NEXT 0.5 % yields a better purification in CD11b and Calnexin than EB2 NEXT 0.1 % Triton. Furthermore, CD11b is much more abundant than Calnexin, differently from what happened in J774 cells, where these two proteins were enriched in a narrower range. These observations underline how different cells can respond differently to the same extraction conditions.

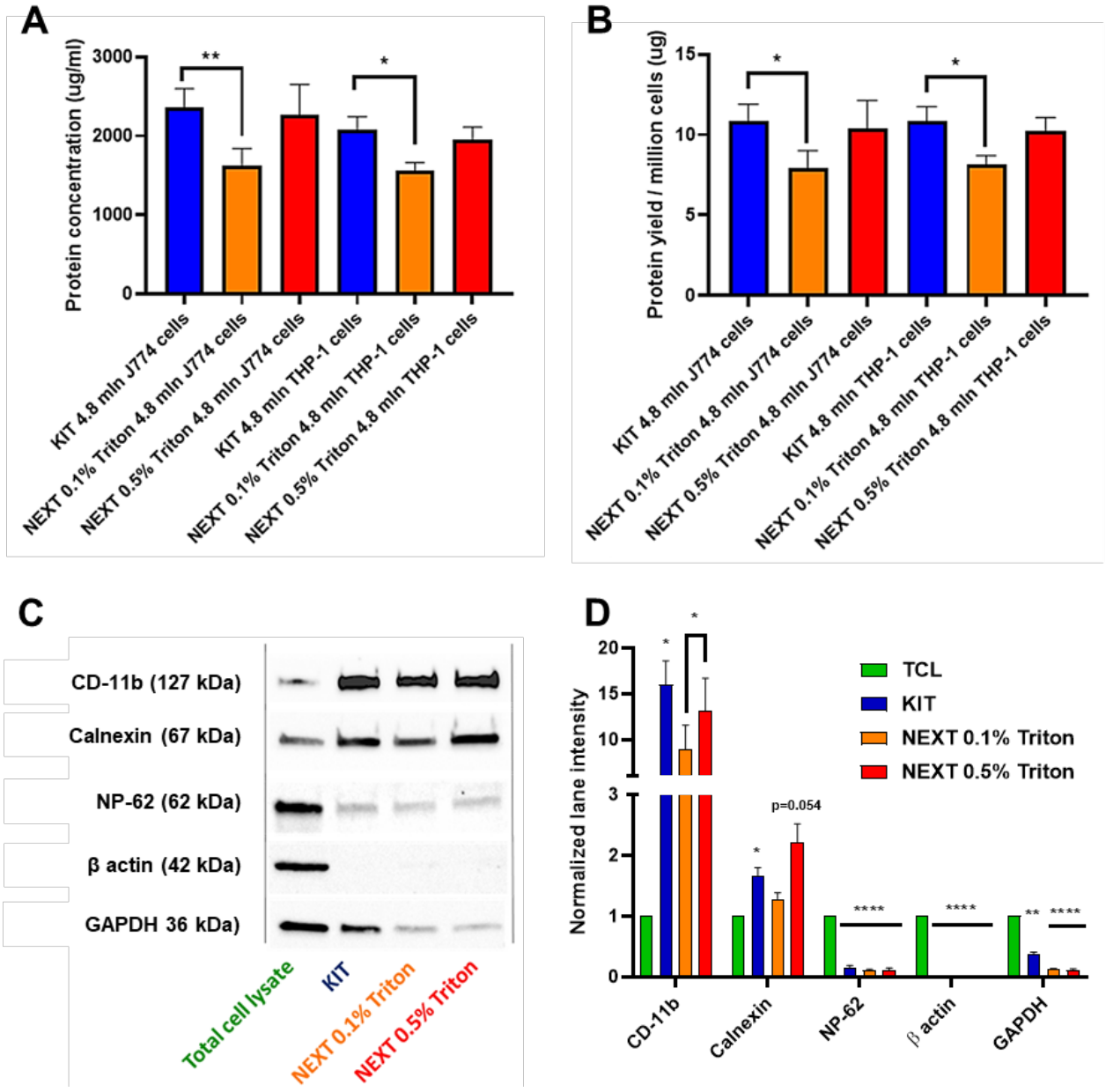


**Figure 17** A) Protein concentration of membrane protein extracts obtained from KIT and NEXT for 4.8 million J774 cells or THP-1 cells; B) Protein yield per milligrams of wet cell pellet of membrane protein extracts obtained from KIT and NEXT for 4.8 million J774 cells or THP-1; C) SDS-PAGE / Western blot profile of THP-1 lysed using RIPA buffer, KIT, NEXT 0.1% Triton X-100 and NEXT 0.5% Triton X-100; D) Relative quantification of THP-1 cells SDS-PAGE / Western Blot profile (n=3 for all the graphs, error bars represent standard deviations; *= $p<0.05$; **=$p<0.01$; ***=$p<0.001$; ****=$p<0.0001$).

NP-62 however is still present in low amount in all the tested protocols, including KIT (40 % of TCL signal). It is possible that THP-1 nuclear envelopes are more sensible to KIT detergents than J774, releasing a small amount of NP-62 in the extract. Conversely, β actin is not detectable in any tested extraction procedure, and GAPDH is also reduced in all three conditions. However, KIT present a significantly higher GAPDH presence than either NEXT 0.1 % Triton or NEXT 0.5 % Triton.

Taken together, these results evidence how the membrane protein extraction protocol can be easily translated without any modification across different cell lines, proving its robustness and versatility.

## Confirmation of Membrane Proteins purification via Mass Spectrometry:

To complement the semi-quantitative information on the protein composition obtained from SDS-PAGE and western blot, we employed qualitative mass spectrometry analysis. Mass spectrometry can elucidate the identity of hundreds of proteins present in the final extracts, giving us a broader overview of their actual composition.

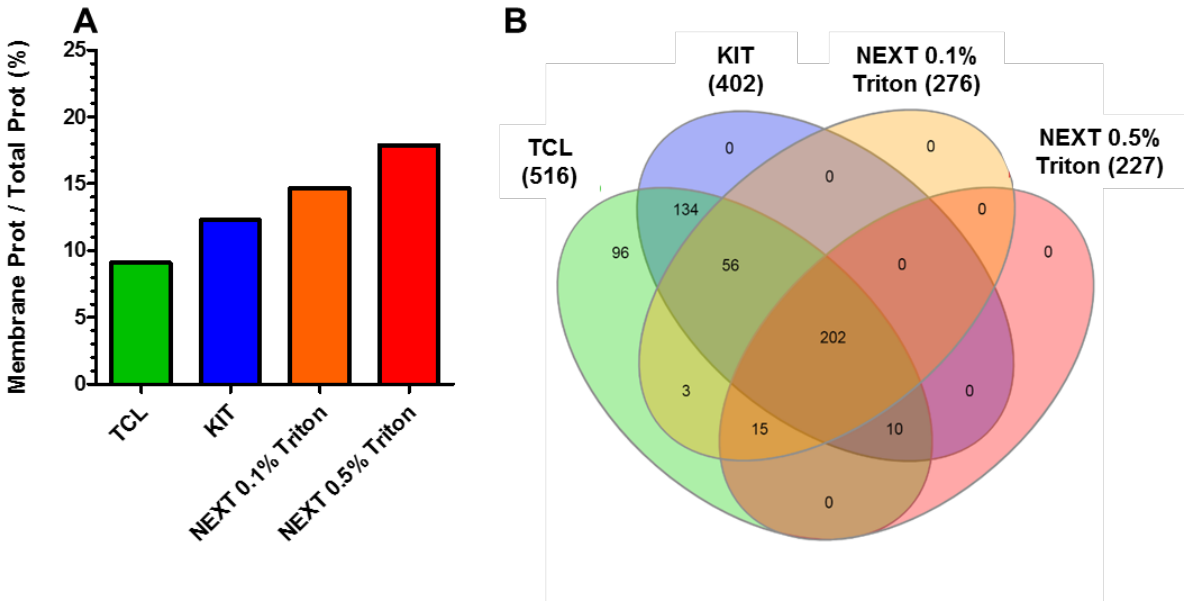


**Figure 18** A) Percentage of membrane proteins detected over the entire pool of proteins for TCL, KIT, NEXT 0.1% Triton, and NEXT 0.5% Triton for THP-1 cells B) Venn diagram presenting the common proteins among the TCL and the different THP-1 cells extracts. The Venn diagram was created using the InteractiVenn website. The data represent proteins that were present only for three different mass spectrometry measurements.

These data were used to test for membrane proteins enrichment using the informatic tool STRING (version 11.5). We used the TCL proteins as a background for enrichment. Despite not evidencing a specific network enrichment, it is interesting to note that the PPI enrichment p-value progressively decreased from TCL (PPI=1.0) to KIT extracts (PPI=0.0621), to NEXT 0.1 % and 0.5

% Triton (PPI=$3.48 \cdot 10^{-9}$ and $5.33 \cdot 10^{-15}$, respectively). This indicates that on a statistical level, the NEXT-derived extracts contain proteins that are somehow related among themselves when compared to the TCL background. However, this analysis does not provide information on the identity of the enriched proteins. To confirm this enrichment, we further analyzed the network by assessing the false discovery ratio for different cellular compartments. In this case, the false discovery ratio for the KIT extracts membrane proteins is 0.00052, while decreases to $6.33 \cdot 10^{-11}$ and to $6.57 \cdot 10^{-13}$. This demonstrated how the membrane compartment is enriched in all the extracts, and particularly in the NEXT-derived ones.

Finally, we manually validated these results by assessing membrane proteins present in all the tested extracts compared over all the identified proteins. As shown in Figure 18A, the percentage of membrane proteins for TCL was 9.1 %, for KIT was 12.3 %, for NEXT 0.1 % Triton was 14.7 % and 17.9 % for NEXT 0.5 % Triton. Ultimately, this confirms how the extracts contain in proportion more membrane proteins compared to TCL, and how NEXT membrane proteins are better purified that KIT, especially when increasing the amount of Triton in the final buffer. As presented in Figure 18B, all the extracts are fractions of TCL, as demonstrated by the absence of proteins exclusive to either KIT, NEXT 0.1 % Triton or NEXT 0.5 % Triton. Furthermore, KIT had 134 exclusively common proteins with TCL, while NEXT 0.1 % Triton and NEXT 0.5 % Triton 3 and 0 respectively. Of note, the NEXT extracts contained fewer overall proteins but also that the NEXT extracts are mostly subunits of KIT and that NEXT 0.5% Triton is even more restricted than KIT 0.1% Triton. Taken together, these data confirm that KIT and NEXT extracts for THP-1 cells are indeed more abundant in membrane proteins compared to TCL, and that NEXT 0.1 % Triton and especially NEXT 0.5 % Triton extracts are purer in their membrane protein contents. Despite this evidence, it is important to note that our analysis is limited by the qualitative nature of our technique, and further studies using more quantitative approaches could give more insights on the proportion of proteins from different cellular compartments.

## Optimization of Leuko using a Design of Experiment Approach

In many cases, the optimization of pharmaceutical formulations presents a daunting challenge, since even relatively simple processes can be affected by many variables, each one with its own contribution to the results. The need to control all these variables often leads to time consuming and very expensive screening studies.

Thus, a much more straightforward trial and error process is often employed. This strategy is cheap ant time efficient but does not provide much insight in the contribution of different

experimental parameters to the experimental outcome. Furthermore, the final solutions found through trial and error are not necessarily the best possible ones, since the scope of the study is quite narrow by its own nature. Furthermore, the large scope nor the trial-and-error screenings allow to understand the potential interplay among the experimental parameters involved.

Design of Experiment (DoE) strategy can overcome these limitations. DoE is a statistical approach that enables the creation of specific combination of qualitative and quantitative experimental parameters under investigations, creating an “experimental space” in which each dimension is represented by one of the experimental parameters (Figure 19A). These combinations are calculated within a specified range of parametric values and are arranged in a pattern that allows obtaining the maximum amount of information regarding the process while performing the minimum amount of experimental runs.

The selection of which DoE pattern to employ for an investigation is a critical choice, and depends on both the structure of the experiment, the number of experimental parameters that are included, and the intended result (170) Specifically, DoE can be used to:

- Understand which among the selected parameters is statistically relevant in determining the results of the process (screening objective).
- Create mathematical models that allow to predict the results based on the specific values of the selected parameters (response surface method objective).
- Troubleshoot, optimize or make more robust a specific process.

In this project, a single DoE was employed both to understand which variables are relevant for the formulation of Leukos and thus significantly influence the process output, and to optimize the process itself via the calculation of parameter that would yield desirable NPs features. This strategy has already been applied successfully on liposomes formulations (13).

To produce Leuko, the Nanoassemblr™ platform was selected. This instrument is based on a microfluidic chip in which two liquid, miscible phases are blended very quickly and efficiently by converging into a “herringbone” mixing device. The mixing of the two phases thus occurs within milliseconds. The principle upon which the Nanoassemblr™ allows the formulation of liposomes relies on the solubilization of lipids or hydrophobic polymers within the organic phase. When this solution mixes with the aqueous phase within the system, the overall polarity of the organic phase suddenly decreases due to the introduction of water. In turn, this increased polarity increases the free energy of the system and induces the self-assembly of the hydrophobic lipids into liposomes. This self-assembly combined with the shear stress caused by the microfluidics components breaks down

the newly formed vesicles into nanovesicles with a narrow size distribution (143).

Considering this approach for the formulations of Leuko, their hydrophobic components are specifically phospholipids and cholesterol, specifically Dipalmitoyl-phosphatidyl-choline (DPPC), dioleyl-phosphatidyl-choline (DOPC), and cholesterol. Among the many different lipid mixtures employed in the formulation of liposomes, a 4:3:3 molar ratio of DPPC: DOPC: Cholesterol, as indicated in the literature for these formulations (143). Thus, this mixture of lipids was dissolved in absolute ethanol in a total concentration of 10mg/mL. Ethanol was selected as a solvent since it is compatible with the Nanoassemblr$^{TM}$ cartridge material, it is easily miscible with water, it is easy to remove via dialysis, and is relatively biocompatible in the case some residues are still present within the final formulations.

On the other hand, the aqueous phase of Leuko is composed of a dispersion of membrane proteins derived from the previously optimized extracts in a 250mM ammonium sulphate buffer. This buffer was selected from previous studies to enable the loading of DOXO using the remote loading approach (171).

During the process of self-assembly occurring in the microfluidics system, lipid nanovesicles and the integration of membrane proteins in their phospholipid bilayer in a single step, ultimately forming Leuko.

Therefore, the main controllable experimental parameters to be optimized in this process are:

- Total for rate in the system (TFR), which is the speed of the overall flow of both phases within the Nanoassemblr$^{TM}$, expressed in mL/min

- Flow rate ratio between the aqueous and the organic phase (FRR), specifically the ratio between the speeds of the organic phase over the flow rate of the aqueous phase.

- The weight ratio between membrane proteins and lipids (Lip/Prot ratio). The mass of lipids was kept constant for simplicity, while the amount of proteins in the aqueous phase was modulated to a specific ratio and was further adjusted by taking into account the FRR. For the formulation of Leuko, THP-1 cells human membrane protein extracts were employed.

| ***Experimental Run*** | **TFR (mL/min)** | **FRR (acq/org)** | **Lip/Prot Ratio** |
|---|---|---|---|
| *1* | 5.5 | 3 | 160 |

| | | | |
|---|---|---|---|
| *2* | 1 | 3 | 20 |
| *3* | 5.5 | 1 | 300 |
| *4* | 1 | 3 | 300 |
| *5* | 10 | 5 | 160 |
| *6* | 1 | 5 | 160 |
| *7* | 10 | 1 | 160 |
| *8* | 5.5 | 5 | 300 |
| *9* | 1 | 1 | 160 |
| *10* | 10 | 3 | 20 |
| *11* | 5.5 | 5 | 20 |
| *12* | 10 | 3 | 300 |
| *13* | 5.5 | 1 | 20 |

**Table 4:** Different experimental parameters combinations generated to perform a single run of DoE for Leuko optimization.

To create the DoE for screening and optimization, the selected range of values for the experimental parameters was: TFR between 1 and 10 mL/min, FRR from 1:1 to 5:1 (aqueous/organic phase), and Lip/Prot ratio from 300:1 to 20:1. Using the Stat Graphics Centurion XIX software, a three level, randomized, Box-Behnken design with three replicates and five center points was generated. The entire set of combinations for a single replicate is listed in Table 4, the visual representation of the design space is presented in Figure 19A. The prediction variance analysis graph (Figure 19B) demonstrated a completely symmetrical trend in variance. This feature of DoE is defined as rotatable. As indicated by the graph, the variance of the design increased from the center of the design. This indicates how the accuracy of the predictions offered by DoE tends to decrease from the center of the experimental space. Furthermore, the symmetry of the variance represents how the design is *per se* unbiased in any direction, giving similarly accurate predictions across all the dimensions of the experimental space. After performing all the experimental runs, all Leuko formulations were dialyzed against PBS to remove ethanol and were characterized using DLS to measure their average size by intensity, their polydispersity index (PDI) and their zeta potential. Zeta potential was used as a proxy for membrane protein integration, since the previous studies on similar formulations evidenced how the integration of membrane proteins onto Leukos decreases the particles zeta potential compared to liposomes with the same composition (138; 137; 172). Using the software, the experimental results were analyzed to understand the influence of experimental parameters or their combinations on the different responses taken into consideration. For the size by

intensity, the only relevant factor appeared to be FRR (Figure 19C), whose increase decreased the particles size. For zeta potential, as expected, the most relevant variable was the Lip/Prot ratio (Figure 19E); specifically, increasing the ratio also increased the zeta potential and vice versa, therefore making it more negative with the increase in proteins. Finally, PDI was influenced by both TFR and FRR and interestingly, their combination as well (Figure 19G), increasing with them. The experimental data were interpolated to create response surfaces for the results, which allow seeing the overall trend in each one depending on the selected variables (Figure 19D, F, H). The creation of response surfaces allows the extrapolation of optimal values of experimental factors for a specific desired outcome.

In the case of Leuko formulation, the desired features for these particles are:

- A diameter in the nano range (between 20 and 200nm specifically) that allows for their long circulation in the blood after IV injection (173). For this formulation, a desired size of 150 nm was selected as the target.
- A low PDI (around or below 0.2) that makes the formulation homogeneous in size and thus with reproducible features and behavior. Thus, the selected PD response was the lowest value within the tested range.
- A low zeta potential. This could appear counterintuitive since most of the literature shows how neutral or slightly negatively charged particles are normally the one with longest circulation time. However, as previously stated, the surface charge of our particles was used as an indication for the presence of membrane proteins on their surfaces. Thus, a minimized zeta potential would correspond to a high protein loading efficiency.

After providing all these formulations to the software, the calculated optimized values were a TFR=1 mL/min, a FRR=4.88, and a Lip/Prot Ratio of 1:20. The software also predicted the expected values of Size, PDI and zeta potential at 150 nm, 0.31 and -25mV, respectively. The overall optimization yielded an overall desirability of 85% of the selected responses (Figure 19I, J). To confirm the validity of these predictions, the optimized parameters were used to formulate actual Leukos. As a negative control, Lipos with the same lipid composition but without membrane proteins in their formulations. Each time, Lipos and Leukos were prepared starting from the same lipid batches and buffers. This control does not only allow to maintain constant all the features of the formulation but also enables to evidence possible discrepancies in NPs behavior and features that can be ascribed to the presence of the membrane proteins themselves. After performing these experimental runs, Lipos and Leukos were analyzed using DLS.

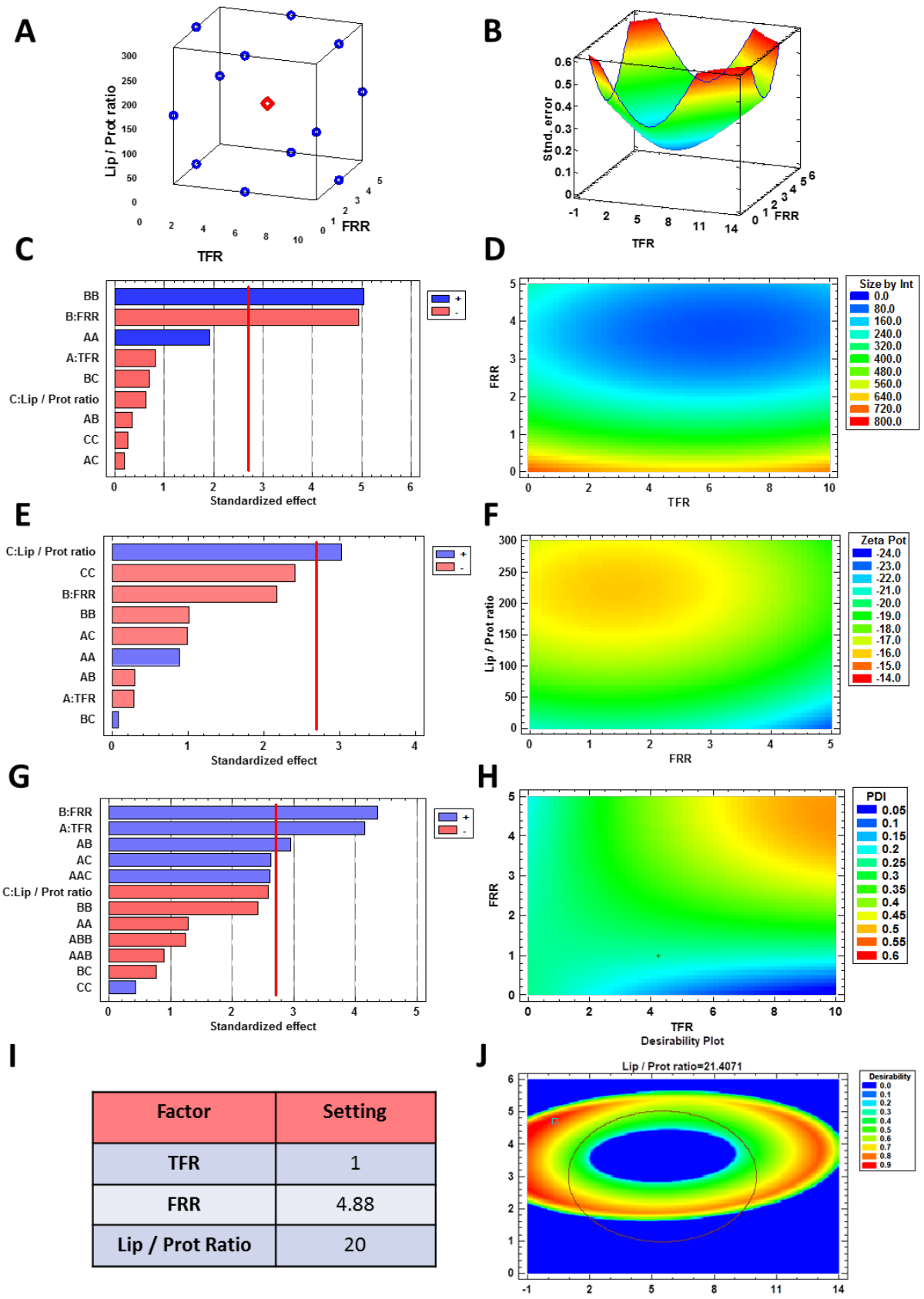


| Factor | Setting |
|---|---|
| TFR | 1 |
| FRR | 4.88 |
| Lip / Prot Ratio | 20 |

**Figure 19** A) Schematic representation of the DoE used for Leuko optimization. B) Analysis of variance used for the DoE. C, E, G) Standardized Pareto Chart for statistical significance of the experimental parameters. D, F, H) Response surface fitted for each analyzed response. I) optimized experimental parameters derived from DoE. J) Desirability plot used to extrapolate the optimized experimental parameters values. (n=3 for all the performed experiments).

Figure 20A shows that the average size by intensity for both Lipos and Leukos was around 137±34 nm and 159±28 nm, respectively.

Conversely, the PDI was 0.179±0.017 for Lipos, while was slightly higher for Leukos (0.237±0.021 Figure 20B). Finally, the zeta potential for Lipo set around -13.6±2.4 mV, while for Leuko it was significantly lower (-24.7±3.4 mV, Figure 20C).

Taken together, these data confirm the reliability of our predictions as calculated by the DoE-derived mathematical model. The number of particles per mL of suspension was also measured using nanoparticle tracking analysis (NTA) via the Nanosight™ equipment. As presented in Figure 20D, Lipos and Leukos had a number of particles $4.8\pm0.17\bullet10^{11}$ particles/mL and $4.45\pm0.24\bullet10^{11}$ particles/mL, respectively.

The PDI value of Leukos was still considered to be above the acceptable threshold of 0.200. To reduce it, particles after dialysis were filtered using a PVDA filter with a 0.22μm cutoff.

This procedure had the dual convenient effect of removing the big particle aggregates from the suspensions, ultimately reducing the PDI, and sterilize the particles when performed in sterile conditions. Interestingly, the filtration managed to decrease the size of both Lipos and Leukos down to 100±21 nm and 99±22 nm. The PDI was lowered to 0.186±0.011 also for Leukos and at the same time, the difference between the zeta potential of Lipos (-14.0±2.4mV) and Leukos (-22.3±2.5mV) and their particles number ($5.3\pm0.3\bullet10^{11}$ particles/mL and $5.2\pm0.5\bullet10^{11}$ particles/mL) was retained, despite a small reduction in the absolute Leuko surface charge.

Finally, fluorescent Lipos and Leukos (Lipo Cy5.5 and Leuko Cy5.5, respectively) were formulated by adding to the lipid phase a fraction of Cy5.5 conjugated phosphatidylethanolamine (Cy5.5-PE) corresponding to 0.5% of the total lipid mass used form the formulation. These formulations were characterized using DLS and Nanosight™, confirming that their size, PDI, zeta potential and particle number were consistent with the other formulations. The Cy5.5 fluorescence of labelled Lipo and Leuko was measured using a plate reader. For both formulations, the fluorescence was very consistent. This feature is important to later quantify these particles uptake in later *in vitro* uptake on cell cultures (Figure 20E).

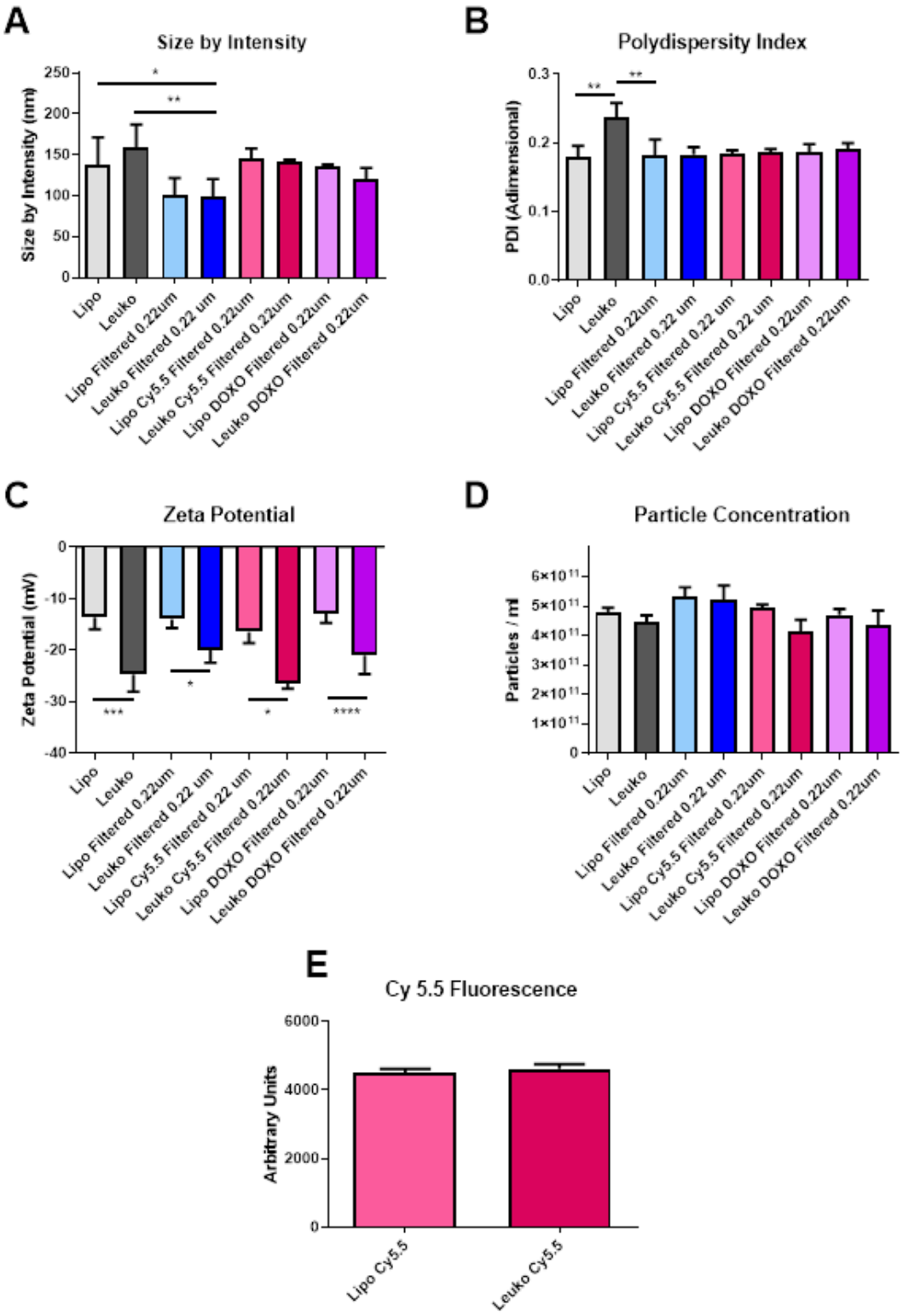


**Figure 20** Size by intensity (A), polydispersity Index (PDI, B) and zeta potential (C) measured by DLS for the different Lipo and Leuko formulations. D) Particles concentrations estimated by Particle tracking analysis using the Nanosight™ platform. E) Fluorescence of Lipo Cy5.5 and Leuko Cy5.5 measured by plate reader. (*: $p<0.05$; **: $p<0.01$; ***: $p<0.001$; ****: $p<0.0001$, n=3 for all the performed experiments).

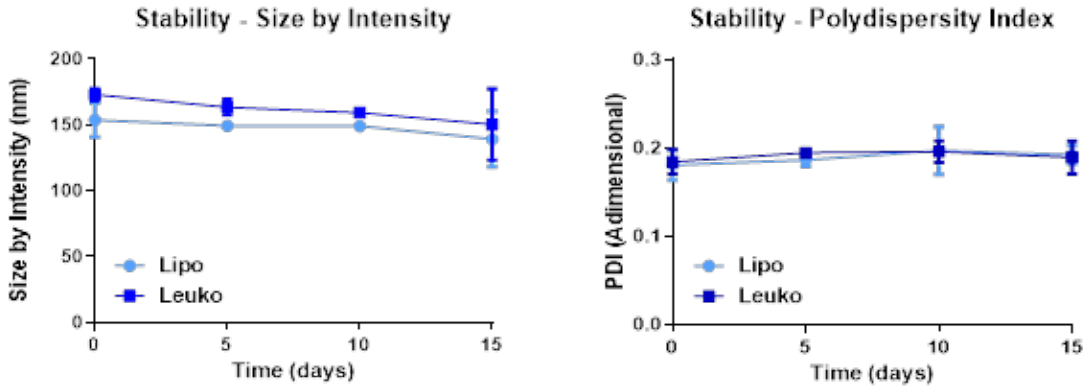


**Figure 21:** Size by intensity (left) and PDI (right) of Lipo and Leuko measured over 15 days of storage in PBS solution, at 4°C. (n=3 for all the performed experiments).

Lipo and Leuko stability under 4°C storage conditions were also assessed with DLS over 15 days, demonstrating that the NPs size and PDI did not change significantly over time (Figure 21A, B, respectively).

To assess both the presence of membrane proteins onto the surface of Leukos, these particles were analyzed using flow cytometry and a panel of antibodies for different surface markers of different immune cell types.

The fluorescence signal of Lipo was subtracted from the one of Leukos to consider the small amount of unspecific antibody binding onto the base lipid surface of Lipos. Since all the antibodies are used normally to identify markers onto the surface of cells and EVs, they are specific for the extracellular domains of the proteins and thus confirm both the presence and the correct orientation of specific molecules.

As shown in Figure 22A, Leukos presented on their surface general markers for leukocytes (CD45) (174), markers for T cells (including CD3, CD8, and HLA-DR) (175), markers for NK cells (CD56) (176), for monocytes (CD40, CD86a and CD1c) (177), for B cells (CD20) (178). This can appear quite puzzling, since the starting material used for membrane proteins extractions were human THP-1 monocytes. However, it is important to remember that THP-1 cells are not primary monocytes, but a stabilized cell culture derived from acute monocytic leukemia and thus are able to aberrantly express many different markers that are not normally associated to healthy monocytes (179). Nevertheless, it is important to note, as presented Figure 22B that Leukos also present on their surface proteins involved in vessels adhesion (CD29 and CD44) (180; 181), which are paramount for their efficient adhesion to the endothelial cells lining the inflamed blood vessels as well as molecules related to activated endothelia (CD146) (182), platelet activation (CD62p and CD42a) (183), and

monocytes activation (CD40 and CD69) (184; 185).

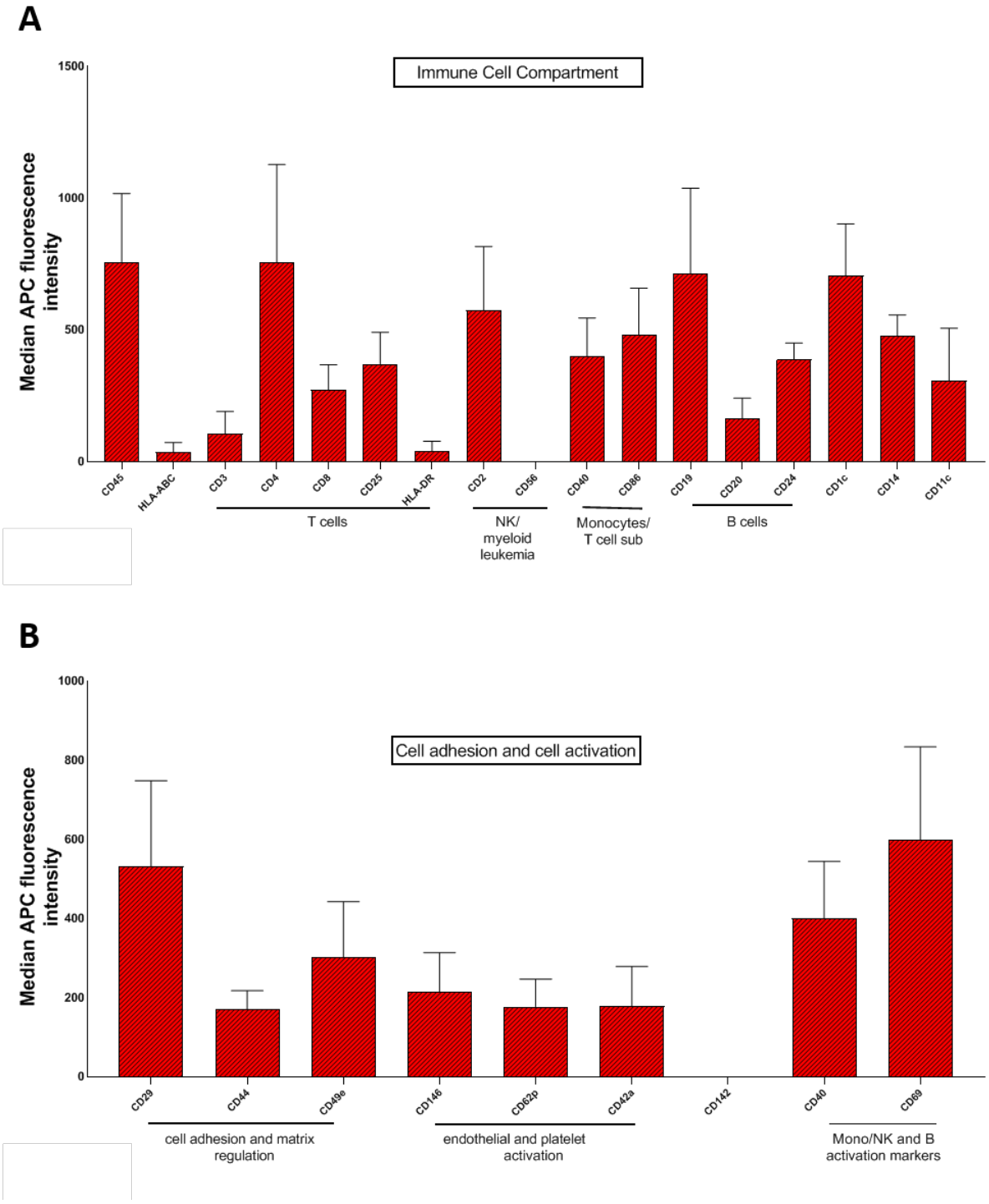


**Figure 22** Flow cytometry analysis of Leuko Markers for immune cells (A) and molecules involved in cells adhesion and activation (B). (n=3).

Despite this approach offering important information regarding the composition of Leuko surface, it is important to note that it has some limitations. Specifically, flow cytometry does not provide information over the overall amount of proteins loaded onto Leukos compared to the starting proteins. Furthermore, this technique can confirm the orientation of the proteins, but does not say how

many are correctly oriented compared to the total amount present onto the NPs. Nevertheless, previous studies using similar flow cytometry and computational approaches demonstrated how most proteins onto Leukos are correctly oriented due to a mixed effect of steric hindrance and lipids membrane curvature (186).

## DOXO loading into Lipo and Leuko using a remote loading strategy

DOXO is an antitumor drug used against many different neoplasms. This molecule can exert its cytotoxic effect via multiple molecular mechanisms, including DNA intercalation, causing oxidative stress to the cells, and activating several signaling pathways that in turn lead to cell death (187). Furthermore, this drug has a low molecular weight (543.52 g/mol), and thus can easily permeate the cells membrane to reach the cells intracellular target via diffusion and it is very soluble in water, a feature which allows the administration of high doses via intravenous injection.

However, many tumors are characterized by multidrug resistance. This phenotype can be enabled by several mechanisms, including the overexpression or mutation or drugs intracellular target, the use of alternative signaling pathways to evade or compensate for the drug action, or even by the expression of extrusion pumps onto the plasma membrane that quickly remove the drug from the cytosol, significantly reducing their cytotoxicity (188). Since DOXO is a traditional chemotherapeutic with multiple and pleiotropic effects on cells biology, the first two mechanism of resistance mentioned above are somewhat overcome by this molecule. However, DOXO is still a substrate for extrusion pumps. When DOXO is loaded within NPs, its uptake follows the same mechanism of the particles, which are internalized normally by endocytosis or phagocytosis, depending on their size, shape, surface proprieties, and on the cell type in study (189). Remarkably, DOXO has been previously encapsulated with success into liposomes in already clinically approved nanoformulations including the first approved NPs for the treatment of tumors (Myocet™), and their PEGylated version (DOXIL™ and CAELYX™) using a remote loading approach.

This technique allows the fast, reliable and efficient loading of DOXO and other small molecules drugs by creating a pH gradient between the external environment (pH=7.4) and the internal aqueous core of nanovesicles (pH=6.5). DOXO is a small molecules low molecular weight and this can permeate the vesicles phospholipid bilayer and reach the hydrophobic core. However, when DOXO molecules meet the acidic pH within liposomes, they become positively charged, losing the ability to permeate the phospholipid bilayer due to their increased polarity. This mechanism is normally defined as “ionic entrapment”. Furthermore, the ionized DOXO molecules in presence of sulphate ions spontaneously precipitate into DOXO sulphate nanocrystals within the nanovesicles. The combination of these equilibria has the net effect of “pulling” DOXO molecules within the

liposomes in high amount. Furthermore, the formation of DOXO sulphate crystals allow the packing of a high amount of drug within a very small volume, ultimately leading to high encapsulation efficiency (190).

DOXO loading thus was performed by testing different ratio between amounts of Lipos or Leukos, expressed as lipid concentration calculated using the Stewart colorimetric assay, and the amount of DOXO used. The incubation was performed by simply mix the empty NPs suspension and DOXO solution (1 mg/mL), and keeping it under stirring for two hours at 37ºC, according to most protocols used in the literature (172). After incubation, the DOXO that was not encapsulated was removed by dialysis overnight at 4ºC, using a Float-A-Lyzer™ system with a 300 kDa molecular weight cutoff. The low temperature of dialysis was used to avoid any drug leakage from the particles during dialysis, keeping the lipids of composing Lipos and Leukos in their "solid" state. After DOXO loading, the particles were characterized again via DLS and Nanosight™, confirming no significant changes in their features compared with empty Lipos and Leukos.

The amount of DOXO loaded within the particles was then calculated using a fluorimetric assay. DOXO is characterized by a high intrinsic fluorescence, which is linearly proportional to its concentration within a limited range. Of note, measurement of DOXO loading was performed after filtration to take into account possible drug retention from the filter.

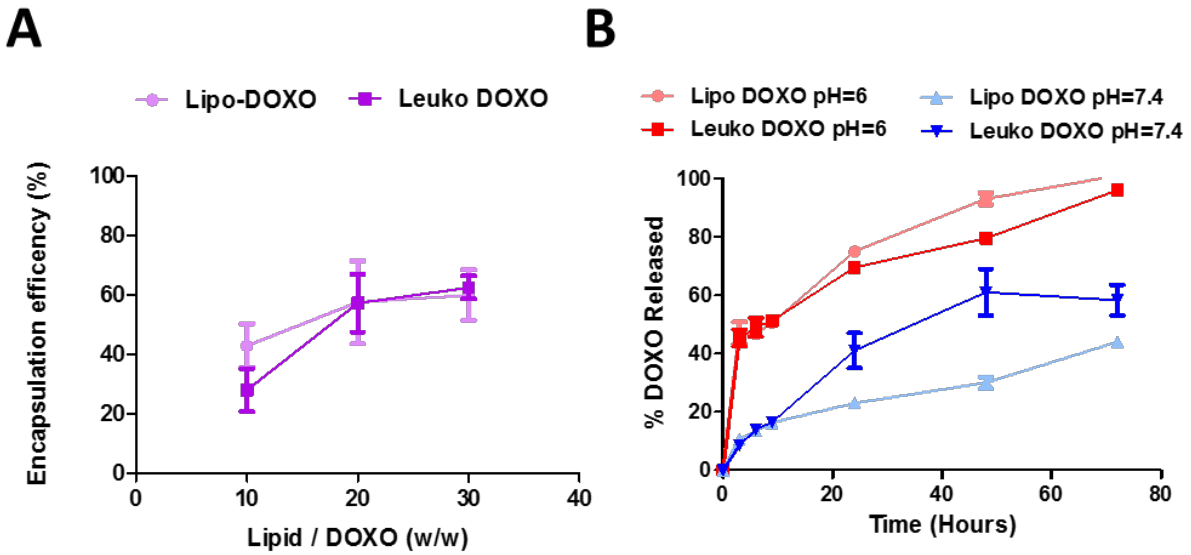


**Figure 23:** A) Encapsulation efficiency of DOXO profile for Lipo and Leuko at different Lipids to DOXO ratios. B) DOXO release profile from Lipo DOXO and Leuko DOXO at pH=7.4 and pH= 6. (n= 3 for all the performed experiments).

However, the DOXO loaded within Lipos and Leukos is present mostly in crystal form, which quenches its fluorescence significantly compared to the free drug (172). Thus, detergents are can be used to disrupt the particles membranes. In turn, this causes the dissolution of the DOXO sulphate

crystals and de-quenches DOXO fluorescence, making it measurable. This approach thus is normally termed as “fluorescence dequenching”. To disrupt our Lipos and Leukos, 0.2% v/v Triton X-100 mixed in a 1:1 volume ratio to a final concentration of 0.1% Triton X-100 was used. After a short stirring DOXO fluorescence was then measured and the encapsulated DOXO was calculated using calibration lines for DOXO dissolved in water or 0.1% Triton X-100 and divided by the initial amount of incubated DOXO to calculate the encapsulation efficiency, expressed as: mg of encapsulated DOXO / initial DOXO•100.

As presented in Figure 23A, the tested lipids to DOXO ratio for drug loading were 10:1, 20:1, and 30:1 (w/w). Interestingly, the encapsulation efficiency tended to increase with the increasing of the ratio. This may appear counterintuitive, since decreasing the relative amount of DOXO results in more of it to be loaded. However, it is important to note that the available space for DOXO encapsulation within the nanovesicles is quite limited and is a very small fraction of the overall NPs suspension. Thus, incubating a very high amount of drug would lead to reaching a maximum of encapsulated DOXO amount, with a high fraction of the drug that is in excess and not successfully loaded within the NPs. Thus, decreasing the total amount of DOXO, it is possible to reduce this excess without compromising the amount of loaded drug, ultimately increasing the encapsulation efficiency. Thus, the lipids to DOXO ratio that was selected for further investigation was 20:1 since it yielded the highest encapsulation efficiency without reducing the DOXO amount too much (55±11% for Lipos and 56±7% for Leukos).

After optimizing DOXO loading, the next step was to assess its release kinetics. To assess this, DOXO loaded Lipos and Leukos were diluted 1:50 in PBS 1X supplemented with 10% v/v of FBS. The presence of FBS was necessary to better replicate the composition of cell culture medium used in further studies. Conversely, PBS 1X was used to replace cell culture basal medium since it contains high amount of phenol red ad pH indicator, which is intrinsically fluorescent and could cover the DOXO signal.

After dispersion, the NPs were then kept on a thermomixer under mild stirring and at 37ºC. At different time points, the suspension was briefly removed from stirring, resuspended via delicate pipetting, and a small aliquot was withdrawn for measurement. DOXO release was measured via fluorimetry. In particular, the released DOXO was measured just by measuring the fluorescence within the aliquot, while the total amount of DOXO within the aliquot was measured via fluorescent dequenching as previously discussed. Thus, the percentage of released DOXO was calculated as the ratio between the released drug and the total DOXO in the suspension, multiplied by 100.

The release was tested for Lipos and Leukos at pH 7.4 to simulate the physiologic pH of the cell culture media and biological fluids, and at pH 6.0 to simulate the conditions of the intracellular lysosomes after NPs uptake. As presented in Figure 23B DOXO release for Lipos and Leukos at pH 6.0 was quite fast, and complete release was achieved within 72 hours. Conversely, the release was significantly slower for both NPs formulations at physiological pH.

This confirms that DOXO sulphate crystals within the NPs dissolve when exposed to acidic pH. This is especially useful since after the particles are internalized by cells via endocytosis, they are normally trafficked to the lysosomal compartment, in which the pH reaches values down to 5.5. In these conditions, the DOXO crystals dissolve and the drug is released within the cells cytosol where it can exert its cytotoxic effect.

Conversely, at the physiologic pH value of 7.4 found in the blood circulation, DOXO is retained within the particles, avoiding the unwanted leakage of drug during NPs circulation that could lead to systemic off target adverse effects. However, it is notable that the release of DOXO from Leukos is significantly faster than bare Lipo. This could be due to the presence of membrane proteins on the surface of Leuko, which could partially disrupt the phospholipids and cholesterol bilayer, making the drug leakage slightly faster.

Nevertheless, it is important to note that most DOXO is retained by both Lipos and Leukos within 24 hours. Since almost all of the NPs are normally cleared from systemic circulation in less than 24 hours, we can expect that both Lipos and Leukos would have already reached their target tissue or have been removed by filtering organs before their release DOXO into the systemic circulation. Ultimately, these studies demonstrate how DOXO can be efficiently loaded within our new biomimetic nanovesicles formulations and is released following a pH dependent and gradual trend.

### *In vitro* assessment of Lipo and Leuko Uptake and Cytotoxicity by tumor cells

After performing the complete characterization of Leukos, it is important to assess their uptake by tumor cells. This is paramount since the endocytic uptake of Leukos is necessary to ensure the internalization of the loaded DOXO cargo, leading to its improved efficacy compared to the free drug.

Cy5.5-labelled fluorescent Lipos and Leukos (Lipos-Cy5.5. and Leukos-Cy5.5) were used to trace and quantify their uptake rate. Thus, CRC HCT-116 cells and osteosarcoma SAOS-2 cell lines were seeded incubated with $5 \bullet 10^9$ particles/mL suspended in complete cell culture medium. At different time points, the medium was removed, cells were stained with DAPI to label their nuclei,

and then were live imaged using a fluorescence microscope.

As shown in Figure 24A and 25A, the Lipos-Cy5.5 and Leukos-Cy5.5 (in red in the fluorescence channel) were internalized by cells even at 6 hours from the initial incubation, as confirmed by the presence of particles within the intracellular space observed in the bright field (BF) channel.

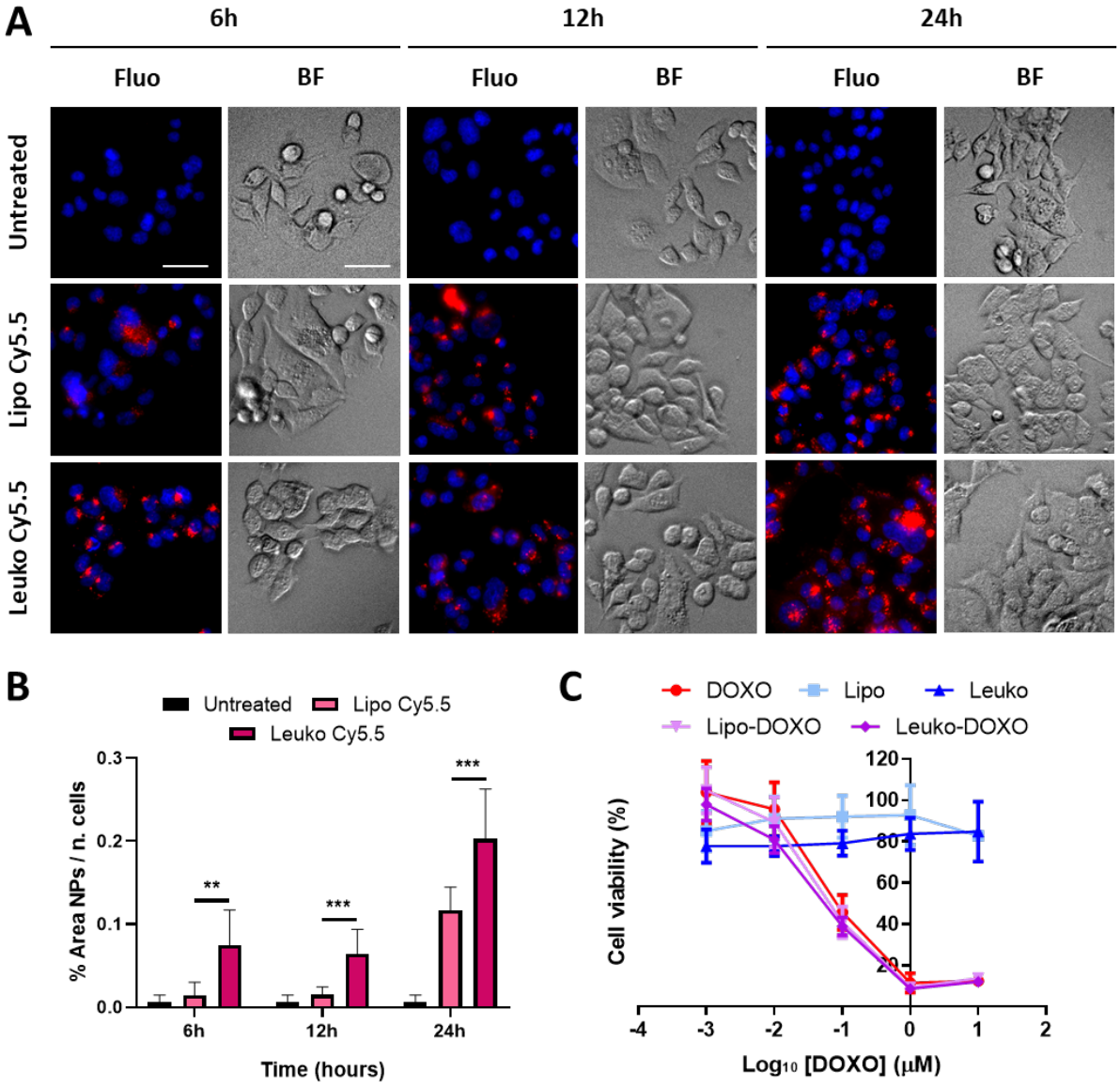


**Figure 24** A) Fluorescence (Fluo) and respective bright field (BF) mages of HCT-116 cells cultured onto flat plates treated with either Lipo Cy5.5 or Leuko Cy5.5 for 6, 12, and 24 hours. B) Quantification of Lipo and Leuko fluorescence at different time points during uptake. C) Resazurin cell viability assay results for DOXO, Lipo, Leuko, Lipo DOXO, and Leuko DOXO on HCT-116 cells. (*: $p<0.05$; **: $p<0.01$; ***: $p<0.001$; ****: $p<0.0001$, n= 3 for all the performed experiments).

Furthermore, the NPs derived fluorescence in all time points appeared as cytosolic fluorescent dots. Since the size of single particles is too small to be visualized by an optical microscope, it is very likely that Lipos-Cy5.5 and Leukos-Cy5.5 are clustered within some form of intracellular

compartment. The most likely hypothesis is that our NPs follow the same fate as many other formulations, and after endocytosis, they are trafficked to the lysosomal compartment. However, the precise identity of this compartment should be defined using *ad hoc* intracellular markers. Another interesting observation is that the NPs signal tends to concentrate in the perinuclear region, which is very suitable for the released DOXO to exert its cytotoxic effects on the tumor cells' DNA.

It is important however also to quantitatively compare the uptake rate of Lipo Cy5.5 compared to Leuko Cy5.5 to see if the presence of membrane proteins can influence the kinetics of NPs uptake. To perform this, NP fluorescence was measured using the FIJI software and was normalized dividing it by the number of cells, that was calculated automatically by counting the fluorescent nuclei.

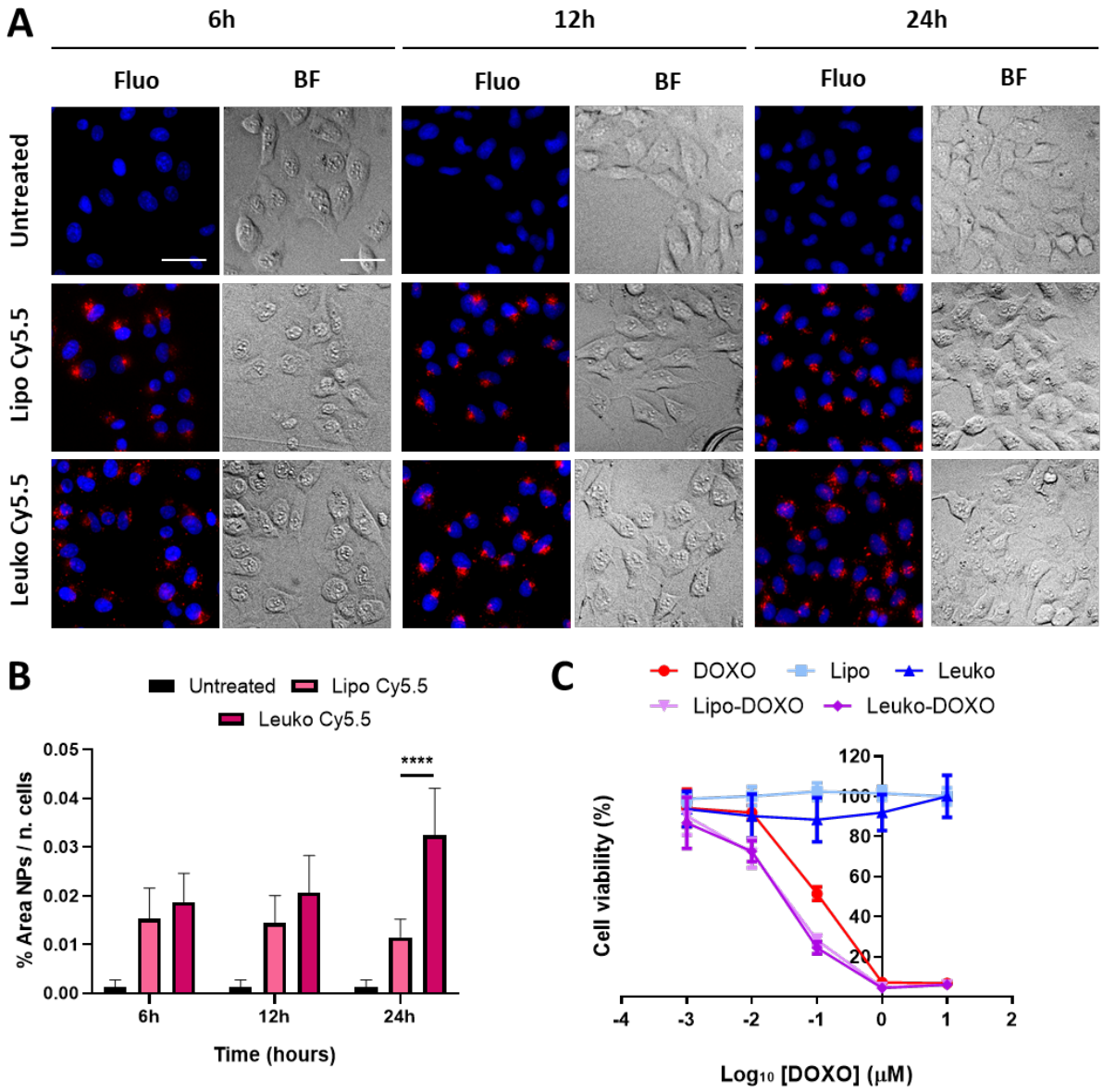


**Figure 25:** A) Fluorescence (Fluo) and respective bright field (BF) mages of SAOS-2 cells cultured onto flat plates treated with either Lipo Cy5.5 or Leuko Cy5.5 for 6, 12, and 24 hours. B) Quantification of Lipo and Leuko fluorescence at different time points during uptake. C) Resazurin cell viability assay results for DOXO, Lipo, Leuko, Lipo DOXO, and Leuko DOXO on SAOS-2 cells. (*: $p<0.05$; **: $p<0.01$; ***: $p<0.001$; ****: $p<0.0001$, n=3 for all the performed

experiments)

As evidenced in Figure 24B and 25B, HCT-116 cells demonstrated a significantly higher uptake of Leukos-Cy5.5 compared to Lipos-Cy5.5 at all time points, with both particles uptake especially increasing between 12h and 24h. Conversely, SAOS-2 cells demonstrated an increase only in Leukos-Cy5.5 uptake over time while Lipos-Cy5.5 internalization underwent a very slight decrease. It is possible that Leukos are not only more efficiently internalized by osteosarcoma cells but are also better retained compared to bare Lipos. These differences in uptake by both amount and overall trend underline how largely different cell lines can interact differently with our NPs, depending on their metabolism, protein expression, and even genetic differences.

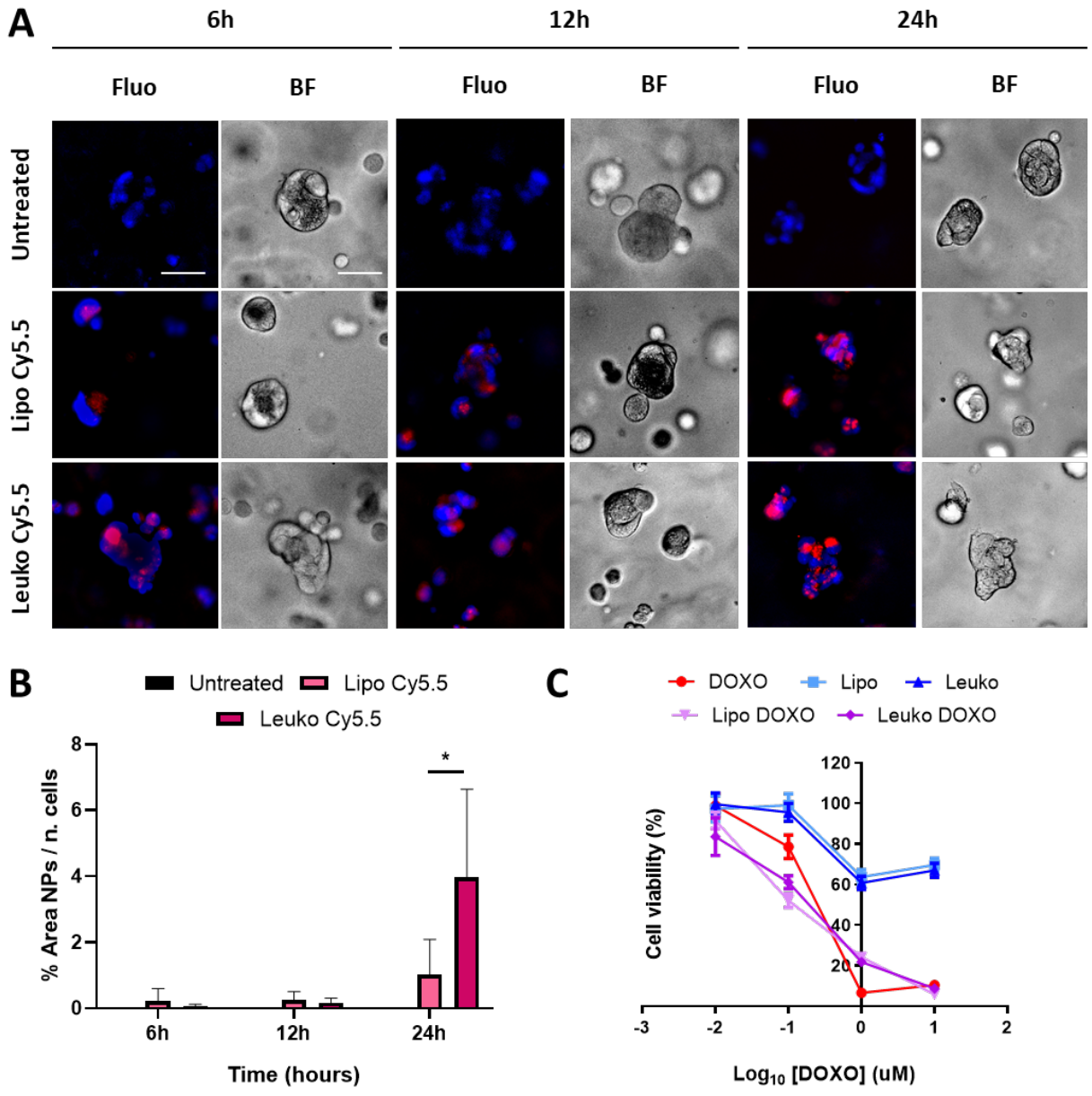


**Figure 26** A) Fluorescence (Fluo) and respective bright field (BF) mages of HCT-116 spheroids cultured into Geltrex™ treated with either Lipo Cy5.5 or Leuko Cy5.5 for 6, 12, and 24 hours. B) Quantification of Lipo and Leuko fluorescence at different time points during uptake. C) Resazurin cell viability assay results for DOXO, Lipo, Leuko, Lipo DOXO, and Leuko DOXO on HCT-116 spheroids. (*: $p<0.05$, n=3 for all the performed experiments).

However, the use of flat cell cultures gives a somewhat reductive insight about the internalization rates of tumor cells. Indeed, in a flat cell culture setting all the cells are equally and directly exposed to the treatment, since they grow on a flat monolayer. This setup thus does not consider the potential barrier effect provided by the tumor tissue, which can limit drug and NPs diffusion, hindering their interaction with tumor cells. Furthermore, the extracellular matrix is known to have important functions in supporting and even promoting tumor development (191; 192), working as a bioactive scaffold.

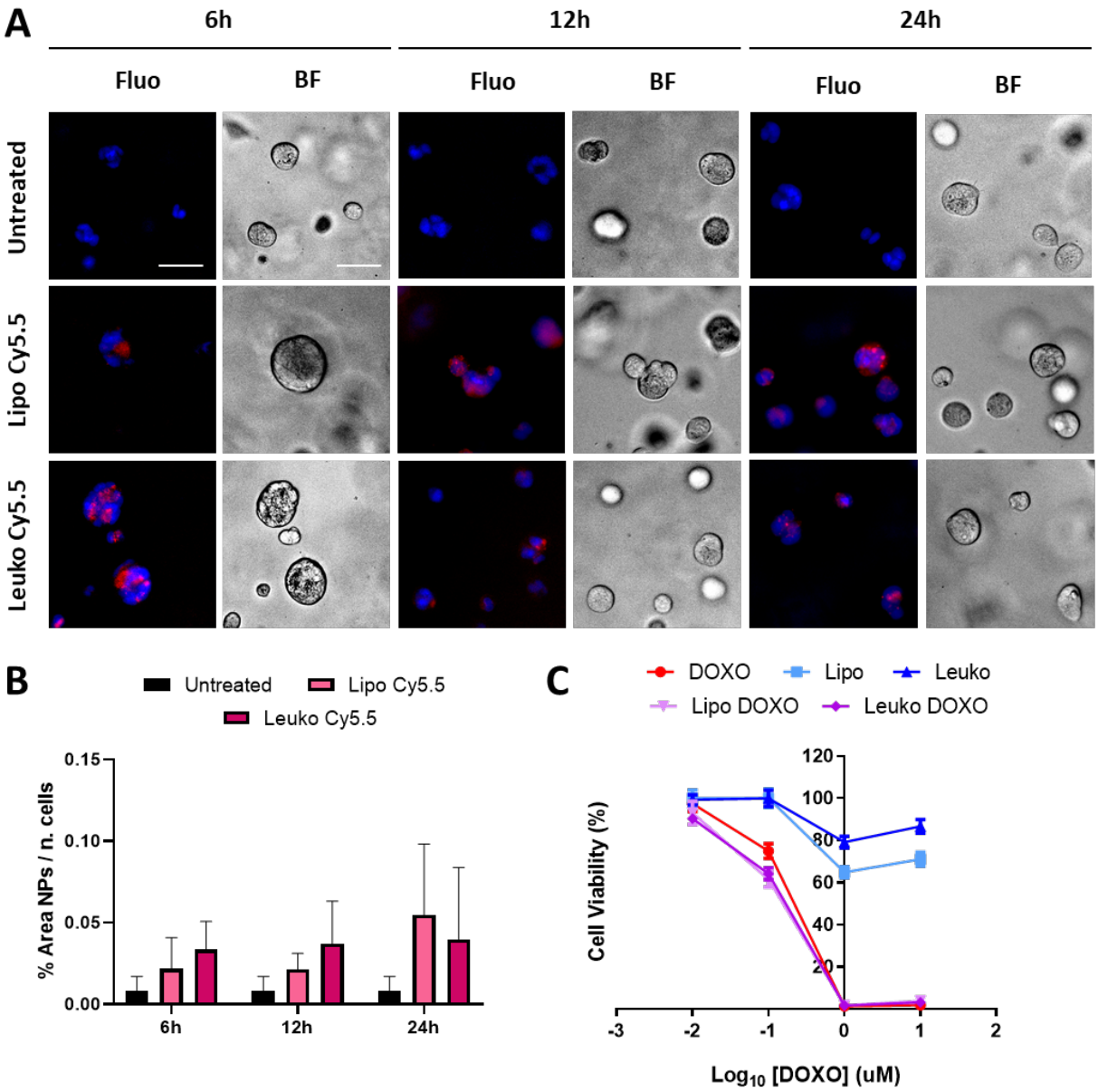


**Figure 27** A) Fluorescence (Fluo) and respective bright field (BF) mages of SAOS-2 spheroids cultured into Geltrex™ treated with either Lipo Cy5.5 or Leuko Cy5.5 for 6, 12, and 24 hours. B) Quantification of Lipo and Leuko fluorescence at different time points during uptake. C) Resazurin cell viability assay results for DOXO, Lipo, Leuko, Lipo DOXO, and Leuko DOXO on SAOS-2 spheroids. (n=3 for all the performed experiments).

To gain further insights into this mechanism, both HCT-116 and SAOS-2 cells were cultured after being dispersed in a collagen based, animal derived hydrogel (Geltrex™). This scaffold has been largely used to create a 3D structure to support tumor cells, but also to induce tumor cells growth into spheroids (193). These structures are clusters of tumor cells that more closely resemble solid tumor structures. Specifically, the presence of external cells, which are exposed more easily to nutrients and treatment, while internal cells that are deprived of both can provide important information about the penetration of treatments into the tumor mass. Furthermore, this peculiar geometry can also modulate the gene expression of tumor cells towards a phenotype that results in higher drug resistance and is associated to more invasive profiles.

Thus, 3D cultured HCT-116 and SAOS-2 cells cultured in Geltrex™ were incubated with $1 \cdot 10^{10}$ Lipos-Cy5.5 or Leukos-Cy5.5 per mL of complete medium, and then stained for their nuclei and imaged at 6, 12 and 24 hours. As shown in Figure 26A and 27A tumor cells in Geltrex™ internalized Lipos-Cy5.5 and Leukos-Cy5.5 even at the shortest time point of 6 hours, and the NPs fluorescence was visible as spots throughout the entire tumor spheroids for both cell lines, demonstrating efficient NPs penetration of the gel. Remarkably, the uptake trend was quite different compared to the respective two-dimensional setup. Specifically, HCT-116 cells demonstrated a marked increase of uptake at 24 hours compared to the other time points (Figure 26B). This appears counterintuitive since we would expect a similar or lower uptake of NPs compared to flat cultures due to the Geltrex™ barrier effect. However, it is possible that HCT-116 cells protein expression and metabolism is altered by the presence of the hydrogel towards a higher endocytic rate, or perhaps expressing more membrane proteins involved in NPs uptake. This was especially visible for Leukos-Cy5.5, which demonstrated a much higher uptake compared to Lipo Cy5.5 at 24h.

On the other hand, SAOS-2 cells did not show the formation of clear tumor spheroids, often presenting in Geltrex™ as either single or randomly close cells. In these cells, the uptake was still visible at early time points (Figure 27A). However, as presented in Figure 27B, the uptake rate was like flat SAOS-2 cells and there was no clear increase in NPs uptake, with no significant increase in Leuko internalization compared to Lipos. These discrepancies between HCT-116 and SAOS-2 cells in 3D again evidence how the genetic makeover of cell lines and also the effect of culture setup onto their behavior are important factors in determining their interactions with Lipos and Leukos.

## Assessment of Lipo and Leuko interaction with inflamed endothelial cells

The ability of Leuko to adhere to the inflamed endothelia associated to either local inflammation or tumor development via their membrane proteins is an essential feature necessary to

enable their efficient active targeting. As a straightforward model of endothelial inflammation, HUVEC cells were cultured onto gelatin-coated plates and were either directly incubated with Lipo Cy5.5 or Leuko Cy5.5, or treated with 100ng/mL of LPS (a component of bacterial walls) for 24 hours beforehand to induce their activation and expression of adhesion molecules that Leuko can use as helve to attach to (138). After 3 hours from treatment, HUVEC cells were stained with DAPI for the nuclei and imaged using fluorescent microscopy. As shown in Figure 28C, Lipo and Leuko were well tolerated by HUVEC cells even at very high concentrations.

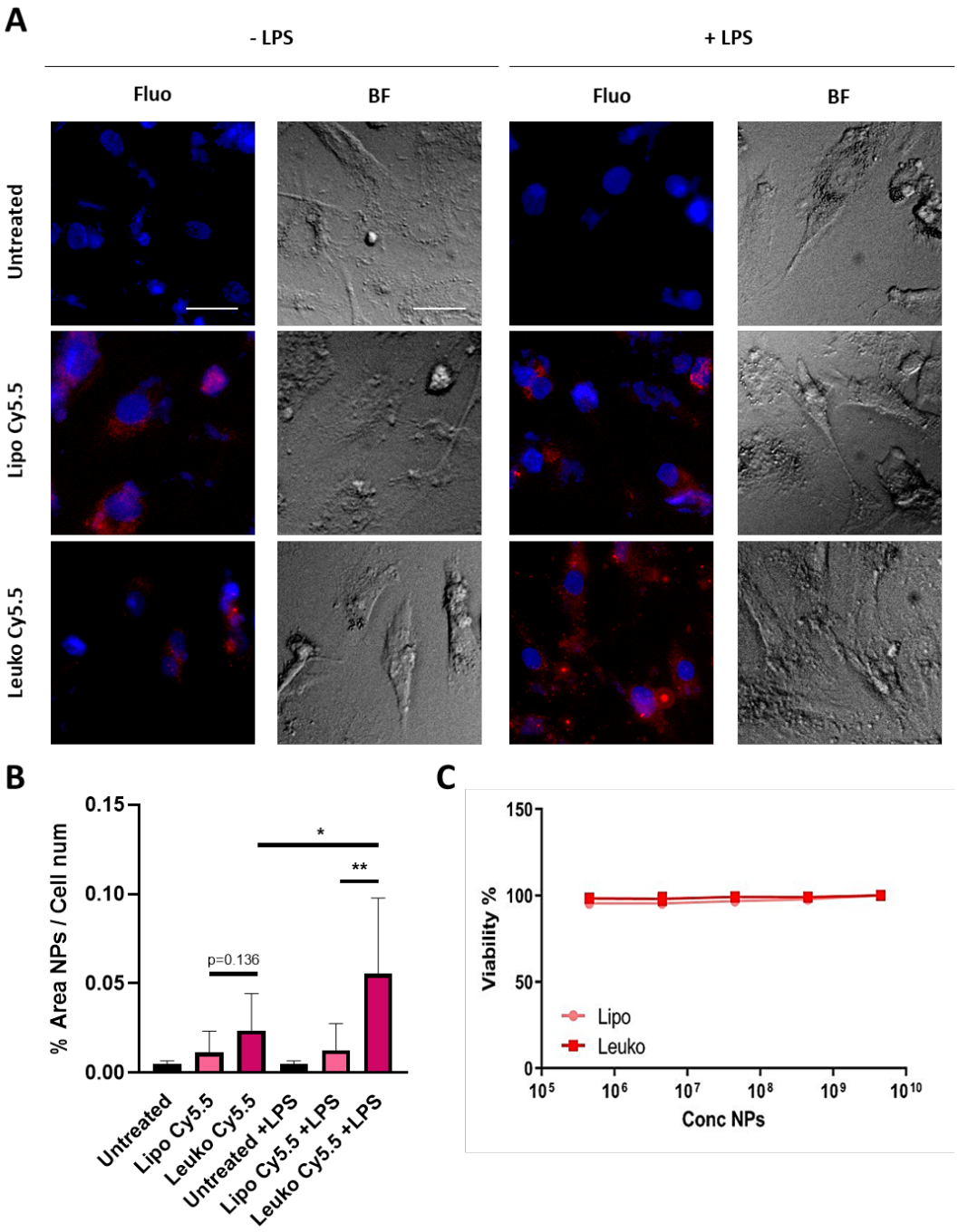


**Figure 28:** A) Fluorescence (Fluo) and respective bright field (BF) mages of HUVEC cells cultured onto gelatin-coated plates and treated with either Lipo Cy5.5 or Leuko Cy5.5 in presence of 100ng/mL of LPS or not, for 3h. B) Quantification of Lipo and Leuko fluorescence at different time points during uptake. C) Resazurin cell viability assay results Lipo and

Leuko on HUVEC cells. (*: $p<0.05$; **: $p<0.01$, n=3 for all the performed experiments).

As shown in Figure 28A and its respective quantification in Figure 28B, the interaction of Lipos-Cy5.5 and Leuko-Cy5.5 was visible to some extent even in HUVEC cells that were not exposed to LPS. In this negative control, Leukos-Cy5.5 still adhered to HUVEC cells slightly more compared to Lipos-Cy5.5, although their difference was not significant ($p=0.136$). However, when HUVEC cells were pre-treated with LPS, the uptake of Lipos-Cy5.5 was not significantly increased, while Leukos-Cy5.5 uptake almost doubled on average, becoming significantly higher.

This simple study demonstrates, in accordance with previous evidence (194; 186), that Leuko are indeed able to interact more efficiently with inflamed endothelia, providing active targeting. Since the only difference between Lipo and Leuko is the presence of membrane proteins on the latter, the higher adhesion of Leuko to HUVEC can be attributed to these surface proteins.

## Assessment of uptake by macrophages

The presence of immune cells such as macrophages in the tumor milieu is an important factor in determining tumors growth and progression, but also in determining the efficacy of treatment (195) . Indeed, local and recruited macrophages can both secrete growth factor to sustain tumor growth or can work as “decoys”, absorbing drug and especially particles and large molecules via their very efficient phagocytosis, hindering their possible interactions with target tumor cells. Furthermore, in many inflammatory pathologies macrophages are recruited to the affected tissue to remove potential external bodies and then sustain tissue remodeling and regeneration.

To create a straightforward model of macrophages, THP-1 human monocytes were stimulated with 100ng/mL of PMA for 48h and then treated with Lipos-Cy5.5 or Leukos-Cy5.5 for 3 hours before staining them for their nuclei with Hoechst.

As shown in Figure 29A, NPs signal was visible even at this early time point, evidencing the efficiency of NPs uptake by macrophages. The uptake quantification presented in Figure 29B evidence how Leukos-Cy5.5 were internalized more efficiently than Lipos-Cy5.5. It is important to consider that Leuko were formulated using THP-1 derived membrane proteins, and thus Leuko could undergo internalization by macrophages through homologous uptake compared to bare Lipo. As presented in Figure 29C, Lipo and Leuko were still well tolerated by THP-1 macrophages at very high concentrations.

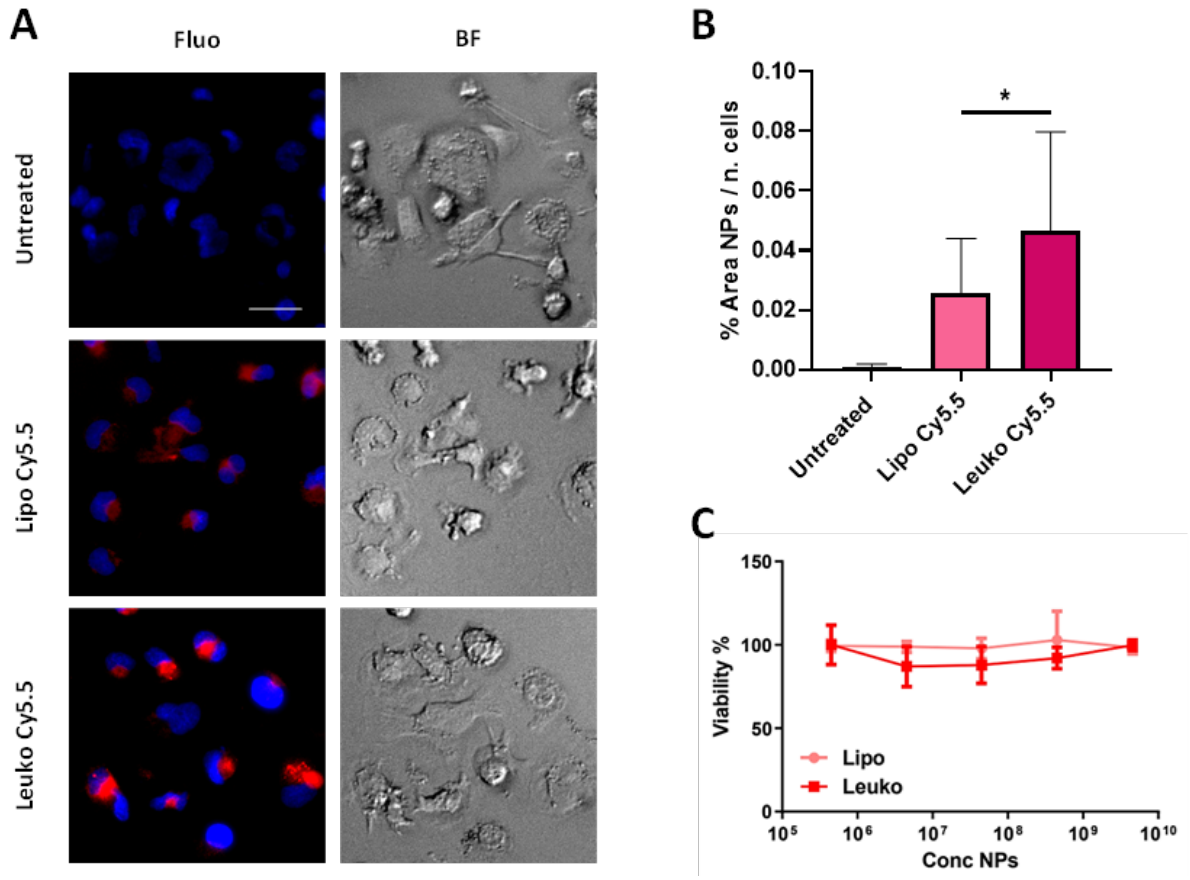


**Figure 29:** A) Fluorescence (Fluo) and respective bright field (BF) mages of THP-1 derived macrophages treated with either Lipo Cy5.5 or Leuko Cy5.5, for 3h after treatment with 100ng/mL of PMA for 48h. B) Quantification of Lipo and Leuko fluorescence at different time points during uptake. C) Resazurin cell viability assay results Lipo and Leuko on THP-1 derived monocytes. (*: $p<0.05$; **: $p<0.01$, n=3 for all the performed experiments).

This higher uptake rate of Leukos could be a drawback in determining their targeting efficiency from tumor cells since macrophages could compete with them for Leuko uptake. However, it is also possible that by internalizing Leukos, macrophages can create a drug depot in proximity to the inflamed tissue or tumor, increasing the retention of the particles in the target tissue.

## Assessment of Cytotoxicity on tumor cells

The cytotoxic effect of Lipos-DOXO and Leukos-DOXO was also assessed both in 2D and in the 3D setting. Specifically, HCT-116 and SAOS-2 cells were seeded onto 96-well plates or in Geltrex in similar conditions to the ones employed for the uptake studies. Then cells were treated with suspensions of either DOXO, Lipos, Leukos, Lipos-DOXO and Leukos-DOXO dispersed in complete culture medium and in the concentration range of 0.01 to 10 μM. Cells were then incubated with the treatment for 72h and then their viability was assessed using the Resazurin assay. The resulting $IC_{50}$ and their respective $R^2$ values are reported in Table 5.

As shown in Figure 24C and 25C, DOXO treatment on HCT-116 cells had an $IC_{50}$ value around 0.1μM. Conversely, it was not possible to calculate the $IC_{50}$ empty Lipo and Leuko, since they

appeared to be well tolerated by tumor cells. Interestingly, Lipos-DOXO and Leukos-DOXO were more toxic compared to the free drug, since they achieved an $IC_{50}$ of 0.075µM and 0.060 µM respectively on CRC cells, demonstrating an improvement on the effect of DOXO when encapsulated in NPs, and especially when delivered through Leuko. A similar trend was also visible for SAOS-2 cells in which free DOXO had an $IC_{50}$ of 0.1µM, but in this case, Lipo-DOXO and Leuko-DOXO demonstrated a much-improved cytotoxicity, with $IC_{50}$ values of 0.031µM and 0.027µM, respectively. Empty Lipos and Leukos were well tolerated also by SAOS-2 cells. These differences in efficacy evidence again how the specific cell lines have a relevant effect in determining the cytotoxic effect of NPs.

However, 3D cultured cell lines treated in analogous conditions present a different toxicity profile (Figure 26 and 27C). Specifically, HCT-116 cells have an $IC_{50}$ for free DOXO that was double of the respective 2D cell culture (0.217 µM). In this case, empty Lipos and Leukos were still well tolerated by the cells, while Lipos-DOXO and Leukos-DOXO demonstrate still a lower $IC_{50}$ (0.120 and 0.185 µM, respectively). SAOS-2 cells showed an $IC_{50}$ value of 0.160 µM for free DOXO, 0.127 µM for Lipos-DOXO, and 0.134 for Leukos-DOXO.

| Conditions | Value | DOXO | Lipo | Leuko | Lipo-DOXO | Leuko-DOXO |
|---|---|---|---|---|---|---|
| HCT-116 2D | IC50 (µM) | 0.100 | NA | NA | 0.075 | 0.060 |
| | $R^2$ | 0.928 | 0.005 | 0.112 | 0.937 | 0.937 |
| SAOS-2 2D | IC50 (µM) | 0.104 | NA | NA | 0.878 | 0.839 |
| | $R^2$ | 0.918 | 0.001 | 0.006 | 0.878 | 0.839 |
| HCT-116 3D | IC50 (µM) | 0.217 | NA | NA | 0.120 | 0.185 |
| | $R^2$ | 0.961 | 0.463 | 0.478 | 0.127 | 0.134 |
| SAOS-2 3D | IC50 (µM) | 0.160 | NA | NA | 0.127 | 0.134 |
| | $R^2$ | 0.997 | 0.456 | 0.262 | 0.990 | 0.994 |

**Table 5:** $IC_{50}$ values and their respective $R^2$ for DOXO, Lipo, Leuko, Lipo DOXO, and Leuko DOXO on HCT-116 cells and SAOS-2 cells in 2D and 3D culture.

These data underline how particles, despite being very well tolerated by tumor cells also in 3D, were able to improve the antitumor effect of DOXO. It is important to note that the difference in the values of $IC_{50}$ is most likely not caused by a barrier effect provided by the Geltrex™. This proven by the fact that during the previously discussed uptake experiments, both Lipo and Leuko were able to reach efficiently the cells embedded in the cells within the 24h from incubation. However, the cells

viability for these experiments was assessed much later, at 72 hours from incubation, leaving for NPs much more time to interact with cells. Furthermore, since free DOXO is a much smaller and hydrophilic molecule compared to NPs, its diffusion through the gels would be much faster. Thus, the difference in the cytotoxic effect of both the free drug is to be attributed to the bioactive stimuli provided by the hydrogel scaffold itself, which supports tumor cells growth and metabolism.

## Conclusions

In the present work, a novel biomimetic nanovesicles formulation was optimized as a potential drug delivery system to target the inflamed vasculature associated with local inflammations and solid tumors. To achieve this, the nanovesicles have been functionalized with leukocyte-derived membrane proteins to provide the particles with long circulation via immune-escaping proteins and active targeting towards the inflamed endothelia via adhesion proteins, defined Leukos.

This project covered the entire production workflow for these particles. The first step thus was the optimization of a protocol for the extraction and purification of membrane proteins from cell cultures. Specifically, the extraction was based on the use of a series of different detergents to first permeabilize the cells using digitonin, allowing the efflux of their cytosolic proteins, and subsequent solubilization of plasma membranes to extract the membrane proteins and stabilize them by including their hydrophobic domains within Triton X-100 detergent micelles. Thus, the optimization of these two steps was performed on murine monocytes, establishing an optimal ratio of 100µl of buffer per million of cells to achieve complete permeabilization. The second step did not require any specific cell number requirement. The final yield of total proteins in fact increased with the initial amount of cells. On the other hand, the purity of the final extract increased with amount of Triton X-100 in the second extraction buffer. The purity was assessed using orthogonal techniques including the semi-quantitative SDS-PAGE and Western Blot, and qualitative proteomic analysis by Mass Spectrometry. This process was also validated on THP-1 human monocytes. Our new protocol demonstrated a similar protein yield and membrane proteins purity compared to a gold standard commercial kit based on the same main principles, demonstrating to be a cheaper and scalable alternative to it.

The second step of the project was the optimization of Leukosomes formulations. The assembly of nanoparticles was performed in a single step using the microfluidics-based platform Nanoassemblr™. To optimize this process in order to achieve monodisperse nano sized Leuko with a high protein loading, a Design of Experiment approach was employed. This allowed the optimization of the lipids to protein ratio and the microfluidics conditions of the system using the minimal amount of experimental runs. Specifically, the DoE strategy allowed the creation of a mathematical model able to predict Leuko features such as size, PDI, and zeta potential depending on the TFR, FRR and proteins to lipids weight ratio used as parameters. Desiring Leuko with a size around 150nm, and a minimized PDI and Zeta Potential, the model retro-calculated as necessary experimental parameters a TFR of 1mL/min, a FRR of 4.88:1 (aqueous phase / organic phase), and a lipid to proteins ratio of 20:1. The predictions were validated formulating Leuko using the calculated parameters, which demonstrated the correctness of the predictions, with Leuko 150nm in diameter, a PDI of 0.24 and a

zeta potential of -25mV that was significantly lower compared to Liposomes with the same composition but without membrane proteins. Thus, this formulation was selected for further studies. These Leuko demonstrated to be colloidally stable, maintaining their main features until 15 days from synthesis. Furthermore, this formulation demonstrated the presence and correct orientation of key membrane proteins on its surface as demonstrated via flow cytometry, retaining important biomolecules involved in endothelial adhesion. The potential of Leukos as DDS however also depends on its ability to efficiently encapsulate therapeutic agents. As a model drug, the antitumor molecule DOXO was encapsulated using a remote loading approach, reaching a maximal encapsulation efficiency of 60% of the incubated drug. Furthermore, the release of DOXO from Leuko was pH dependent, with the drug being released from the particles faster at a slightly acidic pH of 6.0 compared to physiological pH (7.4), which is idea to guarantee the release of DOXO only after particles internalization and trafficking to the acidic lysosomal compartment.

The final part of the project focused on the assessment of Leukos adhesion to inflamed endothelial cells, as well as their cytotoxic effect onto tumor cells. Remarkable, Leukos were able to efficiently adhere to HUVEC endothelial cells inflamed with LPS compared to both Lipo and Leuko incubated onto non-inflamed endothelial cells demonstrating selectivity towards inflamed endothelia. Furthermore, Leukos were also efficiently internalized by HCT-116 and SAOS-2 cells cultured both in flat condition and using the collagen-based Geltrex hydrogel as a bioactive scaffold to induce the formation of tumor spheroids. Importantly, Leukos demonstrated a higher uptake compared to bare Lipos, displaying a second layer of specificity in their active targeting. Since the internalized NPs presented a cytosolic, punctate and perinuclear intracellular accumulation, it is possible to postulate that NPs are internalized via some form of endocytic uptake, although more investigation would be warranted to ensure the specific mechanism involved. Finally, we tested the interaction between Lipos, Leukos and THP-1 derived macrophages as a model for immune cells present into the tumor or inflamed tissue milieu. After 3 hours of incubation, Leuko were internalized more efficiently compared to Lipo, demonstrating the ability to potentially be strongly retained within the tissue creating a local drug depot.

Regarding the therapeutic efficacy of our NPs, Lipo and Leuko loaded with DOXO exerted an improved cytotoxic effect against human CRC HCT-116 cells and SAOS-2 cells compared to free DOXO, while empty NPs did not exert any relevant cytotoxic effect. This improvement in efficacy parallels the higher Leukos uptake compared to Lipos. Furthermore, tumor cells cultured in 3D demonstrated more resilience to the treatments compared to their respective two-dimensional cultures, proving the important contribution of the ECM to tumor cells growth via bioactive functions

and not simply via a barrier effect that prevents drug uptake.

In conclusion, this project constitutes a proof of concept for the creation of a novel framework for the formulation, optimization, and characterization of biomimetic nanoparticles. This was performed starting by the purification of membrane proteins as starting material, to the assembly of the nanovesicles and their physical and chemical characterization, to their biological testing on different tumor and tissue models. Hopefully this workflow can be used in the future for the formulation of biomimetic nanovectors for many other therapeutic applications.

## Acknowledgements

I would like to thank Dr. Marco Agostini and Prof. Paolo Caliceti for offering me the amazing opportunity to work in their laboratories as PhD student, for their constant guidance and encouragement that motivated me to pursue this project among the others I had the privilege to take part to under their supervision.

I would also like to thank Dr. Francesca Taraballi for kindly hosting me in her laboratory at Houston Methodist Research Institute during my time abroad, offering me the opportunity to integrate in her research team and actively participate to their research projects, supporting me with her scientific expertise and motivating me. Thanks to her and her group, my experience in Houston was an incredible opportunity for professional and personal growth.

Thanks also to the post-docs, PhD students, undergraduates and technicians that are part of Dr. Agostini, Prof. Caliceti, and Dr. Taraballi teams, and in particular Dr. Edoardo D'Angelo, Dr. Francesca Sensi, Dr. Federica Giordano, Dr. Sara Crotti, Dr. Laura Moracci, Dr. Andrea Biccari and Dr. Asia Marangio for collaborating with me in the different research projects I had the privilege to take part to, for their suggestions and constant support. They proved to be extraordinary colleagues and friends, and my PhD experience would just not have been as memorable, formative and fun without them.

On a more personal note, I would like to thank my parents, sister, and close relatives, for their constant support in my PhD journey, for their patience with me during difficult times and for believing in me in moments when I couldn't. I can't imagine how these years would have been without them.

Finally, I would like to thank the Ermenegildo Zegna Founder's Scholarship to financially support me during my time abroad, as well as the University of Padova for giving me the possibility to perform my research work and cultivate my passion for science.

# References


1. *Global Cancer Statistics 2020: GLOBOCAN Estimates of Incidence and Mortality Worldwide for 36 Cancers in 185 Countries.* Sung H, Ferlay J, Siegel RL, Laversanne M, Soerjomataram I, Jemal A, Bray F. 3, May 2021, CA Cancer J Clin. , Vol. 71, pp. 209-249.

2. *The cell cycle: a review of regulation, deregulation and therapeutic targets in cancer.* Vermeulen K, Van Bockstaele DR, Berneman ZN. 3, Jun 2003, Cell Prolif., Vol. 36, pp. 131-149.

3. *Hallmarks of cancer: the next generation.* Hanahan D, Weinberg RA. 5, Mar 2011, Cell, Vol. 144, pp. 646 -74.

4. *Cancer classification within tissues and beyond.* . Koch, L. 645, 2014, Nat Rev Genet, Vol. 15.

5. *Microenvironmental regulation of tumour angiogenesis.* De Palma, M., Biziato, D. & Petrova, T. 2017, Nat Rev Cancer , Vol. 17, pp. 457–474 .

6. *Molecular principles of metastasis: a hallmark of cancer revisited.* . Fares, J., Fares, M.Y., Khachfe, H.H. et al. 28, 2020, Sig Transduct Target Ther, Vol. 5.

7. *Mechanisms of Multidrug Resistance in Cancer Chemotherapy.* . Bukowski K, Kciuk M, Kontek R. 9, May 2020, Int J Mol Sci, Vol. 21, p. 3233.

8. *A compendium of mutational cancer driver genes.* Martínez-Jiménez, F., Muiños, F., Sentís, I. et al. 2020, Nat Rev Cancer, Vol. 20, pp. 555–572.

9. *Oncogenes and tumor suppressor genes.* . Lee EY, Muller WJ. 10, Oct 2010, Cold Spring Harb Perspect Biol., Vol. 2, p. a003236.

10. *Spontaneous DNA damage, genome instability, and cancer--when DNA replication escapes control.* . P., Schär. 3, Feb 2001, Cell, Vol. 104, pp. 329-32.

11. *Hereditary cancer predisposition syndromes.* . Garber JE, Offit K. 2, Jan 2005, J Clin Oncol. , Vol. 23, pp. 276-92.

12. *Environmental Determinants of Breast Cancer.* Hiatt RA, Brody JG. Apr 2018, Annu Rev Public Health., Vol. 39, pp. 113-133.

13. *Cancer Initiation, Promotion, and Progression and the Acquisition of Key Behavioral Traits.* author, Carolyn ComptonEmail. May 2020, Cancer: The Enemy from Within, pp. 25-48.

14. *Signal Transduction in Cancer.* Richard Sever, Joan S. Brugge. 5, Apr 2015, p. a006098.

15. *Death and anti-death: tumour resistance to apoptosis.* . Igney, F., Krammer, P. 2002, Nat Rev Cancer , Vol. 2, pp. 277–288.

16. *Mechanisms of Tumor Cell–Intrinsic Immune Evasion.* Gajewski, Stefani Spranger and Thomas F. March 2018, Ann Rev, Vol. 2, pp. 213-228.

17. *Delineating the evolutionary dynamics of cancer from theory to reality.* . Bozic, I., Wu, C.J. 2020, Nat Cancer, Vol. 1, pp. 580–588 .

18. *Tumors: wounds that do not heal. Similarities between tumor stroma generation and wound healing.* HF., Dvorak. 26, Dec 5, 1986, N Engl J Med., Vol. 315, pp. 1650-9.

19. *Many different tumor types have polyclonal tumor origin: evidence and implications.* BL., Parsons. Sep 2008, Mutat Res., pp. 232-47.

20. *Paget's "Seed and Soil" Theory of Cancer Metastasis: An Idea Whose Time has Come.* . Akhtar M, Haider A, Rashid S, Al-Nabet ADMH. 1, Jan 2019, Adv Anat Pathol., Vol. 26, pp. 69-74.

21. *Tumor Hypoxia as a Barrier in Cancer Therapy: Why Levels Matter.* Hompland T, Fjeldbo CS, Lyng H. 3, Jan 2021, Cancers (Basel)., Vol. 13, p. 499.

22. *Role of Reactive Oxygen Species in Cancer Progression: Molecular Mechanisms and Recent Advancements.* Aggarwal V, Tuli HS, Varol A, Thakral F, Yerer MB, Sak K, Varol M, Jain A, Khan MA, Sethi G. 11, Nov 2019, Biomolecules. , Vol. 9, p. 735.

23. *Tumour acidosis: from the passenger to the driver's seat.* Corbet, C., Feron, O. 2017, Nat Rev Cancer, Vol. 17, pp. 577–593.

24. *The 35th Anniversary of the Discovery of EPR Effect: A New Wave of Nanomedicines for Tumor-Targeted Drug Delivery-Personal Remarks and Future Prospects.* H., Maeda. 3, Mar 2021, J Pers Med., Vol. 11, p. 229.

25. *The evolution of cancer surgery and future perspectives.* . Wyld, L., Audisio, R. & Poston, G. 2015, Nat Rev Clin Oncol , Vol. 12, pp. 115–124.

26. *Cancer and radiation therapy: current advances and future directions.* Baskar R, Lee KA, Yeo R, Yeoh KW. 3, 2012, Int J Med Sci., Vol. 9, pp. 193-9.

27. *Chemotherapy and the war on cancer.* Chabner, B., Roberts, T. 2005, Nat Rev Cancer, Vol. 5, pp. 65-72.

28. *The role of hormonal therapy in the management of hormonal-receptor-positive breast cancer with co-expression of HER2.* Prat, A., Baselga, J. 2008, Nat Rev Clin Oncol, Vol. 5, pp. 531-542.

29. *Angiogenesis inhibitors in cancer therapy: mechanistic perspective on classification and treatment rationales.* El-Kenawi AE, El-Remessy AB. 4, Oct 2013, Br J Pharmacol. , Vol. 170, pp. 712-29.

30. *Small molecules in targeted cancer therapy: advances, challenges, and future perspectives.* . Zhong, L., Li, Y., Xiong, L. et al. 201, 2021, Sig Transduct Target Ther, Vol. 6.

31. *A guide to cancer immunotherapy: from T cell basic science to clinical practice.* Waldman, A.D., Fritz, J.M. & Lenardo, M.J. 2020, Nat Rev Immunol , Vol. 20, pp. 651-668.

32. *The Current Status of Gene Therapy for the Treatment of Cancer.* . TM., Belete. Mar 2021, Biologics, Vol. 15, pp. 67-77.

33. *Adverse Effects of Cancer Chemotherapy: Anything New to Improve Tolerance and Reduce Sequelae?* Nurgali K, Jagoe RT, Abalo R. 2018, Front Pharmacol. , Vol. 9, p. 245.

34. *Combination therapy in combating cancer.* . Bayat Mokhtari R, Homayouni TS, Baluch N, Morgatskaya E, Kumar S, Das B, Yeger H. 23, Jun 6, 2017, Oncotarget, Vol. 8, pp. 38022-38043.

35. *A current view on inflammation.* 2017, Nat Immunol, Vol. 18, p. 825.

36. *Tumor inflammatory angiogenesis and its chemoprevention.* Albini A, Tosetti F, Benelli R, Noonan DM. 23, Dec 2005, Cancer Res, Vol. 65, pp. 10637-41.

37. *The hallmarks of cancer are also the hallmarks of wound healing.* MacCarthy-Morrogh L, Martin P. 648, Sep 2020, Sci Signal. , Vol. 13, p. eaay8690.

38. *Inflammation and Cancer: Triggers, Mechanisms, and Consequences.* Greten FR, Grivennikov SI. 1, Jul 2019, Immunity, Vol. 51, pp. 27-41.

39. *Understanding the tumor immune microenvironment (TIME) for effective therapy.* Binnewies M, Roberts EW, Kersten K, Chan V, Fearon DF, Merad M, Coussens LM, Gabrilovich DI, Ostrand-Rosenberg S,

Hedrick CC, Vonderheide RH, Pittet MJ, Jain RK, Zou W, Howcroft TK, Woodhouse EC, Weinberg RA, Krummel MF. 5, 2018, Nat Med, Vol. 24, pp. 541-550.

40. *Immune escape mechanisms as a guide for cancer immunotherapy.* Beatty GL, Gladney WL. 4, Feb 15, 2015, Clin Cancer Res., Vol. 21, pp. 687-92.

41. *Tumor-Associated Macrophages: Recent Insights and Therapies.* Zhou J, Tang Z, Gao S, Li C, Feng Y, Zhou X. 188, Feb 2020 , Front Oncol, Vol. 10.

42. *T Cell Dysfunction in Cancer.* . Thommen DS, Schumacher TN. 4, Apr 2018, Cancer Cell. , Vol. 33, pp. 547-562.

43. *Recent Advances and Strategies in Tumor Vasculature Targeted Nano-Drug Delivery Systems.* Ying M, Chen G, Lu W. 22, 2015, Curr Pharm Des. , Vol. 21, pp. 3066-75.

44. *Therapeutic cancer vaccines.* Saxena M, van der Burg SH, Melief CJM, Bhardwaj N. 6, Jun 2021, Nat Rev Cancer., Vol. 21, pp. 360-378.

45. *Immunogenic cell death in cancer therapy: Present and emerging inducers.* Zhou J, Wang G, Chen Y, Wang H, Hua Y, Cai Z. Aug 2019, J Cell Mol Med, pp. 4854-4865.

46. *A decade of immune-checkpoint inhibitors in cancer therapy.* . Robert, C. 2020, Nat Comm, Vol. 11.

47. *Nanoparticle-Based Medicines: A Review of FDA-Approved Materials and Clinical Trials to Date.* Bobo D, Robinson KJ, Islam J, Thurecht KJ, Corrie SR. 10, 2016, Pharm Res, Vol. 33, pp. 2373-87.

48. *Progress and challenges towards targeted delivery of cancer therapeutics.* Rosenblum, D., Joshi, N., Tao, W. et al. 2018, Nat Comm, p. 1410.

49. *Engineering precision nanoparticles for drug delivery.* Mitchell, M.J., Billingsley, M.M., Haley, R.M. et al. 2021, Nat Rev Drug Discov , Vol. 20, pp. 101–124.

50. *Nanodrugs: pharmacokinetics and safety.* Onoue S, Yamada S, Chan HK. 9, Feb 2014, Int J Nanomedicine., Vol. 20, pp. 1025-37.

51. *Nanovectors Design for Theranostic Applications in Colorectal Cancer.* Rampado R, Crotti S, Caliceti P, Pucciarelli S, Agostini M. Oct 2019, J Oncol., p. 2740923.

52. *Scalable Nanomanufacturing—A Review.* Cooper, Khershed. 1, Jan 2017, Micromachines (Basel), Vol. 8, p. 20.

53. *Nanomedicine: Principles, Properties, and Regulatory Issues.* . Soares S, Sousa J, Pais A, Vitorino C. 6, Aug 2018, Front Chem. , Vol. 20, p. 360.

54. *Walking the line: The fate of nanomaterials at biological barriers.* . Meng H, Leong W, Leong KW, Chen C, Zhao Y. Aug 2018, Biomaterials, Vol. 174, pp. 41-53.

55. *The effect of nanoparticle size on in vivo pharmacokinetics and cellular interaction.* Hoshyar N, Gray S, Han H, Bao G. 6, Mar 2016, Nanomedicine (Lond). , Vol. 11, pp. 673-92.

56. *Recent Advances in Understanding the Protein Corona of Nanoparticles and in the Formulation of "Stealthy" Nanomaterials.* . Rampado R, Crotti S, Caliceti P, Pucciarelli S, Agostini M. Apr 2020, Front Bioeng Biotechnol., Vol. 8, p. 166.

57. *Principles of nanoparticle design for overcoming biological barriers to drug delivery.* . Blanco E, Shen H, Ferrari M. 9, Sep 2015, Nat Biotechnol. , Vol. 33, pp. 941-51.

58. *Form Follows Function: Nanoparticle Shape and Its Implications for Nanomedicine.* . Kinnear C, Moore TL, Rodriguez-Lorenzo L, Rothen-Rutishauser B, Petri-Fink A. Sep 13, 2017, Chem Rev, pp. 11476-11521.

59. *An overview of active and passive targeting strategies to improve the nanocarriers efficiency to tumour sites.* Attia MF, Anton N, Wallyn J, Omran Z, Vandamme TF. 8, Aug 2019, J Pharm Pharmacol., Vol. 71, pp. 1185-1198.

60. *Stimuli-Responsive Nanomaterials for Application in Antitumor Therapy and Drug Delivery.* Pham SH, Choi Y, Choi J. 7, Jul 2020, Pharmaceutics, Vol. 12, p. 630.

61. *Nanomaterials: a review of synthesis methods, properties, recent progress, and challenges* . Nadeem Baig, Irshad Kammakakam, Wail Falathabe. 6 2021, Materials Advances.

62. *H-Responsive Polymer Nanoparticles for Drug Delivery.* Deirram N, Zhang C, Kermaniyan SS, Johnston APR, Such GK. 10, May 2019, Macromol Rapid Commun., Vol. 40, p. e1800917.

63. *H-sensitive nano-systems for drug delivery in cancer therapy.* Liu J, Huang Y, Kumar A, Tan A, Jin S, Mozhi A, Liang XJ. 4, Jul-Aug 2014, Biotechnol Adv, Vol. 32, pp. 693-710.

64. *Redox nanoparticles: synthesis, properties and perspectives of use for treatment of neurodegenerative diseases.* Sadowska-Bartosz I, Bartosz G. 1, Nov 2018, J Nanobiotechnology, Vol. 16, p. 87.

65. *Enzyme-Responsive Nanoparticles for Anti-tumor Drug Delivery.* . Li M, Zhao G, Su WK, Shuai Q. 8, Jul 2020, Front Chem, Vol. 30, p. 647.

66. *Development of therapeutic antibodies for the treatment of diseases.* Lu RM, Hwang YC, Liu IJ, Lee CC, Tsai HZ, Li HJ, Wu HC. 1, Jan 2020, J Biomed Sci., Vol. 27, p. 1.

67. *Viral vector platforms within the gene therapy landscape.* . Bulcha JT, Wang Y, Ma H, Tai PWL, Gao G. 6, 2021, Signal Transduct Target Ther. , Vol. 8, p. 53.

68. *Advances in therapeutic applications of extracellular vesicles.* Wiklander OPB, Brennan MÁ, Lötvall J, Breakefield XO, El Andaloussi S. 492, May 2019, Sci Transl Med. , Vol. 11, p. eaav8521.

69. *Cell therapies in the clinic.* Wang LL, Janes ME, Kumbhojkar N, Kapate N, Clegg JR, Prakash S, Heavey MK, Zhao Z, Anselmo AC, Mitragotri S. 2, Feb 2021, Bioeng Transl Med., Vol. 6, p. e10214.

70. *Cell Membrane Coating Nanotechnology.* Fang RH, Kroll AV, Gao W, Zhang L. Jun 2018, Adv Mater, p. e1706759.

71. *A Review of Biomimetic Nanoparticle Drug Delivery Systems Based on Cell Membranes.* Zhang M, Du Y, Wang S, Chen B. Dec 2020, Drug Des Devel Ther. , Vol. 14, pp. 5495-5503.

72. *Stealth Coating of Nanoparticles in Drug-Delivery Systems.* . Fam SY, Chee CF, Yong CY, Ho KL, Mariatulqabtiah AR, Tan WS. 4, Apr 20, 2020, Nanomaterials (Basel)., Vol. 10, p. 787.

73. *Biomimetic Nanosponges for Treating Antibody-Mediated Autoimmune Diseases.* Jiang Y, Fang RH, Zhang L. 4, Apr 2018, Bioconjug Chem., Vol. 29, pp. 870-877. .

74. *Cell membrane-camouflaged nanoparticles for drug delivery.* Luk BT, Zhang L. Dec 2015, J Control Release, Vol. 220, pp. 600-7.

75. *Cell membrane-derived nanomaterials for biomedical applications.* Fang RH, Jiang Y, Fang JC, Zhang L. Jul 2017, Biomaterials, Vol. 128, pp. 69-83. .

76. *Phospholipids: key players in apoptosis and immune regulation.* . Chaurio RA, Janko C, Muñoz LE, Frey B, Herrmann M, Gaipl US. 12, Nov 2009, Molecules, Vol. 14, pp. 4892-914.

77. *Recent advances of erythrocyte-mimicking nanovehicles: From bench to bedside.* Yang J, Wang F, Lu Y, Qi J, Deng L, Sousa F, Sarmento B, Xu X, Cui W. Nov 2019, J Control Release. , Vol. 314, pp. 81-91.

78. *Platelets and their biomimetics for regenerative medicine and cancer therapies.* Li Z, Hu S, Cheng K. 45, Dec 2018, J Mater Chem B. , Vol. 6, pp. 7354-7365.

79. *White Blood Cell Membrane-Coated Nanoparticles: Recent Development and Medical Applications.* Wang D, Wang S, Zhou Z, Bai D, Zhang Q, Ai X, Gao W, Zhang L. Aug 2021, Adv Healthc Mater. , p. e2101349.

80. *Platelet-vessel wall interaction in health and disease.* . Löwenberg EC, Meijers JC, Levi M. 6, Jun 2012, Neth J Med. , Vol. 68, pp. 242-51.

81. *Getting to the site of inflammation: the leukocyte adhesion cascade updated.* . Ley, K., Laudanna, C., Cybulsky, M. et al. 2007, Nat Rev Immunol, Vol. 7, pp. 678–689.

82. *Mesenchymal stem cells and cancer therapy: insights into targeting the tumour vasculature.* . Aravindhan S, Ejam SS, Lafta MH, Markov A, Yumashev AV, Ahmadi M. 1, Mar 8, 2021, Cancer Cell, Vol. 21, p. 158.

83. *Design of universal cancer vaccines using natural tumor vessel-specific antigens (SANTAVAC).* Lokhov PG, Balashova EE. 3, 2015, Hum Vaccin Immunother. , Vol. 11, pp. 689-98.

84. *Dual-Modified Novel Biomimetic Nanocarriers Improve Targeting and Therapeutic Efficacy in Glioma.* Fu S, Liang M, Wang Y, Cui L, Gao C, Chu X, Liu Q, Feng Y, Gong W, Yang M, Li Z, Yang C, Xie X, Yang Y, Gao C. 2, Jan 2019 , ACS Appl Mater Interfaces, Vol. 11, pp. 1841-1854.

85. *Neuronal mitochondria-targeted therapy for Alzheimer's disease by systemic delivery of resveratrol using dual-modified novel biomimetic nanosystems.* Han Y, Chu X, Cui L, Fu S, Gao C, Li Y, Sun B. 1, Dec 2020, Drug Deliv, Vol. 27, pp. 502-518.

86. *Biomimetic nanoparticles delivered hedgehog pathway inhibitor to modify tumour microenvironment and improved chemotherapy for pancreatic carcinoma.* . Jiang T, Zhang B, Zhang L, Wu X, Li H, Shen S, Luo Z, Liu X, Hu Y, Pang Z, Jiang X. 2018, Artif Cells Nanomed Biotechnol. , Vol. 46, pp. 1088-1101.

87. *ROS-sensitive biomimetic nanocarriers modulate tumor hypoxia for synergistic photodynamic chemotherapy.* Liu H, Jiang W , Wang Q , Hang L , Wang Y , Wang Y. 9, Aug 2019, Biomater Sci. , Vol. 7, pp. 3706-3716.

88. *Safe and Immunocompatible Nanocarriers Cloaked in RBC Membranes for Drug Delivery to Treat Solid Tumors.* . Luk BT, Fang RH, Hu CM, Copp JA, Thamphiwatana S, Dehaini D, Gao W, Zhang K, Li S, Zhang L. 7, Apr 2016, Theranostics., Vol. 6, pp. 1004-11.

89. *Size Dependency of Circulation and Biodistribution of Biomimetic Nanoparticles: Red Blood Cell Membrane-Coated Nanoparticles.* . Li H, Jin K, Luo M, Wang X, Zhu X, Liu X, Jiang T, Zhang Q, Wang S, Pang Z. 8, Aug 2019, Cells, Vol. 8, p. 881.

90. *Sequentially responsive biomimetic nanoparticles with optimal size in combination with checkpoint blockade for cascade synergetic treatment of breast cancer and lung metastasis.* Yu W, He X, Yang Z, Yang X, Xiao W, Liu R, Xie R, Qin L, Gao H. Oct 2019, Biomaterials, Vol. 217, p. 119309.

91. *Anti-EGFR-iRGD recombinant protein modified biomimetic nanoparticles loaded with gambogic acid to enhance targeting and antitumor ability in colorectal cancer treatment.* . Zhang Z, Qian H, Huang J, Sha H, Zhang H, Yu L, Liu B, Hua D, Qian X. Aug 2018, Int J Nanomedicine, Vol. 13, pp. 4961-4975.

92. *Biomimetic Immunomagnetic Nanoparticles with Minimal Nonspecific Biomolecule Adsorption for Enhanced Isolation of Circulating Tumor Cells.* . Meng QF, Cheng YX, Huang Q, Zan M, Xie W, Sun Y, Li R, Wei X, Guo SS, Zhao XZ, Rao L, Liu W. 32, Aug 2019, ACS Appl Mater Interfaces, Vol. 11, pp. 28732-28739.

93. *Oriented Assembly of Cell-Mimicking Nanoparticles via a Molecular Affinity Strategy for Targeted Drug Delivery.* . Xie J, Shen Q, Huang K, Zheng T, Cheng L, Zhang Z, Yu Y, Liao G, Wang X, Li C. 5, May 2019, ACS Nano., Vol. 13, pp. 5268-5277.

94. *Biomimetic Nanosponges Suppress In Vivo Lethality Induced by the Whole Secreted Proteins of Pathogenic Bacteria.* Chen Y, Zhang Y, Chen M, Zhuang J, Fang RH, Gao W, Zhang L. 6, Feb 2019, Small, Vol. 15, p. e1804994.

95. *Cell Membrane-Coated Nanoparticles As an Emerging Antibacterial Vaccine Platform.* . Angsantikul P, Thamphiwatana S, Gao W, Zhang L. 4, Oct 2015, Vaccines (Basel)., Vol. 3, pp. 814-28.

96. *Cell-Membrane-Cloaked Oil Nanosponges Enable Dual-Modal Detoxification.* Chen Y, Zhang Y, Zhuang J, Lee JH, Wang L, Fang RH, Gao W, Zhang L. 6, Jun 2019, ACS Nano, Vol. 13, pp. 7209-7215.

97. *Biomimetic Targeting of Nanoparticles to Immune Cell Subsets via Cognate Antigen Interactions.* Luk BT, Jiang Y, Copp JA, Hu CJ, Krishnan N, Gao W, Li S, Fang RH, Zhang L. 9, Sept 2018, Mol Pharm., Vol. 15, pp. 3723-3728.

98. *A Novel Biomimetic Nanosponge Protects the Retina from the Enterococcus faecalis Cytolysin.* LaGrow AL, Coburn PS, Miller FC, Land C, Parkunan SM, Luk BT, Gao W, Zhang L, Callegan MC. 6, Nov 2017, mSphere, Vol. 2, pp. e00335-17.

99. *Disarming Pore-Forming Toxins with Biomimetic Nanosponges in Intraocular Infections.* . Coburn PS, Miller FC, LaGrow AL, Land C, Mursalin H, Livingston E, Amayem O, Chen Y, Gao W, Zhang L, Callegan MC. 3, May 2019, mSphere. , Vol. 4, pp. e00262-19.

100. *Macrophage-like nanoparticles concurrently absorbing endotoxins and proinflammatory cytokines for sepsis management.* Thamphiwatana S, Angsantikul P, Escajadillo T, Zhang Q, Olson J, Luk BT, Zhang S, Fang RH, Gao W, Nizet V, Zhang L. 43, Oct 2017, Proc Natl Acad Sci U S A, Vol. 114, pp. 11488-11493.

101. *Biomimetic Nanosponges for Treating Antibody-Mediated Autoimmune Diseases.* Jiang Y, Fang RH, Zhang L. 4, Apr 2018, Bioconjug Chem., Vol. 29, pp. 870-877.

102. *Red Blood Cell Membrane Bioengineered Zr-89 Labelled Hollow Mesoporous Silica Nanosphere for Overcoming Phagocytosis.* Lee JY, Vyas CK, Kim GG, Choi PS, Hur MG, Yang SD, Kong YB, Lee EJ, Park JH. 1, May 2019, Sci Rep, Vol. 9, p. 7419.

103. *Mesenchymal Stem Cell/Red Blood Cell-Inspired Nanoparticle Therapy in Mice with Carbon Tetrachloride-Induced Acute Liver Failure.* Liang H, Huang K, Su T, Li Z, Hu S, Dinh PU, Wrona EA, Shao C, Qiao L, Vandergriff AC, Hensley MT, Cores J, Allen T, Zhang H, Zeng Q, Xing J, Freytes DO, Shen D, Yu Z, Cheng K. 7, Jul 2018, ACS Nano , Vol. 12, pp. 6536-6544.

104. *Erythrocyte-Coated Nanoparticles Block Cytotoxic Effects of Group B Streptococcus β-Hemolysin/Cytolysin.* . Koo J, Escajadillo T, Zhang L, Nizet V, Lawrence SM. 7, Nov 2019, Front Pediatr., Vol. 1, p. 410.

105. *Platelet-membrane-biomimetic nanoparticles for targeted antitumor drug delivery.* Wang H, Wu J, Williams GR, Fan Q, Niu S, Wu J, Xie X, Zhu LM. 1, May 2019, J Nanobiotechnology, Vol. 17, p. 60.

106. *Engineering Biomimetic Platesomes for pH-Responsive Drug Delivery and Enhanced Antitumor Activity.* . Liu G, Zhao X, Zhang Y, Xu J, Xu J, Li Y, Min H, Shi J, Zhao Y, Wei J, Wang J, Nie G. 32, Aug 2019, Adv Mater., Vol. 31, p. e1900795.

107. *Platelet-mimicking nanoparticles co-loaded with W18O49 and metformin alleviate tumor hypoxia for enhanced photodynamic therapy and photothermal therapy.* Zuo H, Tao J, Shi H, He J, Zhou Z, Zhang C. Oct 2018, Acta Biomater. , Vol. 80, pp. 296-307.

108. *Platelet Membrane Biomimetic Magnetic Nanocarriers for Targeted Delivery and in Situ Generation of Nitric Oxide in Early Ischemic Stroke.* Li M, Li J, Chen J, Liu Y, Cheng X, Yang F, Gu N. 2, Feb 2020, ACS Nano, Vol. 14, pp. 2024-2035.

109. *A paradigm of endothelium-protective and stent-free anti-restenotic therapy using biomimetic nanoclusters.* Wang B, Chen G, Urabe G, Xie R, Wang Y, Shi X, Guo LW, Gong S, Kent KC. Sep 2018, Biomaterials, Vol. 178, pp. 293-301.

110. *Engineered Biomimetic Platelet Membrane-Coated Nanoparticles Block Staphylococcus aureus Cytotoxicity and Protect Against Lethal Systemic Infection.* al, Jwa-Kyung Kim et. 8, Aug 2021, Engineering, Vol. 7, pp. 1149-1156.

111. *Intratumoral immunotherapy using platelet-cloaked nanoparticles enhances antitumor immunity in solid tumors.* . Bahmani B, Gong H, Luk BT, Haushalter KJ, DeTeresa E, Previti M, Zhou J, Gao W, Bui JD, Zhang L, Fang RH, Zhang J. 1, Mar 2021, Nat Commun. , Vol. 12, p. 1999.

112. *Nanoparticles camouflaged in platelet membrane coating as an antibody decoy for the treatment of immune thrombocytopenia.* Wei X, Gao J, Fang RH, Luk BT, Kroll AV, Dehaini D, Zhou J, Kim HW, Gao W, Lu W, Zhang L. Dec 2016, Biomaterials, Vol. 111, pp. 116-123.

113. *T-Cell-Mimicking Nanoparticles Can Neutralize HIV Infectivity.* . Wei X, Zhang G, Ran D, Krishnan N, Fang RH, Gao W, Spector SA, Zhang L. 45, Nov 2018, Adv Mater, Vol. 30, p. e1802233.

114. *Cellular Nanosponges Inhibit SARS-CoV-2 Infectivity.* Zhang Q, Honko A, Zhou J, Gong H, Downs SN, Vasquez JH, Fang RH, Gao W, Griffiths A, Zhang L. 7, Jul 2020, Nano Lett, Vol. 8, pp. 5570-5574.

115. *Multimodal Enzyme Delivery and Therapy Enabled by Cell Membrane-Coated Metal-Organic Framework Nanoparticles.* . Zhuang J, Duan Y, Zhang Q, Gao W, Li S, Fang RH, Zhang L. 5, May 2020, Nano Lett, Vol. 20, pp. 4051-4058.

116. *Human Cancer Cell Membrane-Coated Biomimetic Nanoparticles Reduce Fibroblast-Mediated Invasion and Metastasis and Induce T-Cells.* . Jin J, Krishnamachary B, Barnett JD, Chatterjee S, Chang D, Mironchik Y, Wildes F, Jaffee EM, Nimmagadda S, Bhujwalla ZM. 8, Feb 2019, ACS Appl Mater Interfaces. , Vol. 11, pp. 7850-7861.

117. *Nanoparticle-Based Manipulation of Antigen-Presenting Cells for Cancer Immunotherapy.* . Fang RH, Kroll AV, Zhang L. 41, Nov 2015, Small, Vol. 11, pp. 5483-96.

118. *Engineered Cell-Membrane-Coated Nanoparticles Directly Present Tumor Antigens to Promote Anticancer Immunity.* . Jiang Y, Krishnan N, Zhou J, Chekuri S, Wei X, Kroll AV, Yu CL, Duan Y, Gao W, Fang RH, Zhang L. 30, Jul 2020, Adv Mater, Vol. 32, p. e2001808.

119. *Nanoparticulate Delivery of Cancer Cell Membrane Elicits Multiantigenic Antitumor Immunity.* . Kroll AV, Fang RH, Jiang Y, Zhou J, Wei X, Yu CL, Gao J, Luk BT, Dehaini D, Gao W, Zhang L. 47, Dec 2017, Adv Mater., Vol. 29, p. 10.1002/adma.201703969.

120. *Cancer Cell-Membrane Biomimetic Boron Nitride Nanospheres for Targeted Cancer Therapy.* . Feng S, Ren Y, Li H, Tang Y, Yan J, Shen Z, Zhang H, Chen F. Mar 2021, Int J Nanomedicine. , Vol. 16, pp. 2123-2136. .

121. *Macrophage-cancer hybrid membrane-coated nanoparticles for targeting lung metastasis in breast cancer therapy.* . Gong C, Yu X, You B, Wu Y, Wang R, Han L, Wang Y, Gao S, Yuan Y. 1, Jun 2020, J Nanobiotechnology, Vol. 18, p. 92.

122. *Erythrocyte-Platelet Hybrid Membrane Coating for Enhanced Nanoparticle Functionalization.* Dehaini D, Wei X, Fang RH, Masson S, Angsantikul P, Luk BT, Zhang Y, Ying M, Jiang Y, Kroll AV, Gao W, Zhang L. 16, Apr 2017, Adv Mater, Vol. 29, p. 10.1002/adma.201606209.

123. *Medical Micro/Nanorobots in Precision Medicine.* Soto F, Wang J, Ahmed R, Demirci U. 21, Oct 2020, Adv Sci (Weinh)., Vol. 7, p. 2002203.

124. *Hybrid biomembrane-functionalized nanorobots for concurrent removal of pathogenic bacteria and toxins.* . Esteban-Fernández de Ávila B, Angsantikul P, Ramírez-Herrera DE, Soto F, Teymourian H, Dehaini D, Chen Y, Zhang L, Wang J. May 2018, Sci Robot, p. eaat0485.

125. *Modulating antibacterial immunity via bacterial membrane-coated nanoparticles.* . Gao W, Fang RH, Thamphiwatana S, Luk BT, Li J, Angsantikul P, Zhang Q, Hu CM, Zhang L. 2, Feb 2015, Nano Lett., Vol. 15, pp. 1403-9. .

126. *Inhibition of Pathogen Adhesion by Bacterial Outer Membrane-Coated Nanoparticles.* Zhang Y, Chen Y, Lo C, Zhuang J, Angsantikul P, Zhang Q, Wei X, Zhou Z, Obonyo M, Fang RH, Gao W, Zhang L. 33, Aug 2019, Angew Chem Int Ed Engl, Vol. 58, pp. 11404-11408.

127. *Coating nanoparticles with gastric epithelial cell membrane for targeted antibiotic delivery against Helicobacter pylori infection.* Angsantikul P, Thamphiwatana S, Zhang Q, Spiekermann K, Zhuang J, Fang RH, Gao W, Obonyo M, Zhang L. 2, Jun 2018, Adv Ther (Weinh)., Vol. 1, p. 1800016.

128. *Reductively dissociable biomimetic nanoparticles for control of integrin-coupled inflammatory signaling to retard atherogenesis.* Gao W, Yang H, Liu X, Liu Z, Tong L, Sun Y, Cao W, Cao Y, Tang B. 77, Sep 2019, Chem Commun (Camb)., Vol. 55, pp. 11535-11538.

129. *Nano-Ghosts: Biomimetic membranal vesicles, technology and characterization.* . Oieni J, Levy L, Letko Khait N, Yosef L, Schoen B, Fliman M, Shalom-Luxenburg H, Malkah Dayan N, D'Atri D, Cohen Anavy N, Machluf M. May 1, 2020, Methods, Vol. 177, pp. 126-134.

130. *Radiolabeling of cell membrane-based nano-vesicles with 14C-linoleic acid for robust and sensitive quantification of their biodistribution.* Letko Khait N, Malkah N, Kaneti G, Fried L, Cohen Anavy N, Bronshtein T, Machluf M. Jan 2019, J Control Release, Vol. 293, pp. 215-223.

131. *Nano-ghosts: Novel biomimetic nano-vesicles for the delivery of antisense oligonucleotides.* Oieni J, Lolli A, D'Atri D, Kops N, Yayon A, van Osch GJVM, Machluf M. May 2021, J Control Release, Vol. 333, pp. 28-40.

132. *Nanoghosts as a Novel Natural Nonviral Gene Delivery Platform Safely Targeting Multiple Cancers.* . Kaneti L, Bronshtein T, Malkah Dayan N, Kovregina I, Letko Khait N, Lupu-Haber Y, Fliman M, Schoen BW, Kaneti G, Machluf M. 3, Mar 2016, Nano Lett. , Vol. 16, pp. 1574-82.

133. *Biomimetic Glyconanoparticle Vaccine for Cancer Immunotherapy.* Reuven EM, Leviatan Ben-Arye S, Yu H, Duchi R, Perota A, Conchon S, Bachar Abramovitch S, Soulillou JP, Galli C, Chen X, Padler-Karavani V. 3, Mar 2019, Acs Nano, Vol. 13, pp. 2936-2947.

134. *Nanoparticle Delivery of Immunostimulatory Agents for Cancer Immunotherapy.* Zhuang J, Holay M, Park JH, Fang RH, Zhang J, Zhang L. 25, Oct 2019, Theranostics, Vol. 9, pp. 7826-7848. .

135. *Remote Loading of Small-Molecule Therapeutics into Cholesterol-Enriched Cell-Membrane-Derived Vesicles.* . Zhang X, Angsantikul P, Ying M, Zhuang J, Zhang Q, Wei X, Jiang Y, Zhang Y, Dehaini D, Chen M, Chen Y, Gao W, Fang RH, Zhang L. Nov 2017, Angew Chem Int Ed Engl. , pp. 14075-14079.

136. *Remote-Loaded Platelet Vesicles for Disease-Targeted Delivery of Therapeutics.* . Ying M, Zhuang J, Wei X, Zhang X, Zhang Y, Jiang Y, Dehaini D, Chen M, Gu S, Gao W, Lu W, Fang RH, Zhang L. May 2018, Adv Funct Mater., p. 1801032. .

137. *Biomimetic nanoparticles with enhanced affinity towards activated endothelium as versatile tools for theranostic drug delivery.* Martinez JO, Molinaro R, Hartman KA, Boada C, Sukhovershin R, De Rosa E, Kirui D, Zhang S, Evangelopoulos M, Carter AM, Bibb JA, Cooke JP, Tasciotti E. 4, Jan 2018, Theranostics

, Vol. 8, pp. 1131-1145.

138. *Biomimetic proteolipid vesicles for targeting inflamed tissues.* Molinaro, R., Corbo, C., Martinez, J. et al. 2016, Nature Mater , Vol. 15, pp. 1037–1046 .

139. *Reproducible and Characterized Method for Ponatinib Encapsulation into Biomimetic Lipid Nanoparticles as a Platform for Multi-Tyrosine Kinase-Targeted Therapy.* al, Assaf Zinger et. 10, 2020, ACS Appl. Bio Mater, Vol. 3, pp. 6737–6745.

140. *Macrophage-derived nanovesicles exert intrinsic anti-inflammatory properties and prolong survival in sepsis through a direct interaction with macrophages.* . Molinaro R, Pastò A, Corbo C, Taraballi F, Giordano F, Martinez JO, Zhao P, Wang X, Zinger A, Boada C, Hartman KA, Tasciotti E. 28, Jul 2019, Nanoscale, Vol. 11, pp. 13576-13586.

141. *Engineered biomimetic nanovesicles show intrinsic anti-inflammatory properties for the treatment of inflammatory bowel diseases.* Corbo C, Cromer WE, Molinaro R, Toledano Furman NE, Hartman KA, De Rosa E, Boada C, Wang X, Zawieja DC, Agostini M, Salvatore F, Abraham BP, Tasciotti E. 38, Oct 2017, Nanoscale, Vol. 9, pp. 14581-14591.

142. *Inflammation and Cancer: In Medio Stat Nano.* Molinaro R, Corbo C, Livingston M, Evangelopoulos M, Parodi A, Boada C, Agostini M, Tasciotti E. 34, 2018, Curr Med Chem. , Vol. 25, pp. 4208-4223.

143. *Design and Development of Biomimetic Nanovesicles Using a Microfluidic Approach.* Molinaro R, Evangelopoulos M, Hoffman JR, Corbo C, Taraballi F, Martinez JO, Hartman KA, Cosco D, Costa G, Romeo I, Sherman M, Paolino D, Alcaro S, Tasciotti E. 15, Apr 2018, Adv Mater., Vol. 30, p. e1702749.

144. *Exosome-mimetic nanoplatforms for targeted cancer drug delivery. J Nanobiotechnology.* Vázquez-Ríos AJ, Molina-Crespo Á, Bouzo BL, López-López R, Moreno-Bueno G, de la Fuente M. 1, Jul 2019, Nanobiotechnology, Vol. 17, p. 85.

145. *Active-Targeting NIR-II Phototheranostics in Multiple Tumor Models Using Platelet-Camouflaged Nanoprobes.* Geng X, Gao D, Hu D, Liu Q, Liu C, Yuan Z, Zhang X, Liu X, Sheng Z, Wang X, Zheng H. 50, Dec 2020, ACS Appl Mater Interfaces. , Vol. 12, pp. 55624-55637. .

146. *Cell-free synthesis of connexin 43-integrated exosome-mimetic nanoparticles for siRNA delivery.* Lu M, Zhao X, Xing H, Liu H, Lang L, Yang T, Xun Z, Wang D, Ding P. Sep 2019, Acta Biomater., pp. 517-536.

147. *Nanodelivery Systems Face Challenges and Limitations in Bone Diseases Management.* Federica Giordano, Stefania Lenna,Riccardo Rampado,Ava Brozovich,Takashi Hirase,Mauro G. Tognon,Fernanda Martini,Marco Agostini,Jason T. Yustein,Francesca Taraballi. Oct 2021, Adv Ther.

148. *Neutralization of cholera toxin with nanoparticle decoys for treatment of cholera.* . Das S, Angsantikul P, Le C, Bao D, Miyamoto Y, Gao W, Zhang L, Eckmann L. 2, Feb 2018, PLoS Negl Trop Dis., Vol. 12, p. e0006266. .

149. *Albumin: An Emerging Opportunity in Drug Delivery.* ahimizadeh, P., Yang, S. & Lim, S.I. 2020, Biotechnol Bioproc E , Vol. 25, pp. 985–995.

150. *Paclitaxel Nano-Delivery Systems: A Comprehensive Review.* . Ma P, Mumper RJ. 2, Feb 2013, J Nanomed Nanotechnol., Vol. 4, p. 1000164.

151. *Secreted Protein Acidic and Rich in Cysteine Mediated Biomimetic Delivery of Methotrexate by Albumin-Based Nanomedicines for Rheumatoid Arthritis Therapy.* Liu L, Hu F, Wang H, Wu X, Eltahan AS, Stanford S, Bottini N, Xiao H, Bottini M, Guo W, Liang XJ. 5, May 2019, ACS Nano, Vol. 13, pp. 5036-5048.

152. *Plasma lipoproteins: genetic influences and clinical implications.* Hegele, R. 2009, Nat Rev Genet , Vol. 10, pp. 109–121 .

153. *Dynamically enhancing plaque targeting via a positive feedback loop using multifunctional biomimetic nanoparticles for plaque regression.* Jiang C, Qi Z, He W, Li Z, Tang Y, Wang Y, Huang Y, Zang H, Yang H, Liu J. Aug 2019, J Control Release, Vol. 308, pp. 71-85.

154. *Lipoprotein-inspired penetrating nanoparticles for deep tumor-targeted shuttling of indocyanine green and enhanced photo-theranostics.* Sheng Y, Wang Z, Ngandeu Neubi GM, Cheng H, Zhang C, Zhang H, Wang R, Zhou J, Ding Y. Aug 2019, Biomater Sci. , pp. 3425-3437.

155. *Low density lipoprotein mimic nanoparticles composed of amphipathic hybrid peptides and lipids for tumor-targeted delivery of paclitaxel.* . Qian J, Xu N, Zhou X, Shi K, Du Q, Yin X, Zhao Z. Sep 7431-7446., 2019, Int J Nanomedicine, Vol. 14.

156. *Microparticle, nanoparticle, and stem cell-based oxygen carriers as advanced blood substitutes.* Tao Z, Ghoroghchian PP. 9, 2014, Trends Biotechnol, Vol. 32, pp. 466-73.

157. *Supramolecular Assembly of High-Density Lipoprotein Mimetic Nanoparticles Using Lipid-Conjugated Core Scaffolds.* Henrich SE, Hong BJ, Rink JS, Nguyen ST, Thaxton CS. 25, Jun 2019, J Am Chem Soc., Vol. 141, pp. 9753-9757.

158. *An optimized method for the isolation and identification of membrane proteins.* Lehner I, Niehof M, Borlak J. 11, Jun 2003, Electrophoresis., Vol. 24, pp. 1795-808.

159. *Differential Detergent Fractionation of Eukaryotic Cells.* Ramsby, M. L. & Makowski, G. S. Vol. 112, pp. 53–66.

160. *Resistance of cell membranes to different detergents.* Schuck, S., Honsho, M., Ekroos, K., Shevchenko, A. & Simons, K. 10, 2003, PNAS, Vol. 100, pp. 5795-5800.

161. Carlson, Owen W. Nadeau and Gerald M. A Review of Methods Used for Identifying Structural. [book auth.] Aron W. Fenton (ed.). *Allostery: Methods and Protocols, Methods in Molecular Biology.* s.l. : Springer Science+Business Media, Vol. 796.

162. *High-throughput stability screening for detergent-solubilized membrane proteins.* Kotov, V. et al. 2019, pp. 1-9.

163. *Human Polymorphonuclear Leukocytes Adhere to Complement Factor H Through an Interaction That Involves α M β 2 (CD11b/CD18).* Discipio, R. G., Daffern, P. J., Schraufstätter, I. U. & Cd, M. C. 2020, Vol. 2.

164. *Palmitoylated calnexin is a key component of the ribosome – translocon complex.* . Lakkaraju, A. K. K. et al. 2012, Vol. 31, pp. 1823–1835.

165. *Nucleoporin Nup62 maintains centrosome homeostasis.* Hashizume, C. et al. 2013.

166. *Nuclear ARP2 / 3 drives DNA break clustering for homology-directed repair.* Schrank, B. R. et al. 2018, Nature.

167. *Subcellular localization of human glyceraldehyde-3-phosphate dehydrogenase is independent of its glycolytic function.* Mazzola, J. L. & Sirover, M. A. 2003, Vol. 1622, pp. 50–56.

168. *CD14 Targets Complement Receptor 3 to Lipid Rafts during Phagocytosis of Borrelia burgdorferi.* Hawley, K. L., Martín-ruiz, I., Iglesias-pedraz, J. M., Berwin, B. & Anguita, J. 2013, Int J Biol Sci, pp. 803-810.

169. *Resistance of cellular membrane antigens to solubilization with Triton X-100 as a marker of their association with lipid rafts--analysis by flow cytometry.* Filatov AV, Shmigol IB, Kuzin II, Sharonov GV, Feofanov AV. Jul 2003, J Immunol Methods. , Vol. 278, pp. 211-9.

170. *Design of experiments (DoE) to develop and to optimize nanoparticles as drug delivery systems.* Tavares Luiz M, Santos Rosa Viegas J, Palma Abriata J, Viegas F, Testa Moura de Carvalho Vicentini F, Lopes Badra Bentley MV, Chorilli M, Maldonado Marchetti J, Tapia-Blácido DR. Aug 2021, Eur J Pharm Biopharm, Vol. 165, pp. 127-148.

171. *Doxil®--the first FDA-approved nano-drug: lessons learned.* Y., Barenholz. Jun 2012, J Control Release, pp. 117-34.

172. *Leukocyte-mimicking nanovesicles for effective doxorubicin delivery to treat breast cancer and melanoma.* . Molinaro R, Martinez JO, Zinger A, De Vita A, Storci G, Arrighetti N, De Rosa E, Hartman KA, Basu N, Taghipour N, Corbo C, Tasciotti E. 1, Jan 2020, Biomater Sci, Vol. 8, pp. 333-341.

173. *Nanoparticle-Based Drug Delivery in Cancer Therapy and Its Role in Overcoming Drug Resistance.* Yao Y, Zhou Y, Liu L, Xu Y, Chen Q, Wang Y, Wu S, Deng Y, Zhang J, Shao A. Aug 2020, Front Mol Biosci, p. 193.

174. *Protein tyrosine phosphatase receptor type C (PTPRC or CD45).* Al Barashdi MA, Ali A, McMullin MF, Mills K. 9, 2021, J Clin Pathol, Vol. 74, pp. 548-552.

175. *Different Subsets of T Cells, Memory, Effector Functions, and CAR-T Immunotherapy.* Golubovskaya V, Wu L. 3, 2016, Cancers (Basel). , Vol. 8, p. 36.

176. *Markers and function of human NK cells in normal and pathological conditions. Cytometry B Clin Cytom.* Del Zotto G, Marcenaro E, Vacca P, Sivori S, Pende D, Della Chiesa M, Moretta F, Ingegnere T, Mingari MC, Moretta A, Moretta L. 2, Cytometry B Clin Cytom. , Vol. 92, pp. 100-114. .

177. *Human Monocyte Subsets and Phenotypes in Major Chronic Inflammatory Diseases.* Kapellos TS, Bonaguro L, Gemünd I, Reusch N, Saglam A, Hinkley ER, Schultze JL. 10, Aug 2019, Front Immunol. , Vol. 30, p. 2035.

178. *Challenges and Opportunities for Consistent Classification of Human B Cell and Plasma Cell Populations.* Sanz I, Wei C, Jenks SA, Cashman KS, Tipton C, Woodruff MC, Hom J, Lee FE. 10, Oct 2019, Front Immunol, Vol. 18, p. 2458.

179. *Aberrant expression of T cell and B cell markers in myelocyte/monocyte/histiocyte-derived lymphoma and leukemia cells. Is the infrequent expression of T/B cell markers sufficient to establish a lymphoid origin for Hodgkin's Reed-Sternberg cells?* Hsu SM, Hsu PL. 1, Jan 1989, Am J Pathol., Vol. 134, pp. 203-12.

180. *beta 1 integrin function in vivo: adhesion, migration and more.* Brakebusch C, Fässler R. 3, 2005, Cancer Metastasis Rev, Vol. 24, pp. 403-11.

181. *CD44: from adhesion molecules to signalling regulators.* Ponta H, Sherman L, Herrlich PA. 1, Jan 2003, Nat Rev Mol Cell Biol, Vol. 4, pp. 33-45.

182. *A dileucine motif targets MCAM-l cell adhesion molecule to the basolateral membrane in MDCK cells.* Guezguez B, Vigneron P, Alais S, Jaffredo T, Gavard J, Mège RM, Dunon D. 15, Jun 2006, FEBS Lett, Vol. 580, pp. 3649-56.

183. *CD62 and endothelial cell-leukocyte adhesion molecule 1 (ELAM-1) recognize the same carbohydrate ligand, sialyl-Lewis x.* Polley MJ, Phillips ML, Wayner E, Nudelman E, Singhal AK, Hakomori S, Paulson JC. 14, Jul 1991, Proc Natl Acad Sci U S A, Vol. 88, pp. 6224-8.

184. *Molecular mechanism and function of CD40/CD40L engagement in the immune system.* Elgueta R, Benson MJ, de Vries VC, Wasiuk A, Guo Y, Noelle RJ. 1, 2009, Immunol Rev., Vol. 229, pp. 152-72.

185. *CD69: from activation marker to metabolic gatekeeper.* Cibrián D, Sánchez-Madrid F. 6, 2017, Eur J Immunol. , Vol. 47, pp. 946-953.

186. *Design and Development of Biomimetic Nanovesicles Using a Microfluidic Approach.* Molinaro R, Evangelopoulos M, Hoffman JR, Corbo C, Taraballi F, Martinez JO, Hartman KA, Cosco D, Costa G, Romeo I, Sherman M, Paolino D, Alcaro S, Tasciotti E. 15, Apr 2018, Adv Mater., Vol. 30, p. e1702749.

187. *Farhat Yaqub.* drugs, Mechanism of action of anthracycline. 8, Jun 2013, Lancet Oncology, Vol. 14.

188. *Cancer Drug Resistance: A Brief Overview from a Genetic Viewpoint.* Rueff J, Rodrigues AS. Methods Mol Biol, Vol. 1395, pp. 1-18.

189. *Understanding nanoparticle endocytosis to improve targeting strategies in nanomedicine.* Sousa de Almeida M, Susnik E , Drasler B , Taladriz-Blanco P , Petri-Fink A , Rothen-Rutishauser B. 9, May 2021, Chem Soc Rev., Vol. 50, pp. 5397-5434.

190. *Remote loading of doxorubicin into liposomes driven by a transmembrane phosphate gradient.* Fritze A, Hens F, Kimpfler A, Schubert R, Peschka-Süss R. 10, Oct 2006, Biochim Biophys Acta., Vol. 1758, pp. 1633-40.

191. *Extracellular Matrix in the Tumor Microenvironment and Its Impact on Cancer Therapy.* Henke E, Nandigama R, Ergün S. Jan 2020, Front Mol Biosci, Vol. 6, p. 160.

192. *Role of Extracellular Matrix in Development and Cancer Progression.* Walker C, Mojares E, Del Río Hernández A. 10, 2018, Int J Mol Sci, Vol. 19, p. 3028.

193. *Three-dimensional cell culture: A powerful tool in tumor research and drug discovery.* Lv D, Hu Z, Lu L, Lu H, Xu X. 6, 2017, Oncol Lett, Vol. 14, pp. 6999-7010.

194. *Biomimetic proteolipid vesicles for targeting inflamed tissues.* . Molinaro R, Corbo C, Martinez JO, Taraballi F, Evangelopoulos M, Minardi S, Yazdi IK, Zhao P, De Rosa E, Sherman MB, De Vita A, Toledano Furman NE, Wang X, Parodi A, Tasciotti E. 9, Sep 2016, Nat Mater., Vol. 15, pp. 1037-46.

195. *Tumor-Associated Macrophages: Recent Insights and Therapies.* Zhou J, Tang Z, Gao S, Li C, Feng Y, Zhou X. 188, Feb 2020, Front Oncol, Vol. 10.

196. *Shedding light on the cell biology of extracellular vesicles.* van Niel, G., D'Angelo, G. & Raposo, G. 2018, Nat Rev Mol Cell Biol , Vol. 19, pp. 213-228.

197. *Minimal information for studies of extracellular vesicles 2018 (MISEV2018): a position statement of the International Society for Extracellular Vesicles and update of the MISEV2014 guidelines.* Théry C, Witwer KW, Aikawa E, Alcaraz MJ, Anderson JD, Andriantsitohaina R, Antoniou A, Arab T, Archer F, Atkin-Smith GK, Ayre DC, Bach JM, Bachurski D, Baharvand H, Balaj L, Baldacchino S, Bauer NN, Baxter AA, Bebawy M, Beckham C, Bedina Zavec A, et al. 1, Nov 2018, J Extracell Vesicles., Vol. 7, p. 1535750.

198. *Overview of Extracellular Vesicles, Their Origin, Composition, Purpose, and Methods for Exosome Isolation and Analysis.* Doyle LM, Wang MZ. 7, 2019, Cells, Vol. 8, p. 727. .

199. *Exosomes: Cell-Derived Nanoplatforms for the Delivery of Cancer Therapeutics.* Kim H, Kim EH, Kwak G, Chi SG, Kim SH, Yang Y. 1, Dec 2020, Int J Mol Sci., Vol. 22, p. 14.

200. *Characterization of Human NK Cell-Derived Exosomes: Role of DNAM1 Receptor In Exosome-Mediated Cytotoxicity Against Tumor.* Di Pace AL, Tumino N, Besi F, Alicata C, Conti LA, Munari E, Maggi E, Vacca P, Moretta L. 3, Mar 2020, Cancers (Basel), Vol. 12, p. 661.

201. *Mesenchymal stem cell exosomes: a two-edged sword in cancer therapy.* Vakhshiteh F, Atyabi F, Ostad SN. Apr 2019, Int J Nanomedicine., Vol. 14, pp. 2847-2859.

202. *Tumor exosomes: a double-edged sword in cancer therapy.* Sun, W., Luo, Jd., Jiang, H. et al. 2018, Acta Pharmacol Sin , Vol. 39, pp. 534–541.

203. *Exosome-based immunotherapy: a promising approach for cancer treatment.* . Xu, Z., Zeng, S., Gong, Z. et al. 2020.

204. *Exosomes: biogenesis, biologic function and clinical potential.* Zhang, Y., Liu, Y., Liu, H. et al. 19, Cell Biosci, Vol. 9.

205. *Pharmacokinetics of Exosomes-An Important Factor for Elucidating the Biological Roles of Exosomes and for the Development of Exosome-Based Therapeutics.* Morishita M, Takahashi Y, Nishikawa M, Takakura Y. 9, 2017, J Pharm Sci. , Vol. 106, pp. 2265-2269.

206. *Routes and mechanisms of extracellular vesicle uptake.* Mulcahy LA, Pink RC, Carter DR. 3, Aug 2014, J Extracell Vesicles., Vol. 4.

207. *Perspectives in Manipulating EVs for Therapeutic Applications: Focus on Cancer Treatment.* Nazimek K, Bryniarski K. 13, Jun 2020, Int J Mol Sci. , Vol. 21, p. 4623.

208. *The "sugar-coated bullets" of cancer: Tumor-derived exosome surface glycosylation from basic knowledge to applications.* . Lin S, Zhou S, Yuan T. 6, Oct 2020, Clin Transl Med. , Vol. 10, p. e204.

209. *Engineering exosomes as refined biological nanoplatforms for drug delivery.* . Luan, X., Sansanaphongpricha, K., Myers, I. 2017, Acta Pharmacol Sin , Vol. 38, pp. 754-763.

210. *Macrophage-derived exosome-mimetic hybrid vesicles for tumor targeted drug delivery.* Rayamajhi S, Nguyen TDT, Marasini R, Aryal S. Aug 2019, Acta Biomater., Vol. 94, pp. 482-494.

211. *Employing mesenchymal stem cells to support tumor-targeted delivery of extracellular vesicle (EV)-encapsulated microRNA-379.* O'Brien KP, Khan S, Gilligan KE, Zafar H, Lalor P, Glynn C, O'Flatharta C, Ingoldsby H, Dockery P, De Bhulbh A, Schweber JR, St John K, Leahy M, Murphy JM, Gallagher WM, O'Brien T, Kerin MJ, Dwyer RM. 16, Apr 2018, Oncogene, Vol. 37, pp. 2137-2149.

212. *Engineered exosomes for targeted co-delivery of miR-21 inhibitor and chemotherapeutics to reverse drug resistance in colon cancer.* Liang, G., Zhu, Y., Ali, D.J. et al. 10, 2020, Nanobiotechnol , Vol. 18.

213. *Tumor Cell-Derived Extracellular Vesicle-Coated Nanocarriers: An Efficient Theranostic Platform for the Cancer-Specific Delivery of Anti-miR-21 and Imaging Agents.* Bose RJC, Uday Kumar S, Zeng Y, Afjei R, Robinson E, Lau K, Bermudez A, Habte F, Pitteri SJ, Sinclair R, Willmann JK, Massoud TF, Gambhir SS, Paulmurugan R. 11, Nov 2018, ACS Nano, Vol. 12, pp. 10817-10832. .

214. *Engineering macrophage-derived exosomes for targeted paclitaxel delivery to pulmonary metastases: in vitro and in vivo evaluations.* . Kim MS, Haney MJ, Zhao Y, Yuan D, Deygen I, Klyachko NL, Kabanov AV, Batrakova EV. 1, Jan 2018, Nanomedicine, Vol. 14, pp. 195-204.

215. *Aptamer-Conjugated Extracellular Nanovesicles for Targeted Drug Delivery.* . Wan Y, Wang L, Zhu C, Zheng Q, Wang G, Tong J, Fang Y, Xia Y, Cheng G, He X, Zheng SY. 3, Feb 2018, Cancer Res, Vol. 78, pp. 798-808.

216. *Nucleolin-targeted Extracellular Vesicles as a Versatile Platform for Biologics Delivery to Breast Cancer.* . Wang Y, Chen X, Tian B, Liu J, Yang L, Zeng L, Chen T, Hong A, Wang X. 5, Mar 2017, Theranostics, Vol. 7, pp. 1360-1372.

217. *Interleukin 3- receptor targeted exosomes inhibit in vitro and in vivo Chronic Myelogenous Leukemia cell growth.* . Bellavia D, Raimondo S, Calabrese G, Forte S, Cristaldi M, Patinella A, Memeo L, Manno M, Raccosta S, Diana P, Cirrincione G, Giavaresi G, Monteleone F, Fontana S, De Leo G, Alessandro R. 5, Mar 2017, Theranositcs, Vol. 7, pp. 1333-1345.

218. *Tumor exosome-based nanoparticles are efficient drug carriers for chemotherapy.* Yong T, Zhang X, Bie N, Zhang H, Zhang X, Li F, Hakeem A, Hu J, Gan L, Santos HA, Yang X. 1, Aug 2019, Nat Commun, Vol. 10, p. 3838.

219. *Microfluidic Sonication To Assemble Exosome Membrane-Coated Nanoparticles for Immune Evasion-Mediated Targeting.* . Liu C, Zhang W, Li Y, Chang J, Tian F, Zhao F, Ma Y, Sun J. 11, Nov 2019, Nano Lett, Vol. 19, pp. 7836-7844.

220. *Development and MPI tracking of novel hypoxia-targeted theranostic exosomes.* . Jung KO, Jo H, Yu JH, Gambhir SS, Pratx G. Sep 2018, Biomaterials., Vol. 177, pp. 139-148.

221. *Heterologous and cross-species tropism of cancer-derived extracellular vesicles.* . Garofalo M, Villa A, Crescenti D, Marzagalli M, Kuryk L, Limonta P, Mazzaferro V, Ciana P. 19, 2019, Theranostics, Vol. 9, pp. 5681-5693.

222. *The Biological Function and Therapeutic Potential of Exosomes in Cancer: Exosomes as Efficient Nanocommunicators for Cancer Therapy.* Choi JU, Park IK, Lee YK, Hwang SR. 19, Oct 2020, Int J Mol Sci., Vol. 21.

223. *Extracellular vesicle-mediated delivery of miR-101 inhibits lung metastasis in osteosarcoma.* Zhang K, Dong C, Chen M, Yang T, Wang X, Gao Y, Wang L, Wen Y, Chen G, Wang X, Yu X, Zhang Y, Wang P, Shang M, Han K, Zhou Y. 1, Jan 2020, Theranostics, Vol. 10, pp. 411-425.

224. *Cancer-derived exosomes from HER2-positive cancer cells carry trastuzumab-emtansine into cancer cells leading to growth inhibition and caspase activation.* Barok M, Puhka M, Vereb G, Szollosi J, Isola J, Joensuu H. 1, May 2018, BMC Cancer, Vol. 18, p. 504.

225. *Macrophage cell-derived exosomes/staphylococcal enterotoxin B against fibrosarcoma tumor.* Behzadi E, Hosseini HM, Halabian R, Fooladi AAI. Oct 2017, Microb Pathog. , Vol. 111, pp. 132-138.

226. *Antibody-directed enzyme prodrug therapy (ADEPT) for cancer.* KD., Bagshawe. 10, Oct 2006, Expert Rev Anticancer Ther. , Vol. 6, pp. 1421-31.

227. *Extracellular vesicle-mediated suicide mRNA/protein delivery inhibits glioblastoma tumor growth in vivo.* Erkan EP, Senfter D, Madlener S, Jungwirth G, Ströbel T, Saydam N, Saydam O. 1, Jan 2017, Cancer Gene Ther. , Vol. 24, pp. 38-44.

228. *Possibility of Exosome-Based Therapeutics and Challenges in Production of Exosomes Eligible for Therapeutic Application.* Yamashita T, Takahashi Y, Takakura Y. 6, 2018, Biol Pharm Bull., Vol. 41, pp. 835-842.